



University of Kentucky  
UKnowledge

---

Theses and Dissertations--Chemistry

Chemistry

---

2014

## STABILITY STUDIES OF MEMBRANE PROTEINS

Cui Ye

University of Kentucky, cuicuicake@gmail.com

[Right click to open a feedback form in a new tab to let us know how this document benefits you.](#)

---

### Recommended Citation

Ye, Cui, "STABILITY STUDIES OF MEMBRANE PROTEINS" (2014). *Theses and Dissertations--Chemistry*. 33.

[https://uknowledge.uky.edu/chemistry\\_etds/33](https://uknowledge.uky.edu/chemistry_etds/33)

This Doctoral Dissertation is brought to you for free and open access by the Chemistry at UKnowledge. It has been accepted for inclusion in Theses and Dissertations--Chemistry by an authorized administrator of UKnowledge. For more information, please contact [UKnowledge@lsv.uky.edu](mailto:UKnowledge@lsv.uky.edu).

## **STUDENT AGREEMENT:**

I represent that my thesis or dissertation and abstract are my original work. Proper attribution has been given to all outside sources. I understand that I am solely responsible for obtaining any needed copyright permissions. I have obtained needed written permission statement(s) from the owner(s) of each third-party copyrighted matter to be included in my work, allowing electronic distribution (if such use is not permitted by the fair use doctrine) which will be submitted to UKnowledge as Additional File.

I hereby grant to The University of Kentucky and its agents the irrevocable, non-exclusive, and royalty-free license to archive and make accessible my work in whole or in part in all forms of media, now or hereafter known. I agree that the document mentioned above may be made available immediately for worldwide access unless an embargo applies.

I retain all other ownership rights to the copyright of my work. I also retain the right to use in future works (such as articles or books) all or part of my work. I understand that I am free to register the copyright to my work.

## **REVIEW, APPROVAL AND ACCEPTANCE**

The document mentioned above has been reviewed and accepted by the student's advisor, on behalf of the advisory committee, and by the Director of Graduate Studies (DGS), on behalf of the program; we verify that this is the final, approved version of the student's thesis including all changes required by the advisory committee. The undersigned agree to abide by the statements above.

Cui Ye, Student

Dr. Yinan Wei, Major Professor

Dr. Dong-sheng Yang, Director of Graduate Studies

STABILITY STUDIES OF MEMBRANE PROTEINS

---

DISSERTATION

---

A dissertation submitted in partial fulfillment of the requirements for the degree of Doctor of Philosophy in the College of Arts and Sciences at the University of Kentucky

By  
Cui Ye

Lexington, Kentucky

Director: Dr. Yinan Wei, Professor of Chemistry

Lexington, Kentucky

2014

Copyright © Cui Ye 2014

## ABSTRACT OF DISSERTATION

### STABILITY STUDIES OF MEMBRANE PROTEINS

The World Health Organization has identified antimicrobial resistance as one of the top three threats to human health. Gram-negative bacteria such as *Escherichia coli* are intrinsically more resistant to antimicrobials. There are very few drugs either on the market or in the pharmaceutical pipeline targeting Gram-negative pathogens. Two mechanisms, the protection of the outer membrane and the active efflux by the multidrug transporters, play important roles in conferring multidrug resistance to Gram-negative bacteria. My work focuses on two main directions, each aligning with one of the known multidrug resistance mechanisms.

The first direction of my research is in the area of the biogenesis of the bacterial outer membrane. The outer membrane serves as a permeability barrier in Gram-negative bacteria. Antibiotics cross the membrane barrier mainly via diffusion into the lipid bilayer or channels formed by outer membrane proteins. Therefore, bacterial drug resistance is closely correlated with the integrity of the outer membrane, which depends on the correct folding of the outer membrane proteins. The folding of the outer membrane proteins has been studied extensively in dilute buffer solution. However, the cell periplasm, where the folding actually occurs, is a crowded environment. In Chapter 2, effects of the macromolecular crowding on the folding mechanisms of two bacterial outer membrane proteins (OmpA and OmpT) were examined. Our results suggested that the periplasmic domain of OmpA improved the efficiency of the OmpA maturation under the crowding condition, while refolding of OmpT was barely affected by the crowding.

The second direction of my research focuses on the major multidrug efflux transporter in Gram-negative bacteria, AcrB. AcrB is an obligate trimer, which exists and functions exclusively in a trimeric state. In Chapter 3, the unfolding of the AcrB trimer was investigated. Our results revealed that sodium dodecyl sulfate induced unfolding of the trimeric AcrB started with a local structural rearrangement. While the refolding of secondary structure in individual monomers could be achieved, the re-association of the trimer might be the limiting factor to obtain folded wild type AcrB. In Chapter 4, the

correlation between the AcrB trimer stability and the transporter activity was studied. A non-linear correlation was observed, in which the threshold trimer stability was required to maintain the efflux activity. Finally, in Chapter 5, the stability of another inner membrane protein, AqpZ, was studied. AqpZ was remarkably stable. Several molecular engineering approaches were tested to improve the thermal stability of the protein.

**KEYWORDS:** Multidrug resistance, multidrug efflux pump, outer membrane proteins, protein stability, AcrB

Cui Ye

---

Apr. 26<sup>th</sup>, 2014

---

STABILITY STUDIES OF MEMBRANE PROTEINS

By

Cui Ye

Yinan Wei, Ph.D.

Director of Thesis

Dong-sheng Yang, Ph. D.

Director of Graduate Studies

April 26<sup>th</sup>, 2014

## ACKNOWLEDGEMENTS

This Ph.D dissertation would have not been possible without the help of many people in various ways. Foremost, I would like to express my sincere gratitude to my advisor, Dr. Yinan Wei, for her continuous support and encouragement during my doctoral study. She taught me how to think independently and helped me to believe in myself. When facing difficulties in my research, she always gives me some inspiration and encourages me to look for solutions by myself. After the training, I felt confident to tackle problems and come up with solutions. I would also like to thank her for taking time and efforts to help me improve my oral presentation and writing skills.

Beside my advisor, I would like to thank my other committee members, Dr. Selegue, Dr. Testa, Dr. Hastings, and my outside examiner Dr. LeVine for providing me with insightful advice for my work. I would also like to thank my past and present colleagues: Dr. Linliang Yu, Dr. Meng Zhong, Ms. Maria Wu, Mr. Brent Ferrell, Ms. Geng Shen, Dr. Wei Lu, Ms. Qian Chai, Ms. Xinyi Zhang and Mr. Zhaoshuai Wang. I really appreciate their help in both my research and presentations.

I would like to acknowledge the University of Kentucky, the Department of Chemistry, the National Science Foundation (MCB 1158036, YW), the National Institute of Health (1R21AI103717, YW) and the Kentucky NASA EPSCoR program for their financial support.

Last but not least, I would like to thank my parents, my uncle and aunt, and all my friends for their love and support over the past many years.

## TABLE OF CONTENTS

CHAPTER I. INTRODUCTION.....	1
1.1 What are antibiotics? How do antibiotics work? .....	1
1.2 Threat of antibiotic resistance .....	2
1.3 Mechanism of bacterial antibiotic resistance .....	3
1.4 Gram-negative and Gram-positive bacteria .....	3
1.5 Mechanisms of drug resistance in Gram-negative bacteria .....	5
1.5.1 Role of outer membrane of Gram-negative bacteria in antimicrobial resistance .....	5
1.5.2 Role of active multidrug efflux transporters in antimicrobial resistance .....	8
1.6 AcrAB-TolC drug efflux pump from <i>E. coli</i> .....	12
1.7 A conformational cycling model of AcrB for drug transport.....	20
1.8 A brief summary of the thesis work .....	21
CHAPTER II. EFFECT OF CROWDING BY FICOLLS ON OMPA AND OMPT REFOLDING AND MEMBRANE INSERTION .....	23
2.1 Introduction .....	23
2.2 Materials and Methods .....	26
2.2.1 Protein cloning, expression, and purification .....	26
2.2.2 Preparation of small unilamellar vesicles .....	29
2.2.3 Folding and membrane insertion of OMPs.....	29



2.2.4 Residual structure of OMPs detected by far Ultraviolet (UV) Circular Dichroism (CD) spectroscopy and fluorescence spectroscopy .....	30
2.2.5 Residual structure of OMPs detected by limited protease digestion experiment .....	30
2.3 Results .....	32
2.3.1 Effect of the crowding condition on the rate of membrane insertion of OmpA and OmpT .....	32
2.3.2 The refolding and membrane insertion mechanism of OMPs .....	36
2.3.3 Crowding had similar effect on the secondary structures of OmpA and OmpT as revealed by far UV CD spectroscopy .....	37
2.3.4 Crowding had little influence on tertiary structure of OMPs monitored using intrinsic fluorescence .....	39
2.3.5 Unfolded OmpA assumed a more compact structure under the crowded condition as revealed by limited protease digestion experiment .....	41
2.3.6 Effect of the crowding condition on the rate of membrane insertion of the transmembrane domain of OmpA .....	46
2.4 Discussion .....	47
2.5 Conclusions .....	48
<b>CHAPTER III. UNFOLDING STUDY OF A TRIMERIC MEMBRANE PROTEIN ACRB.....</b>	<b>50</b>
3.1 Introduction .....	50

3.2 Materials and Methods .....	53
3.2.1 Plasmid construction, protein expression and purification.....	53
3.2.2 Unfolding of trimeric AcrB .....	54
3.2.3 BN- PAGE analysis and far UV CD spectroscopy.....	55
3.2.4 Refolding of AcrB .....	56
3.3 Results .....	56
3.3.1 Chemical denaturation of trimeric AcrB monitored by intrinsic fluorescence .....	56
3.3.2 Contribution of signal change from trimer dissociation.....	59
3.3.3 Unfolding of a triple AcrB mutant .....	62
3.3.4 Chemical denaturation of trimeric AcrB monitored by CD spectroscopy .	64
3.3.5 Comparison of AcrB unfolding plots monitored using fluorescence and CD spectroscopy .....	65
3.3.6 Refolding of chemically denatured AcrB.....	66
3.4 Discussion .....	69
3.5 Conclusion.....	72
 CHAPTER IV. THE CORRELATION BETWEEN ACRB TRIMER ASSOCIATION AFFINITY AND EFFLUX PUMP ACTIVITY.....	 73
4.1 Introduction .....	73
4.2 Materials and Methods .....	75

4.2.1 Protein cloning, expression and purification .....	75
4.2.2 Structural characterization using CD and fluorescence spectroscopy .....	76
4.2.3 Measurement of drug susceptibility, ethidium bromide accumulation and nile red efflux.....	76
4.2.4 Method to calculate apparent trimer affinity of AcrB in detergent micelles .....	77
4.3 Results .....	77
4.3.1 AcrB variants with mutations at the inter-subunit interface.....	77
4.3.2 AcrB variants displayed partial or full activities .....	80
4.3.3 Most AcrB variants used in this study have similar expression levels.....	83
4.3.4 Mutations introduced in TH8 had little influence on the structure of monomers. ....	86
4.3.5 Determination of the trimer association constant of purified AcrB variants .....	90
4.3.6 Correlation between AcrB trimer stability and transport activity. ....	93
4.4 Discussion .....	95
4.5 Conclusion.....	98
CHAPTER V. MOLECULAR ENGINEERING OF AQUAPORIN Z .....	100
5.1 Introduction .....	100
5.2 Materials and Methods .....	103
5.2.1 Plasmid construction, protein expression and purification.....	103

5.2.2 Quantification of the disulfide bonds formed in AqpZ <sub>G91C</sub> .....	104
5.2.2 Protein thermal denaturation monitored using CD spectroscopy and fluorescence spectroscopy .....	105
5.3 Results and Discussion.....	106
5.3.1 A rational design of positions to be mutated .....	106
5.3.2 None of mutations increased the thermal stability of AqpZ.....	110
5.3.3 Disulfide bond formations in AqpZ <sub>G91C</sub> .....	114
5.4 Prospectus.....	116
REFERENCES .....	119
VITA.....	145

## LIST of TABLES

Table 1.1 Multidrug efflux systems in Gram-negative bacteria. ....	12
Table 2.1 Primers used in the construction of plasmids containing OmpA, OmpT and OmpA171.....	27
Table 2.2 Refolding rate constants ( $\text{min}^{-1}$ ) .....	34
Table 2.3 Parameters of trypsin and chymotrypsin activities measured with small substrates in the absence and presence of 20% Ficoll 70. ....	43
Table 4.1 MIC and EtBr accumulation rate of BW25113 $\Delta$ <i>acrB</i> containing plasmid encoding the corresponding protein, and monomer stability of AcrB constructs.....	82
Table 4.2 Trimer stabilities of AcrB constructs.....	92
Table 4.3 Oligomer association constant and energy reported in literature. ....	98

## LIST OF FIGURES

Figure 1.1 Diagrams of cell envelopes of the Gram-negative (A) and Gram-positive bacteria (B).....	5
Figure 1.2 Ribbon diagrams of the structures of the representative $\alpha$ -helical and $\beta$ -barrel membrane protein created using Pymol <sup>18</sup> .....	7
Figure 1.3 Schematic illustrations of the cooperation between the energy uptake and drug efflux for bacterial drug efflux pumps.....	10
Figure 1.4 Representative substrates of the AcrAB-TolC efflux system.....	13
Figure 1.5 Structure model of the AcrAB-TolC efflux system of Gram-negative <i>E. coli</i> .....	15
Figure 1.6 Structures of three proteins constituting the tripartite AcrAB-TolC efflux system (AcrA, AcrB and TolC) created using Pymol.....	17
Figure 1.7 Structure of a single AcrB subunit .....	19
Figure 1.8 Schematic representation of the AcrB alternating site functional rotation mechanism as described in the text.....	21
Figure 2.1 The diagram of the biogenesis of OMPs as described in the text .....	24
Figure 2.2 Crystal Structures of OmpA .....	26
Figure 2.3 Dynamic light scattering results of small unilamellar vesicle in the absence (triangles) and presence (5%, diamonds; 10%, circles; 20%, squares) of Ficoll 70...	33
Figure 2.4 OMP refolding and membrane insertion. ....	35
Figure 2.5 Scheme of refolding kinetics of OMPs <i>in vitro</i> .....	37
Figure 2.6 Far UV CD spectra of BSA (A), unfolded OmpA (B) and OmpT (C) in the absence (open) and the presence (filled) of Ficoll 70. ....	39

Figure 2.7 Fluorescence emission spectra of BSA (A), unfolded OmpA (B) and OmpT (C) in the absence (open) and the presence (filled) of Ficoll 70.....	41
Figure 2.8. Plots of trypsin (A) and chymotrypsin (B) digestion rate in the absence (open) and the presence (filled) of 20% Ficoll 70 versus the concentration of small molecule substrates fitted by Michaelis-Menton equation. ....	43
Figure 2.9 Trypsin and chymotrypsin digestion pattern of BSA (A), OmpA (B) and OmpT (C) in pure buffer solution (open) and in 20% Ficoll 70 (filled).....	45
Figure 2.10 OmpA171 refolding and membrane insertion. ....	47
Figure 3.1 Structure of AcrB .....	52
Figure 3.2 Chemical denaturation of AcrB monitored using the intrinsic fluorescence .....	58
Figure 3.3 AcrB trimer dissociation observed in BN-PAGE gel.....	60
Figure 3.4 SDS-induced unfolding of wild type AcrB and AcrB $_{\Delta}$ loop. ....	62
Figure 3.5 SDS-induced AcrB $_{W13F/W515F/W895F}$ unfolding.....	64
Figure 3.6 SDS-induced denaturation of AcrB monitored by CD.....	65
Figure 3.7 Refolding of AcrB. ....	67
Figure 3.8 Refolding of AcrB $_{\Delta}$ loop.....	69
Figure 4.1 Structure of AcrB. ....	74
Figure 4.2 Sequence alignment of residues in the loop (A) and TH8 (B), residues at the interface are shown as white fonts in black box).....	80
Figure 4.3 Western blot analysis of expression levels of all AcrB constructs.....	85
Figure 4.4 CD spectrum of each AcrB construct (grey) superimposed onto the spectrum of wild type AcrB (black). ....	87

Figure 4.5 Stability characterizations .....	89
Figure 4.6 BN-PAGE gel of purified AcrB constructs. ....	92
Figure 4.7 Correlation between AcrB trimer affinity and substrate efflux activity....	94
Figure 5.1 Structure of AqpZ (created from 2ABM.pdb .....	102
Figure 5.2 $\beta$ -Turns and their presence in AqpZ structure.....	107
Figure 5.3 Sequence alignment of AqpZ with its homologues with known structures. .....	108
Figure 5.4. Ribbon diagram of AqpZ monomer structure (1RC2.pdb.....	109
Figure 5.5 Thermal denaturation of AqpZ monitored using far UV CD spectroscopy. .....	110
Figure 5.6 Effect of urea on secondary structure and melting point of AqpZ. ....	111
Figure 5.7 Thermal stabilities of AqpZ and its mutants measured by CD spectroscopy. .....	113
Figure 5.8 Disulfide bond formation in AqpZ <sub>G91C</sub> .....	115
Figure 5.9 Thermal unfolding of AqpZ monitored using intrinsic fluorescence. ....	118



## LIST OF ABBREVIATIONS

- ABC: ATP-binding cassette
- ASA: Accessible surface area
- BAM:  $\beta$ -barrel assembly machinery
- BN-PAGE: Blue native polyacrylamide gel electrophoresis
- BSA: Bovine serum albumin
- BTEE: *N*-benzoyl-L-tyrosine ethyl ester
- CD: Circular dichroism
- CPM: *N*-[4-(7-diethylamino-4-methyl-3-coumarinyl) phenyl]-maleimide
- DDM: *n*-dodecyl- $\beta$ -maltoside
- DLS: Dynamic light scattering
- DTT: Dithiothreitol
- EDTA: Ethylenediaminetetraacetic acid
- EtBr: Ethidium bromide
- Ery: Erythromycin
- FP: Fluorescence polarization
- F-MAL: 5-maleimido-fluorescein
- IAM: Iodoacetamide
- IM: Inner membrane
- IPTG: Isopropyl- $\beta$ -D-1-thiogalactopyranoside
- LPS: Lipopolysaccharide
- MATE: Multidrug and toxic compound extrusion
- MDR: Multidrug resistance

MFP: Membrane fusion protein

MFS: Major facilitator superfamily

MIC: Minimum inhibitory concentration

Nov: Novobiocin

OM: Outer membrane

OMP: Outer membrane protein

PAGE: Polyacrylamide gel electrophoresis

PG: Peptidoglycan

PL: Phospholipid

PMSF: Phenylmethylsulfonyl fluoride

R6G: Rhodamine-6-G

RND: Resistance-nodulation-cell division

SDS: Sodium dodecyl sulfate

SMR: Small multidrug resistance

SUV: Small unilamellar vesicle

TAME: *N*<sub>α</sub>-p-toyl-L-arginine methyl ester hydrochloride

TCA: Trichloroacetic acid

TH: Transmembrane helix

TPP: Tetraphenylphosphonium

UV: Ultraviolet

## CHAPTER I. INTRODUCTION

### 1.1 What are antibiotics? How do antibiotics work?

Antibiotics, also known as antibacterials, are compounds interfering with the normal life process of bacteria or viruses, either killing them or stopping their reproduction. The Greek word “antibiosis” was first introduced by Jean Paul Vuillemin, a French bacteriologist, as a descriptive name of functions of these antimicrobial drugs in 1889.<sup>1</sup> The “anti” means “against,” while the “biosis” means “life.” Selman Waksman, an American microbiologist, later changed this term to “antibiotic” in 1942.<sup>2</sup> Most antibiotics are relatively small with the molecular mass less than 2000 atomic mass units, which is around 200 times the size of a water molecule. Antibiotics were originally discovered in organisms that display antibacterial actions. Nowadays, the majority of the antibiotics are semisynthetic, variants derived from natural products for specific clinical applications.<sup>3, 4</sup>

Based on their actions on microorganisms, antibiotics can be divided into two groups: bacteriostatic agents that inhibit bacterial growth, and bactericidal agents that kill bacteria. Bacteriostatic antibiotics slow down the growth of bacteria through disrupting DNA replication and repair (e.g. quinolones<sup>5</sup>), protein biosynthesis (e.g. macrolides<sup>6</sup>) or other cellular metabolism processes. Bactericidal antibiotics kill the bacteria usually by interrupting bacterial cell wall biosynthesis (e.g.  $\beta$ -lactam antibiotics<sup>7</sup>), altering the cell membrane permeability (e.g. polypeptide antibiotics<sup>8</sup>), or targeting essential bacterial enzymes (e.g. rifamycins<sup>9</sup>). The target bacterial type and compound dosage are also crucial to distinguish between bacteriostatic and bactericidal effects. The same

drug may be lethal to one type of bacteria, while only inhibitory to another. A high dose of a bacteriostatic drug may also lead to cell death.

## **1.2 Threat of antibiotic resistance**

Antibiotics are one of the most successful and powerful forms of chemotherapy in the history of medicine. One of the famous antibiotics was penicillin discovered (more accurately rediscovered) by the Scottish microbiologist Alexander Fleming in 1929. The discovery and the successful usage of penicillin in the treatment of bacterial infection ushered an era of antibiotics. Since then, numerous antibiotics have been discovered and became the primary treatments of infectious diseases in humans, animals, and plants. There is no doubt that the discovery and development of the antibiotic drugs have saved hundreds of millions of lives and also brought tremendous economic benefits to animal husbandry and agriculture. However, overuse of antibiotics soon began to cause problems. Only three years after the mass production of penicillin, one strain of staphylococcal bacterium was found to be no longer susceptible to penicillin. Today, especially in hospitals, there are bacterial strains resistant to nearly all known antibiotics. This phenomenon was later referred to as bacterial multidrug resistance (MDR). Antibiotics are no longer as effective at killing bacteria as when they were first discovered. People are dying from diseases that used to be readily treatable. According to the statistical results, antibiotic resistant bacteria lead to the death of at least 23,000 people each year.<sup>10</sup> Nowadays, the World Health Organization has identified antimicrobial resistance as one of the top three threats to human health.<sup>11</sup>

### **1.3 Mechanism of bacterial antibiotic resistance**

The targets of most antibiotics are inside the bacterial cells. Bacteria gain resistance to antimicrobials via five major mechanisms: a) active efflux of antibiotics through the efflux pumps located in the cell membrane, b) enzymatic degradation of antibacterial drugs, c) chemical alteration and inactivation of antimicrobials, d) reduction of the permeability of the cell membrane, and e) mutation of the drug target or expression of functionally redundant enzymes.<sup>12-14</sup> Bacteria originally acquire their resistance genes from genetic mutations that occur readily and spontaneously in bacterial cells. Resistance genes stored in the bacteria genome or carried by small plasmids are passed on to offspring through DNA replication and cell division. The latter can also be readily shared among bacteria via cell conjugation, transduction, or transformation. The combination of a rapid emergence and rapid sharing of the bacterial resistant genes leads to the appearance and expansion of MDR bacterial strains.

### **1.4 Gram-negative and Gram-positive bacteria**

While the majority of bacterial species are harmless or even beneficial to human, a small fraction are pathogenic. In general, bacteria can be divided into Gram-negative and Gram-positive bacteria on the basis of a staining procedure by Danish bacteriologist Hans Christian Gram in 1884.<sup>15</sup> After staining, the violet color is washed away by alcohol and leave cells with red/pink appearance under the microscope, since the Gram-negative bacteria do not retain the crystal violet dye, while the Gram-positive bacteria take up the dye and become purple/blue. This difference is ascribed to the presence of a much thicker peptidoglycan layer in the Gram-positive bacteria cell wall

(Figure 1.1). Peptidoglycan is a mesh-like structure located between the inner and outer membranes. It consists of alternating copolymers of *N*-acetylglucosamine and *N*-acetylmuramic acid. The copolymer chains are crosslinked by short (3-5) oligopeptides, the N-terminal amine groups of which form amide bonds with the carboxyl groups of *N*-acetylmuramic acid. The peptidoglycan layer strengthens the bacterial cell wall and helps counteract the osmotic pressure of the cell cytoplasm. The peptidoglycan layer is 20-80 nm thick in the Gram-positive bacteria but only 1.5-15 nm in the Gram-negative bacteria.<sup>16</sup> With such a thin layer of peptidoglycan, the Gram-negative bacteria do not retain the violet dye in their cell wall.

Another distinctive feature of the cell wall of Gram-negative bacteria is the presence of an outer membrane (Figure 1.1A). The outer membrane is located outside of the peptidoglycan layer and provides extra barrier protection for the Gram-negative bacteria. This feature results in the Gram-negative bacterium being intrinsically more resistant to antibiotics than the Gram-positive bacterium.

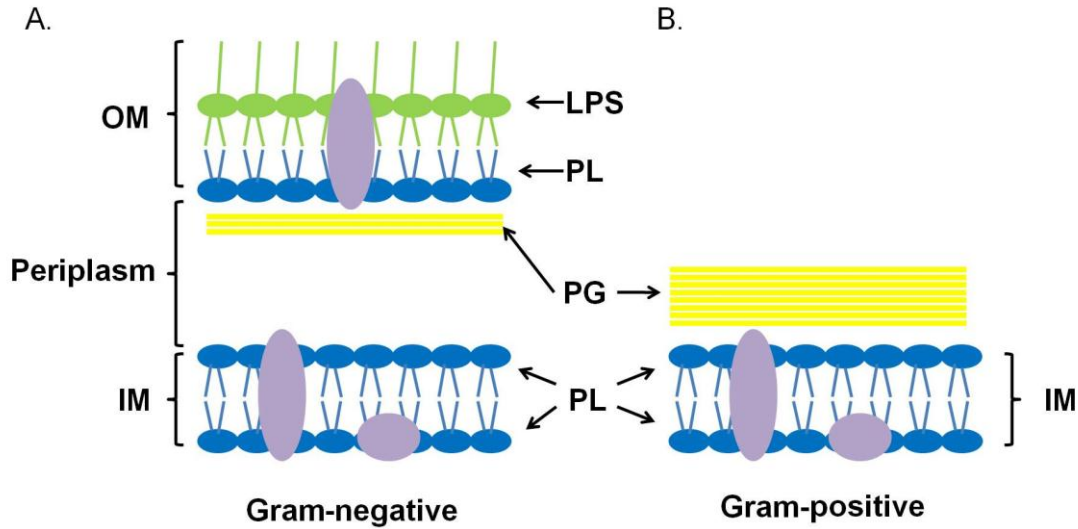


Figure 1.1 Diagrams of cell envelopes of the Gram-negative (A) and Gram-positive bacteria (B). The cell envelope of the Gram-negative bacteria comprises an inner membrane (IM) and a cell wall including the periplasm and the outer membrane (OM), while the Gram-positive bacteria contain an IM and a thick peptidoglycan-containing cell wall. The essential components of the cell wall and the IM are indicated: phospholipids (PL, blue), peptidoglycan layer (PG, yellow), membrane proteins (purple); lipopolysaccharides (LPS, green).

## 1.5 Mechanisms of drug resistance in Gram-negative bacteria

### 1.5.1 Role of outer membrane of Gram-negative bacteria in antimicrobial resistance

Compared with Gram-positive bacteria, Gram-negative bacteria are intrinsically more resistant to antimicrobials. A survey of reported antibiotics of the natural origin showed that more than 90% of the antibiotics that are active against the Gram-positive bacteria are not effective against *Escherichia coli*.<sup>17</sup> The lower sensitivity of the Gram-negative bacteria to antibiotic drugs is due to the extra protection from the outermost

semipermeable bacterial outer membrane (OM). The Gram-negative bacteria such as *E. coli* contain two lipid bilayer membranes: the inner membrane (IM) and the OM, separated by the periplasm (Figure 1.1A). These two membranes define the boundary between the intracellular components of the bacterial cell and the outside world to maintain an intrinsic homeostatic environment for cellular machinery. The composition of these two membranes is different: the IM is a phospholipid bilayer containing  $\alpha$ -helical transmembrane proteins (Figure 1.2A), and the OM is an asymmetrical bilayer (where the inner leaflet facing to periplasmic space has a similar composition to the IM, and the outer leaflet is composed of both phospholipids and lipopolysaccharides (LPS)). Unlike the inner membrane proteins, the outer membrane proteins (OMPs) adopt a  $\beta$ -barrel conformation and are thus termed  $\beta$ -barrel proteins (Figure 1.2B).



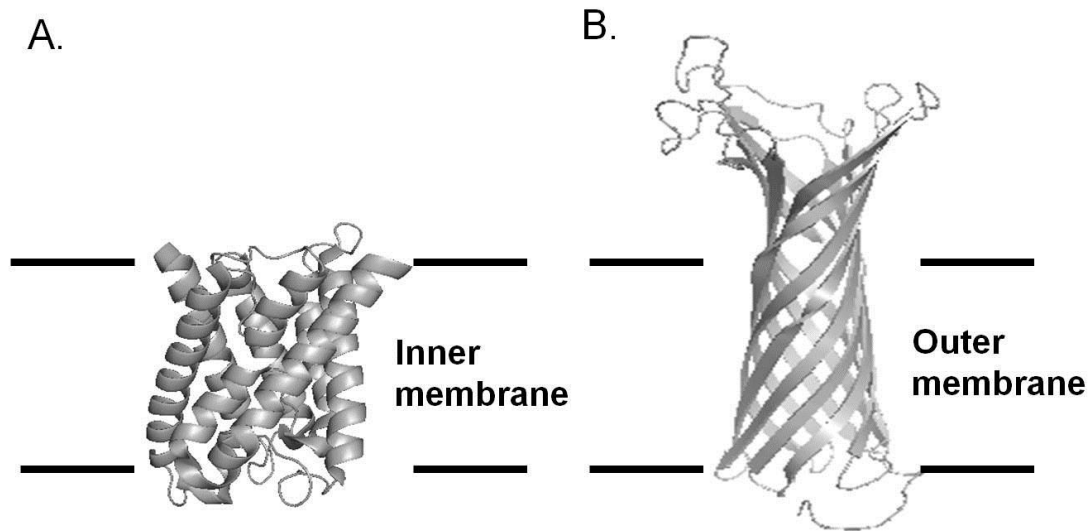


Figure 1.2 Ribbon diagrams of the structures of the representative  $\alpha$ -helical and  $\beta$ -barrel membrane protein created using Pymol<sup>18</sup>. A. AqpZ monomer (PDB: 2ABM<sup>19</sup>). B. OmpT (PDB: 1I78<sup>20</sup>)

The OM acts as a selective barrier and is composed of a highly hydrophobic lipid bilayer with pore-forming proteins with specific size-exclusion properties embedded. The targets of most antibiotics exist either in the periplasmic space or in the cytoplasm. Therefore, the permeability of the membrane barrier plays an important role on the susceptibility of the microorganism to antibiotics. Antibiotics cross the OM through two pathways. Small hydrophilic antibiotic drugs, such as  $\beta$ -lactams, use porin channels formed by OMPs (e.g. OmpC) to cross the OM. Macrolides and other large hydrophobic or amphiphilic drugs cross the OM barrier by passive diffusion into lipid bilayer.<sup>21</sup> Many existing bacteria strains develop their resistance through the modification of the phospholipid or LPS composition and the reduction of the porin permeability in the OM. For instance, polymyxin B, a positive charged antibiotic,

penetrates the barrier via binding to the negative charged LPS, the outer leaflet of OM.<sup>22</sup> Polymyxin-resistant *Salmonella typhimurium* mutant strains decrease the negative charges of LPS molecules by substitution of phosphate groups, located in the core oligosaccharide and the lipid A component, by 4-amino-4-deoxy-L arabinose. Such modification decreases the binding affinity of polymyxin to LPS molecules by approximately 75%.<sup>23, 24</sup> These mutants tolerate a concentration of polymyxin B up to 100 times higher than their parent strains. Certain drug tolerant mutants modify their OMP composition to gain antimicrobial resistance. Two porin-based resistance mechanisms have been observed in clinical isolates: a) alterations of the OM profile, including either severe reduction in expression or replacement of major drug-relevant porins, and b) mutations to alter the porin specificity or reduce its permeability.<sup>21</sup> In summary, the existence of multiple drug-tolerant bacterial species (due to modifications in the lipid or protein composition of the OM) highlights the importance of the OM as a major mechanism of antibiotic resistance.

#### *1.5.2 Role of active multidrug efflux transporters in antimicrobial resistance*

Active multidrug efflux mediated by membrane transporters is another major bacterial antibiotic-resistance mechanism noted in Section 1.3. The OM of the Gram-negative bacteria blocks the entrance of a large number of antibiotics. However, it is not the sole reason for the observed high level of resistance. Even with a diminished influx rate (due to the presence of the OM), the concentration of many antibiotics in periplasm could reach 50% of their external concentration in 10 to 30 s, due to the large surface-to-volume ratio of the bacterial cell.<sup>25</sup> Therefore, a second defense mechanism

involving the multidrug resistance pumps plays an important role in preventing drug access to intracellular targets. The multidrug transporters actively remove toxic substances and antibiotics from the interior of the bacterial cell. Many transporters have a broad range of substrates, and thus contribute to the resistance to multiple drugs. There are five superfamilies of the transporters that utilize various energy source.<sup>26</sup> These families include a) the major facilitator superfamily (MFS), b) the small multidrug resistance protein family (SMR), c) the multidrug and toxic compound extrusion transporters (MATE), d) the ATP-binding cassette superfamily (ABC), and e) the resistance-nodulation-cell division superfamily (RND). A schematic illustration of the coupling between the energy uptake and drug efflux of the bacterial drug efflux pumps is shown in Figure 1.3. SMR, RND and MFS families utilize a proton gradient to power transport activity, while the ABC and MATE pumps are driven by ATP hydrolysis and sodium counter transport towards the cytoplasm, respectively.

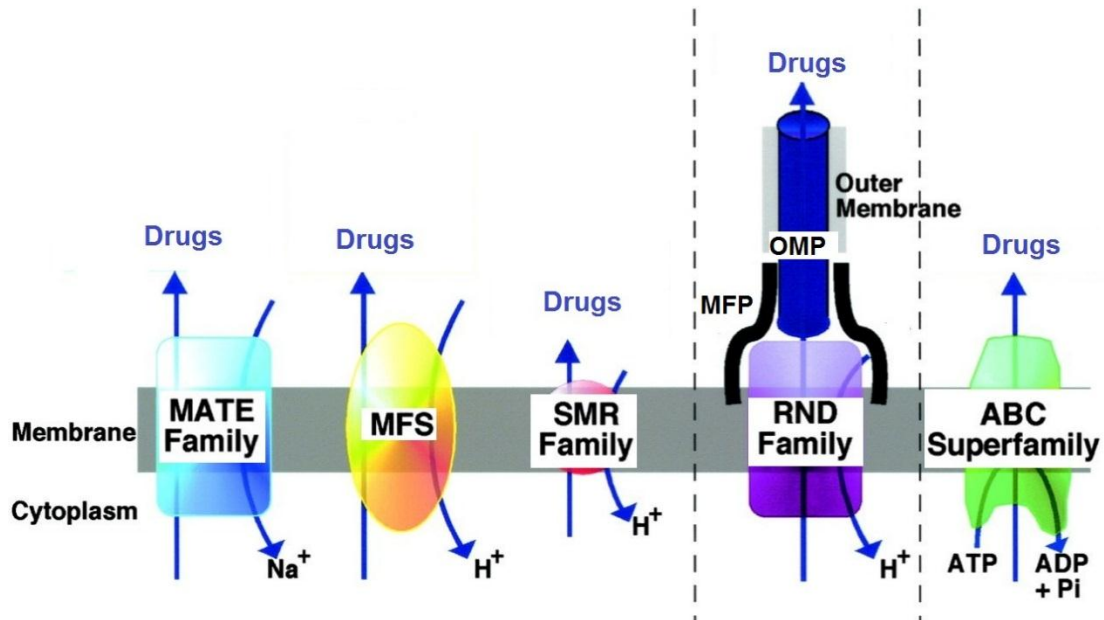


Figure 1.3 Schematic illustrations of the cooperation between the energy uptake and drug efflux for bacterial drug efflux pumps.<sup>27</sup> Five major drug efflux pumps are indicated: MFS, the major facilitator superfamily; SMR, the small multidrug resistance protein; MATE, the multidrug and toxic compound extrusion transporters; ABC, the ATP-binding cassette; and RND, the resistance-nodulation-cell division. The RND transporter functionally associates with a membrane fusion protein (MFP) and an OMP to form a drug efflux complex. Reprinted with permission from “Pidcock, L. J. V. Clinically relevant chromosomally encoded multidrug resistance efflux pumps in bacteria, *Clin. Microbiol. Rev.* 19, 382-402.” ©2006 American Society for Microbiology

Multidrug resistance pumps from several families of the transporters can be expressed simultaneously in the Gram-negative bacteria cells and act synergistically to expel toxic compounds. Multidrug efflux systems in the Gram-negative bacteria are reviewed by

Dr. Nikaido in one of his papers listed in Table 1.1.<sup>28</sup> Among the multidrug efflux transporters, the RND superfamily is the most clinically relevant antibiotic transport system.<sup>29, 30</sup> A systematic deletion of the multidrug resistant pumps in *Escherichia coli* revealed that only the AcrAB-TolC (RND member) knockout strain displayed an observable increase of sensitivity in 25 out of 35 tested antibiotics, whereas the removal of other transporters demonstrated no alternation or only a minor influence on the drug susceptibility.<sup>31</sup> Despite their prominent role in antimicrobial resistance, few RND transporters have been well characterized. So far, X-ray crystal structures of only four RND efflux pumps have been reported. These are AcrB<sup>32</sup> and CusA<sup>33</sup> from *E. coli*, MexB from *Pseudomonas aeruginosa*,<sup>34</sup> and ZneA from *Cupriavidus metallidurans* CH34.<sup>35</sup> Because of the available high-resolution structures, AcrB and MexB are the most extensively studied bacterial RND pumps.

Table 1.1 Multidrug efflux systems in Gram-negative bacteria.<sup>28, 36-42</sup>

Transporter	Linker	OM channel	Organism <sup>1</sup>	Examples of substrates <sup>2</sup>
SMR-type				
EmrE			<i>E. coli</i>	Lipophilic cations (TPP, EtBr)
MF-type				
EmrB	EmrA	TolC	<i>E. coli</i>	CCCP, nalidixic acid, thiolactomycin
RND-type				
AcrB	AcrA	TolC	<i>E. coli</i>	TC, CP, FQ, $\beta$ -lactams, Nov, Ery, FuA, Rif, EtBr, AF, CV, SDS, DOC
MexB	MexA	OprM	<i>P. aeruginosa</i>	TC, CP, FQ, $\beta$ -lactams (except carbapenems), Nov, EM, FuA, Rif
MexD	MexC	OprJ	<i>P. aeruginosa</i>	TC, CP, FQ
MexF	MexE	OprN	<i>P. aeruginosa</i>	CP, FQ, carbapenems
MtrD	MtrC	MtrE	<i>N. gonorrhoeae</i>	TC, CP, $\beta$ -lactams, Ery, FuA, AF, CV, TX, DOC

1. *E. coli*, *Escherichia coli*; *P. aeruginosa*, *Pseudomonas aeruginosa*; *N. gonorrhoeae*, *Neisseria gonorrhoeae*
2. TPP, tetraphenylphosphonium; EtBr, ethidium bromide; TC, tetracycline; CP, chloramphenicol; FQ, fluoroquinolones; Nov, novobiocin; Ery, erythromycin; FuA, fusidic acid; Rif, rifampin; AF, acriflavin; CV, crystal violet; SDS, sodium dodecyl sulfate; DOC, deoxycholate; TX, Tween X-100.

### 1.6 AcrAB-TolC drug efflux pump from *E. coli*

AcrAB-TolC is the main RND pump in *E. coli* that is responsible for extruding detergents, dyes, bile salts, multiple classes of antibiotics, and even organic solvents.<sup>43</sup>

Its substrates are structurally and chemically diverse, linear, cyclic, aliphatic or aromatic, charged or neutral, and drastically different in molecular weights.<sup>43</sup>

Structures of the representative substrates of AcrAB-TolC are shown in Figure 1.4. They include fluoroquinolones,  $\beta$ -lactams, tetracyclines, macrolides, and oxazolidinones.

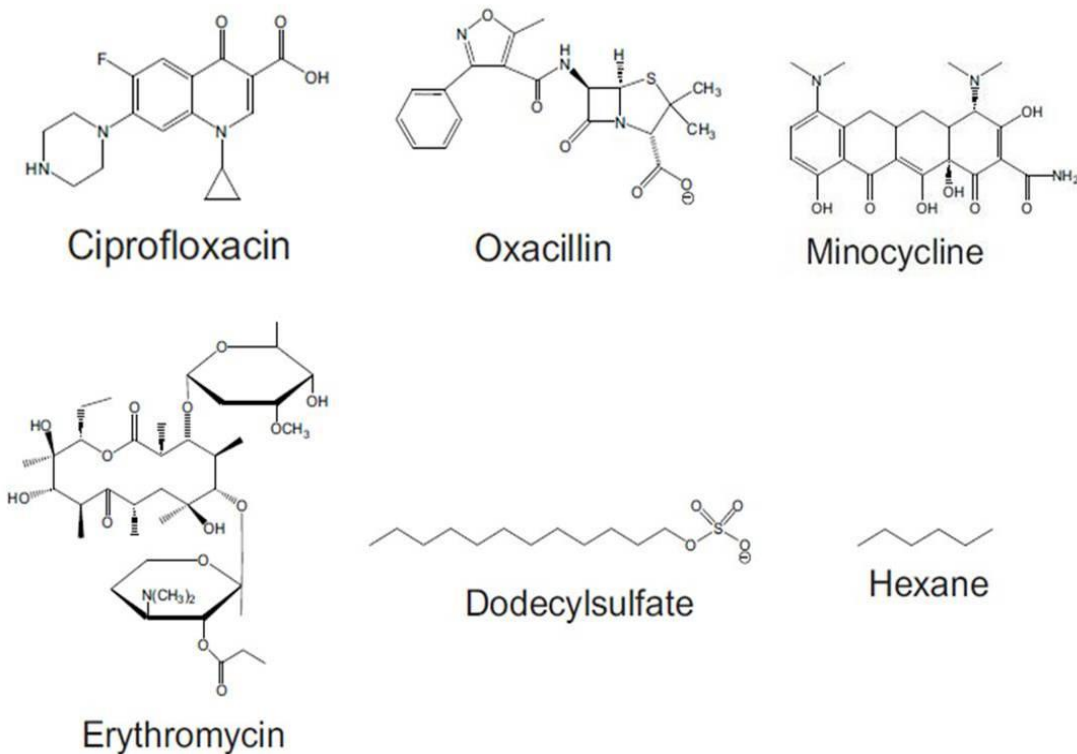


Figure 1.4 Representative substrates of the AcrAB-TolC efflux system. The system accepts a broad range of substrates, including fluoroquinolones (ciprofloxacin),  $\beta$ -lactam (e.g. oxacillin), tetracyclines (e.g. minocycline), macrolides (e.g. erythromycin), detergent (dodecylsulfate), and organic solvents (hexane).

Unlike the transporters from other families with only one IM element, all RND members are functionally associated with two other components: membrane fusion proteins in the periplasmic space and OMPs (Figure 1.3). Even though the crystal structure of the assembled three components has not been determined yet, a model has been established using the high-resolution crystal structures of three separated components, and tested by cross-linking studies.<sup>44, 45</sup> In the AcrAB-TolC efflux system, AcrA is the periplasmic linker that facilitates the interaction between the IM transporter AcrB and the OM channel TolC to form the entire export system (Figure 1.5).<sup>43</sup> The tripartite organization allows the pump to expel its substrates all the way out of cells bypassing accumulation in the periplasm.



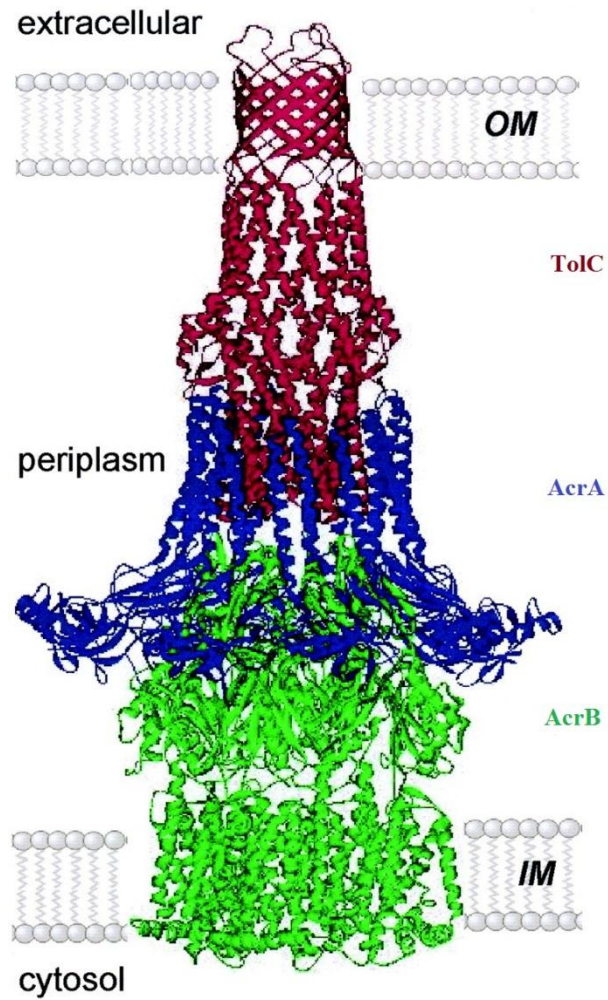


Figure 1.5 Structure model of the AcrAB-TolC efflux system of Gram-negative *E. coli*.<sup>27</sup> The system is composed of AcrB (IM component, in green color), TolC (OM component, red), and AcrA (periplasmic linker, blue). Reprinted with permission from “Piddock, L. J. V. Clinically relevant chromosomally encoded multidrug resistance efflux pumps in bacteria, *Clin. Microbiol. Rev.* 19, 382-402.” ©2006 American Society for Microbiology

Structures of three proteins constituting the tripartite AcrAB-TolC efflux system were shown separately in Figure 1.6. AcrA is a membrane fusion protein consisting of three

periplasmic domains ( $\alpha$ -helical hairpin, lipoyl domain, and  $\beta$ -barrel domain) and an N-terminal lipid anchor attached to the IM (Figure 1.6C).<sup>40</sup> The N-terminal lipid linker is not believed to be essential for drug efflux activity.<sup>46</sup> AcrA binds to TolC through its  $\alpha$ -helical hairpin, whereas the exact interface of the adaptor with AcrB remains unknown.<sup>45, 47</sup> The oligomeric state of AcrA also remains to be determined, which could be a trimer or a hexamer. TolC is the OM component of the system. TolC trimer forms a channel of 35Å diameter through its  $\beta$ -barrel domain in OM and extends its  $\alpha$ -helical domain into the periplasm to form a conduit that accepts the substrate extruded from AcrB (Figure 1.6A).<sup>48</sup> TolC is not exclusively used by AcrAB to transport substrates across the OM. It is also recruited by other RND efflux systems in *E. coli* (MdtEF and MdtAB for instance) as an exit duct.<sup>49</sup>

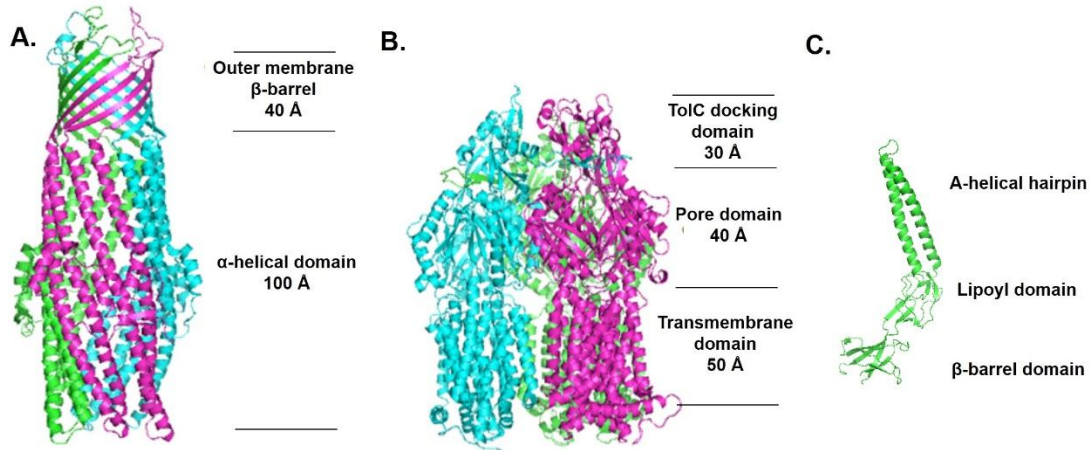


Figure 1.6 Structures of three proteins constituting the tripartite AcrAB-TolC efflux system (AcrA, AcrB and TolC) created using Pymol.<sup>18</sup> Dimensions and domains of each component are indicated. A. Structure of TolC trimer (created from 1TQQ.pdb<sup>50</sup>). B. Structure of AcrB trimer (created from 2GIF.pdb<sup>51</sup>). C. Structure of AcrA monomer (created from 2F1M.pdb<sup>52</sup>).

AcrB is the actual active pump of this efflux system that utilizes the inward flow of proton across the IM to drive substrate efflux. The crystal structure of AcrB has long been known.<sup>32, 53</sup> It is composed of three identical 1,049-residue subunits with the symmetry axis perpendicular to the membrane plane (Figure 1.6B). The structure of a single AcrB subunit is diagrammed in Figure 1.7. Each subunit contains 12 transmembrane helices (THs) and a periplasmic domain with a mixed secondary structures and is formed by two long loops between TH 1 and TH2 and between TH 7 and TH8. The AcrB trimer is divided into three domains: a transmembrane domain, a pore domain and a TolC docking domain. The proton translocation is related with residues Asp407, Asp 408, and Lys940 located in the transmembrane domain, while the substrate transportation and TolC interaction occur in the pore domain and the TolC

docking domain, respectively. Substrates of AcrB are captured in the periplasm and the outer leaflet of the IM, then transported through the binding pocket and finally to the AcrB funnel that connects AcrB to TolC.<sup>54</sup> Details of substrate transport in AcrB will be discussed in the following section.

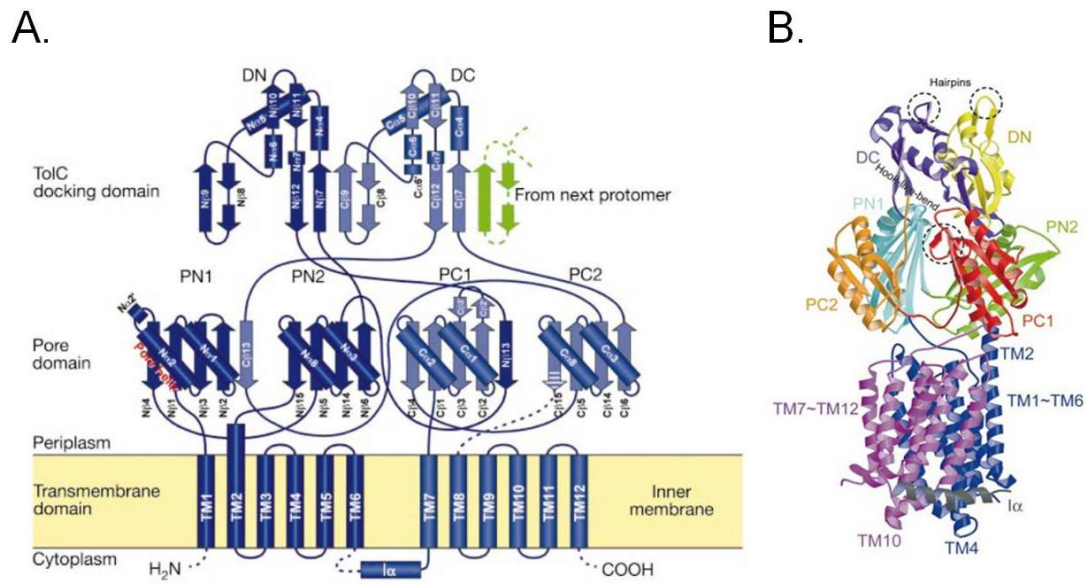


Figure 1.7 Structure of a single AcrB subunit.<sup>32</sup> A. Topology diagram of one AcrB subunit. The subunit is divided into N-terminal half (dark blue) and C-terminal half (light blue). Secondary structure elements are indicated: TM, transmembrane helices; N $\alpha$  and N $\beta$ , helices and strands, respectively in the N-terminal half; C $\alpha$  and C $\beta$ , helices and strands, respectively in the C-terminal half; I $\alpha$ , a helix attached to the cytoplasmic surface of the membrane. Dotted lines represent disordered polypeptide segments. The pore domain is divided into four subdomains: PN1, PN2, PC1 and PC2, while the TolC docking domain is divided into two parts: DN and DC. B. Crystal structure of one AcrB subunit (side view). Subdomains are depicted in different colors: DC (purple), DN (yellow), PN1 (cyan), PN2 (green), PC1 (red), PC2 (orange), N-terminal transmembrane segment (magenta), C-terminal transmembrane segment (blue), and I $\alpha$  (dark). Reprinted by permission from Macmillan Publishers Ltd: Nature (Murakami, S., Nakashima, R., Yamashita, E., and Yamaguchi, A. Crystal structure of bacterial multidrug efflux transporter AcrB, *419*, 587-593) ©2002

## 1.7 A conformational cycling model of AcrB for drug transport

AcrB is an obligate trimer that exists and functions exclusively in a trimeric state. The structure of AcrB was first solved as a homotrimer.<sup>32, 53</sup> However, later studies on the crystal structure of AcrB indicated that AcrB actually functions in an asymmetric trimer form and suggested a conformational cycling model for drug transport.<sup>51, 55</sup> According to the current model, within the asymmetric AcrB, each monomer adopts a different conformation with various substrate affinities: loose (L), tight (T), and open (O) states corresponding to the access, binding and extrusion of substrate activities. The stepwise AcrB-catalyzed drug transport is shown in Figure 1.8. The substrate enters the lower part of the periplasmic cleft (a large lateral indentation defined by the PC1 and PC2 subdomains<sup>54</sup>) and loosely binds to the monomer in the L conformation. The substrate is subsequently directed to a high-affinity deep binding pocket (consisting of multiple phenylalanine residues, such as Phe178, Phe610, Phe615 and Phe617). This step is associated with a conformational change of monomer from L to T. Finally, the substrate is extruded through the funnel towards TolC during the transition from T to O state. Subdomains PC1 and PC2 close the lateral access to prevent the backsliding of the drug.<sup>56</sup> After releasing the substrate, the monomer is reset to the L conformation and ready for drug uptake. The entire process is coupled with proton translocation, which drives the transition between different states.

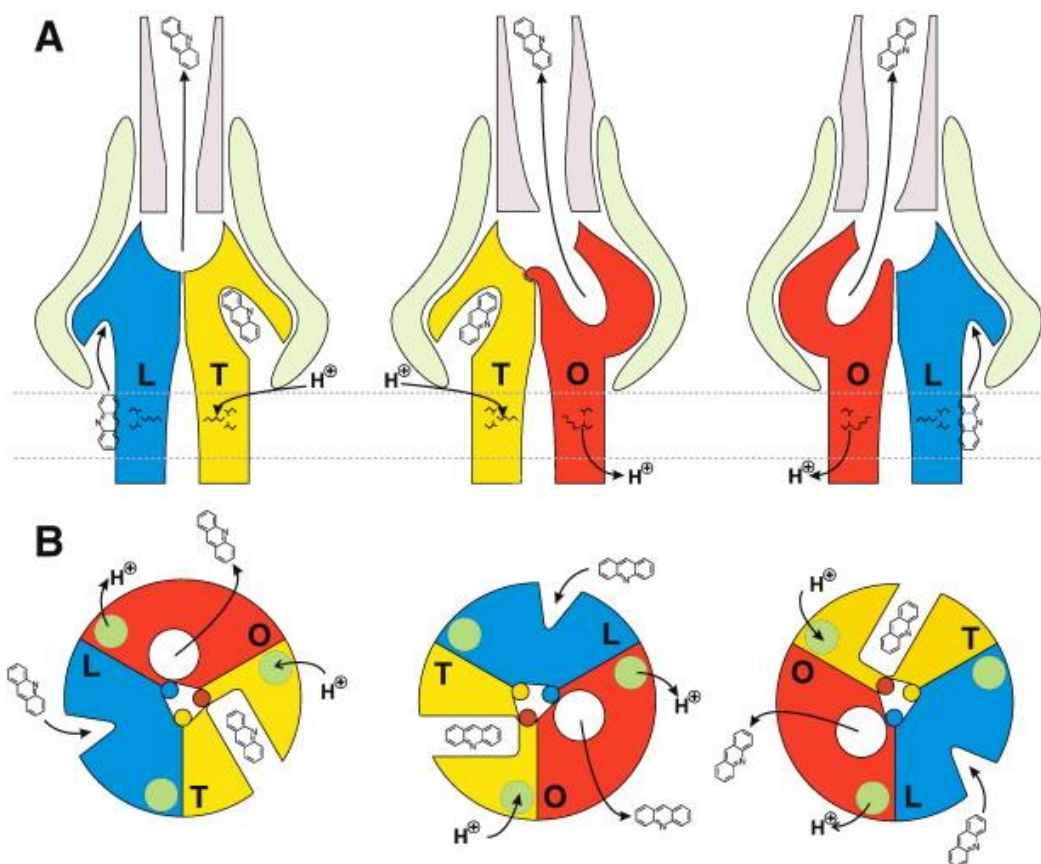


Figure 1.8 Schematic representation of the AcrB alternating site functional rotation mechanism as described in the text.<sup>57</sup> Three conformations of AcrB monomer are depicted in different colors: L (blue), T (yellow) and O (red). Substrate shown is acridine. A. Side view of AcrB and substrate binding. AcrA and TolC are indicated in light green and light purple colors, respectively. B. Wheel view of AcrB trimer during the operation. Reprint from *Biochimica et Biophysica Acta*, 1794, Pos, K. M. Drug transport mechanism of the AcrB efflux pump, 782-793 ©2009 with permission from Elsevier.

### 1.8 A brief summary of the thesis work

As discussed above, two major mechanisms, the protection of the OM and the active efflux of the multidrug transporters, confer potent multidrug resistance to the Gram-negative bacteria. My research focuses on the folding, assembly, and stability of the

membrane proteins involved in those two bacterial cellular defense mechanisms. In Chapter 2, the crowding effect on the refolding mechanism of two model OMPs, OmpA and OmpT, was examined. Our results indicated that the refolding of OmpA was slowed down by the crowding, while that of OmpT was hardly affected. Full length OmpA slowed down its refolding rate to ensure correct folding under the crowded condition, which is mediated by the periplasmic domain. In Chapter 3, the unfolding of the trimeric AcrB induced by SDS and urea was investigated using intrinsic fluorescence and circular dichroism spectroscopy. Our results suggested that unfolding of the trimeric AcrB started with a local structural rearrangement. While the refolding of secondary structure in individual monomers could be achieved, the re-association of the trimer might be the limiting factor to obtain folded wild type AcrB. In Chapter 4, I investigated the relationship between the stability and transporter activity of the AcrB trimer. A non-linear correlation between the two was determined, in which a threshold value was required to maintain the efflux activity of the transporter. To extend the work on the membrane protein stability, I studied another inner membrane protein Aquaporin Z (AqpZ). In Chapter 5, several molecular engineering approaches were tested to increase the thermal stability of AqpZ.



## CHAPTER II. EFFECT OF CROWDING BY FICOLLS ON OMPA AND OMPT REFOLDING AND MEMBRANE INSERTION

Part of this chapter are taken from “Effect of crowding by Ficolls on OmpA and OmpT refolding and membrane insertion”, 2013, *Protein Sci.* 22, 239-245

### 2.1 Introduction

Gram-negative bacteria such as *E. coli* contain two layers of membranes, separated by the periplasmic space. Proteins embedded in these two membranes are different. While the IM contains mainly  $\alpha$ -helical transmembrane proteins, the OMPs form  $\beta$ -barrels.<sup>58</sup> <sup>59</sup> OMPs serve various functions that are crucial to cell viability and activity, including structural support, catalysis, and are involved in both active transport and passive diffusion.<sup>60, 61</sup> The biogenesis of OMPs is a complicated process (Figure 2.1).<sup>62-64</sup> Briefly, all proteins are originally synthesized on ribosomes in the cytosol. OMP protein precursor containing an N-terminal signal peptide is first translocated across the IM through translocons (for instance, SecYEG translocation machinery). Once reaching the periplasm, the leader signal peptide of OMP is removed by signal peptidase. Molecular chaperones including Skp, DegP, and SurA stabilize OMPs in the periplasm and assist their folding and insertion into the OM through the  $\beta$ -barrel assembly machinery (BAM) to form the  $\beta$ -barrel structure.<sup>65-68</sup>

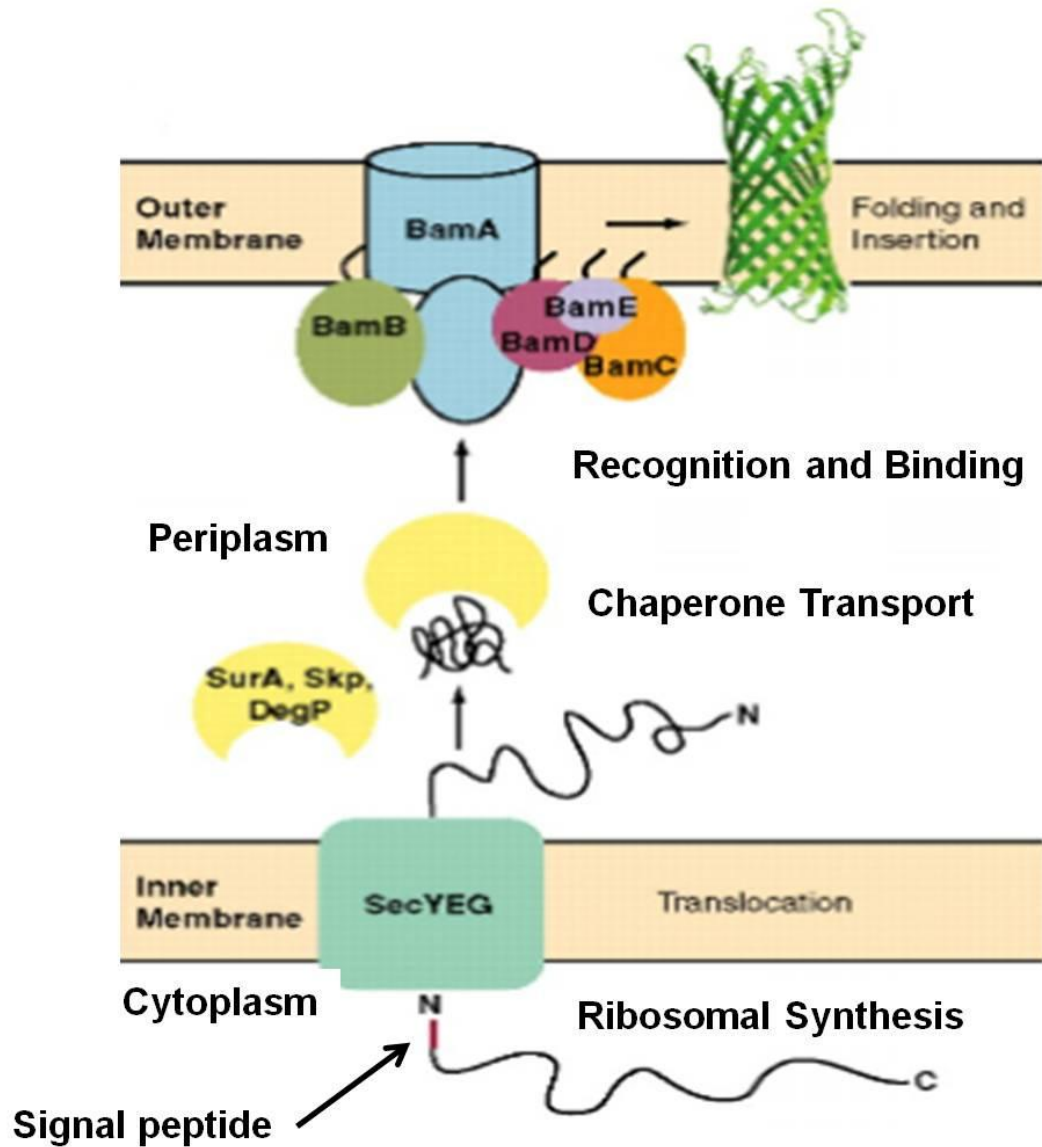


Figure 2.1 The diagram of the biogenesis of OMPs as described in the text.<sup>69</sup> From “Hagan, C. L., Kim, S., and Kahne, D. (2010) Reconstitution of Outer Membrane Protein Assembly from Purified Components, *Science* 328, 890-892.” Reprinted with permission from AAAS

Most current understanding of OMP folding has been obtained from *in vitro* studies conducted in dilute buffer solution.<sup>70-76</sup> However, the actual bioproduction of OMPs

occurs in a very crowded environment. The intracellular space is filled with a variety of macromolecules including proteins, polysaccharides, nucleic acids, and lipids.<sup>77, 78</sup> The periplasm has been described as a “gel-like” environment with macromolecules occupying ~30% of the overall space.<sup>79</sup> Under this crowded condition, proteins may behave differently than in dilute solution. This phenomenon is called the “macromolecular crowding” effect, first proposed by Minton and coworker in 1981.<sup>80</sup> It is later summarized by Minton as “the influence of volume exclusion upon the energetic and transport properties of macromolecules within a crowded or highly volume-occupied medium”.<sup>81</sup> The impact of macromolecular crowding on biological systems is attracting increased attention from the research community in recent years. Studies on soluble proteins have shown that the crowding condition affects the stability of proteins and alters their unfolding/refolding processes.<sup>82-87</sup> In this study we investigated the macromolecular crowding effect on the refolding and membrane insertion of OMPs, using OmpA and OmpT as model proteins (Figure 2.2<sup>88, 89</sup>) and Ficoll 70 as crowding agent to mimic the crowded condition in the periplasm. Ficoll 70 is a sucrose polymer that has been used as an inert co-solute in many studies investigating the crowding effect on protein properties.<sup>90-92</sup>

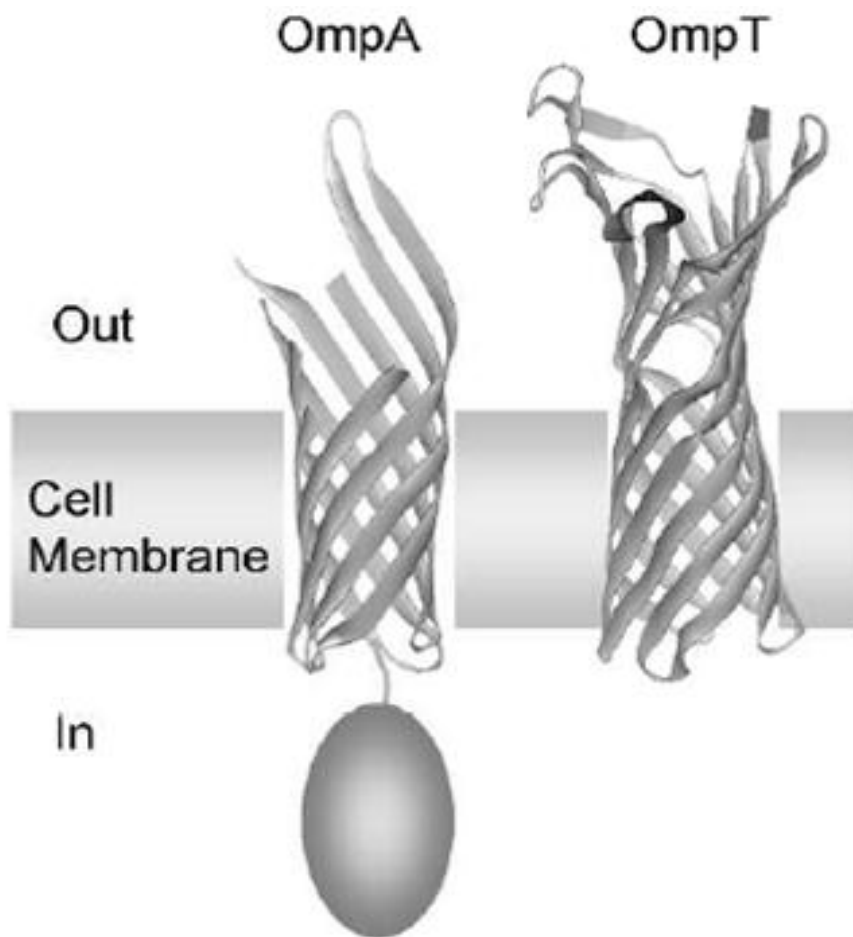


Figure 2.2 Crystal Structures of OmpA<sup>88</sup> (1QJP.pdb) and OmpT<sup>89</sup> (1I78.pdb) viewed from the side. The oval in OmpA represents its periplasmic domain, the structure of which remains unknown.

## 2.2 Materials and Methods

### 2.2.1 Protein cloning, expression, and purification

Genes encoding OmpA, OmpT, and the transmembrane domain of OmpA (OmpA171) without the signal peptide were amplified from the genomic DNA of *E. coli* K-12 and inserted into plasmid pET22b, which introduced a six-histidine tag at the C terminus of the protein. Primers used in the construction of expression plasmids are listed in

Table 2.1. Plasmid containing the OMP gene and the ampicillin resistance marker was then transformed into *E. coli* strain ER2566 for protein expression. Cells were cultured at 37 °C in Lysogeny Broth media (1% tryptone, 0.5% yeast extract, 1% NaCl) containing 100 µg mL<sup>-1</sup> ampicillin to an OD<sub>600nm</sub> of approximately 0.6. The expression of protein was induced by the addition of isopropyl-beta-D-thiogalactopy-ranoside (IPTG) to a final concentration of 1 mM. After three hours, cells were harvested by centrifugation at 7,000 g for 10 min at 4 °C. Cell pellets were stored at -20 °C for purification next day.

Table 2.1 Primers used in the construction of plasmids containing OmpA, OmpT and OmpA171. Restriction enzyme digestion sites are underlined.

---

OmpA

F: 5'-GCTCATATGGCTCCGAAAGATAACACCTGGTAC-3'

R: 5'-GCCTCGAGAGCCTGCGGCTGAGTTACAACGTC-3'

OmpT

F: 5'-GACCATATGTCTACCGAGACTTTATCGTTTACTC-3'

R: 5'-GACTCGAGAAATGTGTACTTAAGACCAGCAGTAG-3'

OmpA171

F: 5'-GACCATATGGCTCCGAAAGATAACACCTGGTAC-3'

R: 5'-AACTCGAGACC GAA ACG GTA GGA AAC ACC-3'

---

The purification procedures for OmpA and OmpT were the same. Briefly, cell pellets were resuspended in a lysis buffer (30 mM Tris base, 0.5 M NaCl, 1% Triton, 1 mM phenylmethylsulfonyl fluoride (PMSF), pH 8.0) and then sonicated on ice for 15 min with 10 sec on/off intervals to lyse cells. After centrifugation at 10,000 g for 30 min at 4 °C, the supernatant containing soluble proteins was discarded, while the pellet was dissolved in the sonication buffer (30 mM Tris base, 0.5 M NaCl, 6 M guanidine, pH 8.0) and sonicated again with the same setting. After sonication, the mixture was centrifuged at 25,000 g for 20 min at 4 °C. The supernatant containing dissolved OMPs was loaded on a Ni-nitrilotriacetic acid column, washed with a buffer containing a low concentration of imidazole (30 mM Tris base, 0.5 M NaCl, 8 M urea, 20 mM imidazole, pH 8.0) and eluted using an elution buffer (20 mM sodium acetate, 0.5 M NaCl, 8 M urea, pH 4.0). The pH of protein solution was adjusted to 8.0 after elution. OmpA171 was purified as described with slight modifications.<sup>73</sup> Briefly, cell pellets were resuspended in the lysis buffer, sonicated on ice, and then centrifuged to obtain the inclusion bodies as described for the purification of OmpA and OmpT. The inclusion bodies were washed twice with 20 mM sodium acetate, 0.5 M NaCl, 2 M urea, 1% Triton, pH 8.0 followed by centrifugation (2900 g, 30 min, 4 °C). Before refolding, OmpA171 pellet was dissolved in a buffer containing 8 M urea (2 mM Ethylenediaminetetraacetic acid (EDTA), and 10 mM borate, pH 10.0).

Purified protein was analyzed using sodium dodecyl sulfate-polyacrylamide gel electrophoresis (SDS-PAGE) and visualized by staining with Coomassie Blue.

Concentrations of all three proteins were determined using Pierce BCA Protein Assay Kit (Thermal Scientific INC., TX).

### *2.2.2 Preparation of small unilamellar vesicles*

Small unilamellar vesicles (SUVs) were prepared as described with slight modifications.<sup>73</sup> *E. coli* Lipid Total Extract (Avanti Polar Lipids, INC.) dissolved in chloroform was dried to form a thin film in a glass vial under a gentle stream of nitrogen. The lipid film was then placed under vacuum at room temperature overnight to remove residual solvent. Prior to the insertion studies, the dry lipid film was hydrated in a borate buffer (10 mM Na-borate, 2 mM EDTA, pH 10) at a lipid concentration of 3.2 mg mL<sup>-1</sup> at 4 °C overnight. An appropriate amount of Ficoll 70 (GE Healthcare, PA) were added to the borate buffer during hydration when indicated. The SUV suspension was prepared by sonicating hydrated lipid solution for 50 min using a Branson digital Sonic Dismembrator at 50% pulse cycle in an ice/water bath. The SUV solution was equilibrated overnight at 4 °C and used within 48 hours after preparation. The size of SUVs in solutions containing different amount of Ficoll 70 was determined using a Wyatt DynaPro Dynamic Light Scattering (DLS) System.

### *2.2.3 Folding and membrane insertion of OMPs*

OMP refolding experiments were performed following a published protocol.<sup>73</sup> Refolding was initiated by rapidly diluting a stock solution of OMP (in 8 M urea) into a buffer solution containing 3.2 mg mL<sup>-1</sup> SUV (1 M urea, 2 mM EDTA, 10 mM borate, pH 10.0, in the presence or absence of Ficoll 70) at 37 °C to a final concentration of 4

$\mu\text{M}$  OMP (25  $\mu\text{M}$  for OmpA171). After folding was initiated, at different time points small aliquots of the mixture were collected, quenched by adding SDS gel-loading buffer, and kept on ice. At the last time point, two aliquots were taken – one was treated similarly to the other samples, and the other boiled for 5 min and used as a control. Samples were then analyzed by SDS-PAGE on a 12% gel. After electrophoresis, gels were stained with Coomassie Blue. Gel images were analyzed using software ImageJ to obtain the percentage of refolding.<sup>93</sup>

#### *2.2.4 Residual structure of OMPs detected by far Ultraviolet (UV) Circular Dichroism (CD) spectroscopy and fluorescence spectroscopy*

The OMP stock solution dissolved in a buffer containing 8 M urea (30 mM Tris base, 0.5 M NaCl, pH 8) was quickly diluted using the same buffer without urea to a final urea concentration of 1 M and protein concentration of 0.375 mg/mL, and then scanned from 210 nm to 250 nm. The same sample was recovered for measurement of its fluorescence spectrum exciting at 280 nm and scanning the emission from 320 nm to 450 nm. The CD and fluorescence emission measurements were performed by Ms. Qian Chai.

#### *2.2.5 Residual structure of OMPs detected by limited protease digestion experiment*

Effect of crowding on protease activity. Standard protease digestion assay was used to determine the protease activity of trypsin and chymotrypsin<sup>94</sup>. Specifically, a buffer solution containing synthetic small molecule substrate of different concentrations was incubated in UV/vis spectrophotometer at room temperature for three to four minutes



until its absorbance stabilized. Protease was then added into the solution to a final concentration of 3 µg/mL and the solution was mixed thoroughly. The increase of absorbance was recorded at the indicated wavelength over time. Trypsin activity was monitored using *N*<sub>α</sub>-p-toyl-L-arginine methyl ester hydrochloride (TAME) as the substrate at 247 nm in a buffer containing 0.0046 M Tris HCl, 0.0115 M calcium chloride, pH 8.1. The reaction rate was calculated using the following equation:

$$Rate(AU / mg) = \frac{\Delta A_{247} / \text{min} \times V(mL)}{540 \times M(mg)}$$

in which  $\Delta A_{247}$  is the absorbance change at 247 nm,  $V$  is the total reaction volume in milliliter,  $M$  is the amount of trypsin in the reaction mixture in milligram, and 540 is the extinction coefficient of TAME at 247 nm. Chymotrypsin activity was monitored using *N*-benzoyl-L-tyrosine ethyl ester (BTEE) as the substrate at 256 nm in a buffer containing 0.08 M Tris HCl, 0.1 M calcium chloride, pH 7.8. The reaction rate was calculated using a similar equation:

$$Rate(AU / mg) = \frac{\Delta A_{256} / \text{min} \times V(mL)}{964 \times M(mg)}$$

in which  $\Delta A_{256}$  is the absorbance change at 256 nm,  $V$  is the total reaction volume in milliliters,  $M$  is the amount of chymotrypsin in the reaction mixture in milligrams, and 964 is the extinction coefficient of BTEE at 256 nm.

Limited protease digestion of protein substrate. Digestion was initiated by mixing protein substrate with protease in the digestion buffer at the room temperature. The mass ratio of substrate to protease was adjusted for different proteins to get a clear digestion pattern on SDS-PAGE gel. For trypsin digestion, the substrate to protease

mass ratio for all proteins was 100. For chymotrypsin digestion, the mass ratio for Bovine Serum Albumin (BSA) (Bioworld, OH), OmpA, and OmpT was 33, 200 and 100, respectively. The concentration of all substrate proteins was constant at 0.3 mg/mL. BSA was used as a control protein substrate to examine the effect of crowding on the activity of the proteases. After the reaction started, small aliquots of reaction mixture were removed and quenched by the addition of PMSF and SDS-gel loading buffer. Samples were boiled in a water bath for 5 min before analyzing by 12% SDS-PAGE. After electrophoresis, gels were stained with Coomassie Blue. Images of gels were analyzed by ImageJ software.

## **2.3 Results**

### *2.3.1 Effect of the crowding condition on the rate of membrane insertion of OmpA and OmpT*

To investigate the crowding effect on the folding and membrane insertion of OMPs, we monitored refolding and membrane insertion of OmpA and OmpT in SUV solution in the absence or presence of Ficoll 70. Three different Ficoll 70 concentrations, 5%, 10%, and 20%, were used in this experiment. At concentrations above 20% the high viscosity of the solution drastically decreased the efficiency of sonication and thus the formation of liposomes. To examine the effect of crowding on liposome formation, sizes of SUV vesicles prepared in the absence or presence of Ficoll 70 were measured using DLS. Sizes of SUVs were in the range of 10 to 100 nm, and Ficoll 70 at concentrations up to 20% had little effect on the size distribution of the SUVs (Figure 2.3).

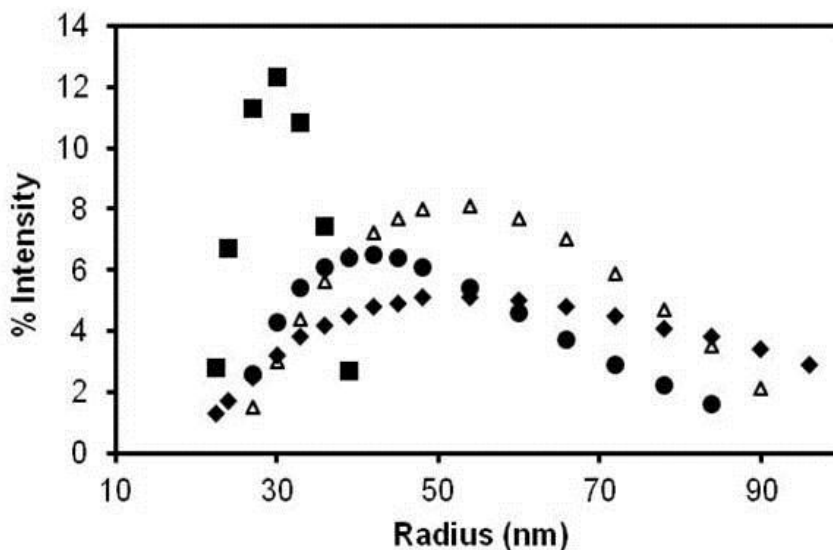


Figure 2.3 Dynamic light scattering results of small unilamellar vesicle in the absence (triangles) and presence (5%, diamonds; 10%, circles; 20%, squares) of Ficoll 70.

Folding and membrane insertion of OMPs were followed by SDS-PAGE. Previous studies have shown that the folded and unfolded OMPs usually migrate differently on SDS polyacrylamide gel.<sup>73</sup> As shown in Figure 2.4A, after Coomassie blue stain, two bands were clearly visible on the gel. The bands with lower and higher apparent molecular weight were the folded and unfolded species, respectively. Intensities of bands were quantified using software ImageJ, and converted into fraction of folded protein through the following equation:

$$Folding \% = \frac{I_F}{I_T} \times 100\%$$

in which  $I_F$  and  $I_T$  are the intensities of the bands corresponding to the folded OMP at different time and the total OMP, respectively. Several studies have shown that the folding kinetics of OMPs can be fitted using a single exponential equation.<sup>71, 73, 95</sup>

Similarly, we fitted the folding data over time using a single exponential equation (Figure 2.4B):

$$y = y_0 + Ae^{-kt}$$

where  $y$  is the folded fraction at certain time point,  $t$  is the time, and  $y_0$  is the fraction folded as time approaches infinity. The rate constant  $k$  could be obtained through fitting. The rate constants of refolding obtained in the presence or absence of Ficoll 70 were shown in Table 2.2. We found that at low Ficoll 70 concentration (5%), little effect could be observed on the refolding rate of OmpA. The rate constant decreased significantly in 10% and 20% Ficoll 70. However, Ficoll 70 at a concentration as high as 20% had little effect on the refolding rate of OmpT, while the overall folding efficiency decreased with the increase of Ficoll 70 concentration (Figure 2.4B).

Table 2.2 Refolding rate constants ( $\text{min}^{-1}$ )

OMP	No Ficoll 70	5% Ficoll 70	10% Ficoll 70	20% Ficoll 70
OmpA	0.016±0.004	0.019±0.005	0.0049±0.0001	0.0020±0.0002
OmpT	0.20±0.04	0.14±0.03	0.24±0.03	0.18±0.02
OmpA 171	0.014±0.002	/	/	0.028±0.002

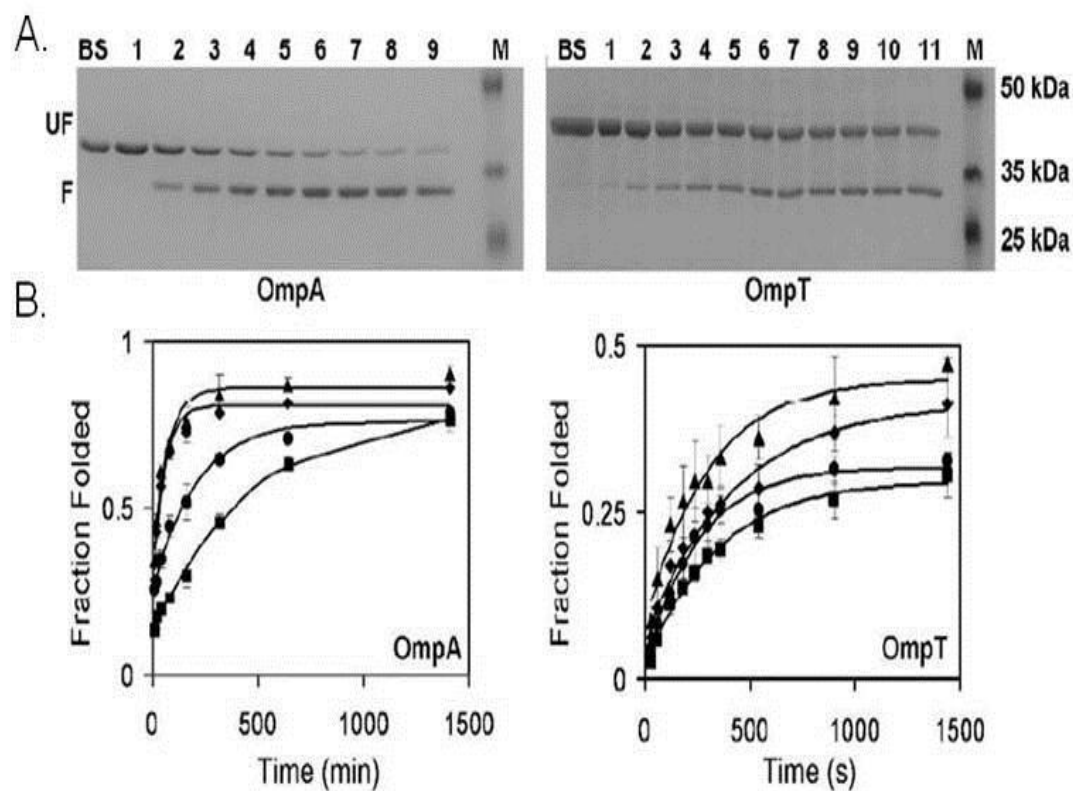


Figure 2.4 OMP refolding and membrane insertion. A. Representative SDS-PAGE images of OmpA and OmpT refolding. BS: boiled sample. M: protein molecular weight marker. For OmpA, lanes 1 to 9 correspond to 0, 10, 20, 40, 80, 160, 320, 640, and 1410 min of incubation. For OmpT, lanes 1 to 11 correspond to 0, 30, 60, 120, 180, 240, 300, 360, 540, 900, and 1440 s of incubation. B. Kinetics of OmpA and OmpT refolding, in buffer (triangles), 5% Ficoll 70 (diamonds), 10% Ficoll 70 (circles), and 20% Ficoll 70 (squares). Data were averages of three independent experiments and fitted to a single exponential equation.

### 2.3.2 *The refolding and membrane insertion mechanism of OMPs*

Kleinschmidt and coworkers proposed a model describing the folding and membrane insertion mechanism of a  $\beta$ -barrel membrane protein in several steps (Figure 2.5).<sup>96, 97</sup> Refolding occurs spontaneously when the unfolded OMPs dissolved in 8 M urea are diluted into the refolding buffer in the presence of the model phospholipid membrane. The first step involves a rapid hydrophobic collapse in which a completely denatured, unstructured polypeptide folds into a conformation with a detectable residual structure (water-soluble intermediate). This step is too fast to detect on the time scale of seconds. The next step is much slower and occurs in the minute time scale, which can be easily monitored by fluorescence spectrometry. In this step, the water-soluble intermediate interacts and adsorbs to the surface of the lipid bilayer, accompanied by the structure rearrangement on the surface of the lipid bilayer. The last step is the formation of the secondary and tertiary structures of OMP. It is an even slower step, usually finishes in minutes to hours. The refolded OMPs are fully functional with native-like structures, as revealed by FT-IR spectroscopy,<sup>98</sup> CD spectroscopy,<sup>99</sup> and single channel conductivity measurements.<sup>100</sup>

To understand the mechanism underlying the different crowding effect on the refolding and membrane insertion of OmpA and OmpT, we examined the crowding effects on the structures of water-soluble intermediate of OMPs using CD spectroscopy, intrinsic fluorescence, and protease digestion.

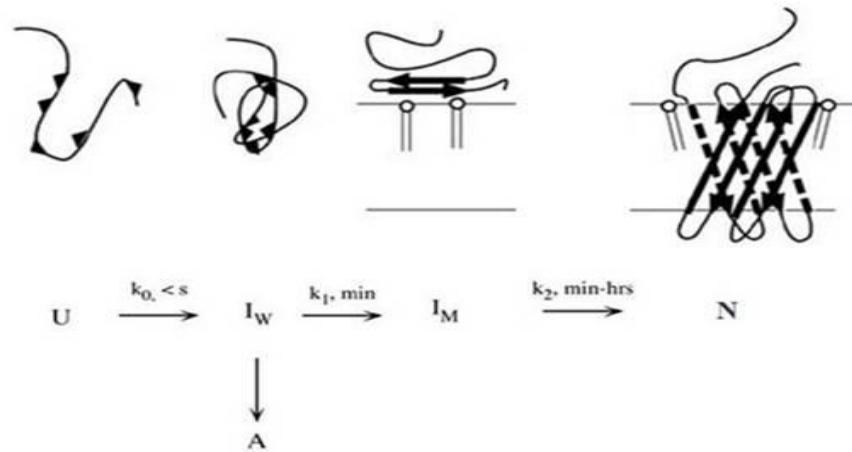


Figure 2.5 Scheme of refolding kinetics of OMPs *in vitro*.<sup>97</sup> U represents unfolded protein; A, aggregation state; I<sub>w</sub>, water-soluble state; I<sub>M</sub>, intermediate state; N, native structure of protein. K represents the rate constant of each step. Reprinted with permission from “Kleinschmidt, J. H., and Tamm, L. K. Folding Intermediates of a  $\beta$ -Barrel Membrane Protein. Kinetic Evidence for a Multi-Step Membrane Insertion Mechanism, *Biochemistry* 35, 12993-13000.” ©1996 American Chemical Society

### 2.3.3 Crowding had similar effect on the secondary structures of OmpA and OmpT as revealed by far UV CD spectroscopy

The far UV CD spectrum is routinely used to assess the secondary structure content of the proteins. The spectrum of the  $\alpha$ -helix displays two negative peaks at around 208 nm and 222 nm, the  $\beta$ -sheet shows one negative peak at around 218 nm, and the random coil has a single negative peak at approximately 198 nm. We collected CD spectra of OmpA and OmpT in the presence and absence of Ficoll 70. BSA was utilized as a control for the non-specific interference. Since Ficoll 70 is a well-established inert co-solute used in studies of many proteins, it should not affect the structure of a well-folded stable protein such as BSA. As shown in Figure 2.6A, the spectrum of BSA

collected in the presence or absence of Ficoll 70 overlaid well with each other, indicating that Ficoll 70, even at a concentration as high as 20%, had little non-specific effect on the far UV CD spectrum. Therefore, any changes of the spectra of OMPs collected in the presence of Ficoll 70 would be a result of the structural changes of the proteins due to the Ficoll. As the CD spectra revealed (Figure 2.6B and C), the presence of the crowding agent caused a decreased in the peak intensities and a red shift of the peak positions for both OMPs. An effort to deconvolute the spectra quantitatively into specific secondary structure compositions was not successful. This is not surprising since the reference data sets used to develop the deconvolute software are mostly the spectra of folded water soluble proteins rather than membrane proteins. However, a similar change in the spectra of OmpA and OmpT suggested a similar effect of Ficoll 70 on the protein secondary structure.



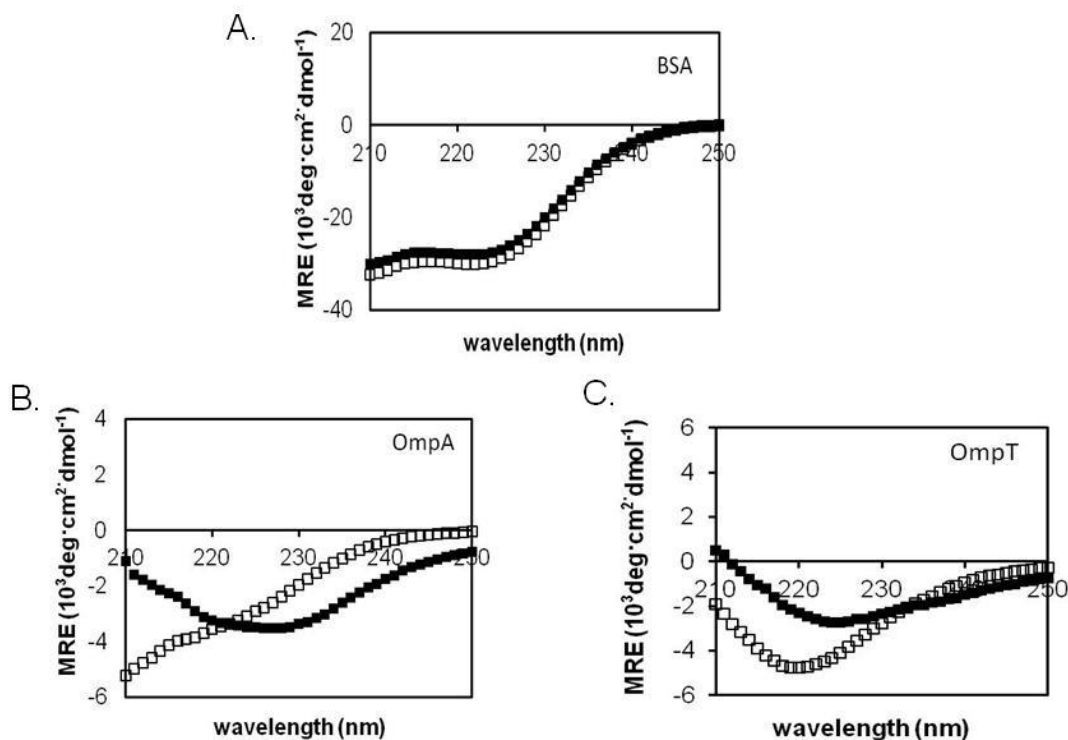


Figure 2.6 Far UV CD spectra of BSA (A), unfolded OmpA (B) and OmpT (C) in the absence (open) and the presence (filled) of Ficoll 70.

### 2.3.4 Crowding had little influence on tertiary structure of OMPs monitored using intrinsic fluorescence

The fluorescence spectra of OmpA and OmpT were collected in the presence and absence of Ficoll 70. A structural change would cause a change of the microenvironment of the aromatic residuals in a protein, including tryptophan, tyrosine and phenylalanine, which would in turn affect their fluorescence emission. Specifically, a blue shift of the peak position and an increase of the emission intensity usually indicate that the aromatic residues have moved into a more hydrophobic environment while a red shift of the peak position and a decrease of its intensity indicate that the residues have moved into a more hydrophilic environment. First we used BSA as a

control sample to determine if the presence of 30% Ficoll 70 had any effect on the fluorescence emission of the protein. We found the Ficoll 70 decreased the intensity of fluorescence emission by about 70%, indicating that it affected the fluorescence signal non-specifically. Since the fluorescence intensity was very sensitive to the solution environment, the presence of Ficoll 70 quenched the fluorescence emission of BSA. However, non-specific interference should not change the wavelength of the emission, while it could have a significant influence on its intensity. As shown in Figure 2.7A, after normalizing each spectrum to its own maximum intensity, the normalized spectra of BSA obtained in the absence or presence of Ficoll 70 overlapped well. Next, we collected fluorescence emission spectra of two OMPs, normalized the spectra, and examined whether the presence of Ficoll 70 affected the emission wavelength. We found that the OmpA (Figure 2.7B) spectrum did not have a shift, while OmpT spectrum (Figure 2.7C) had a slight red shift, indicating either there was no structural change, or the change did not generate net effect on the fluorescence signal of both OMPs.

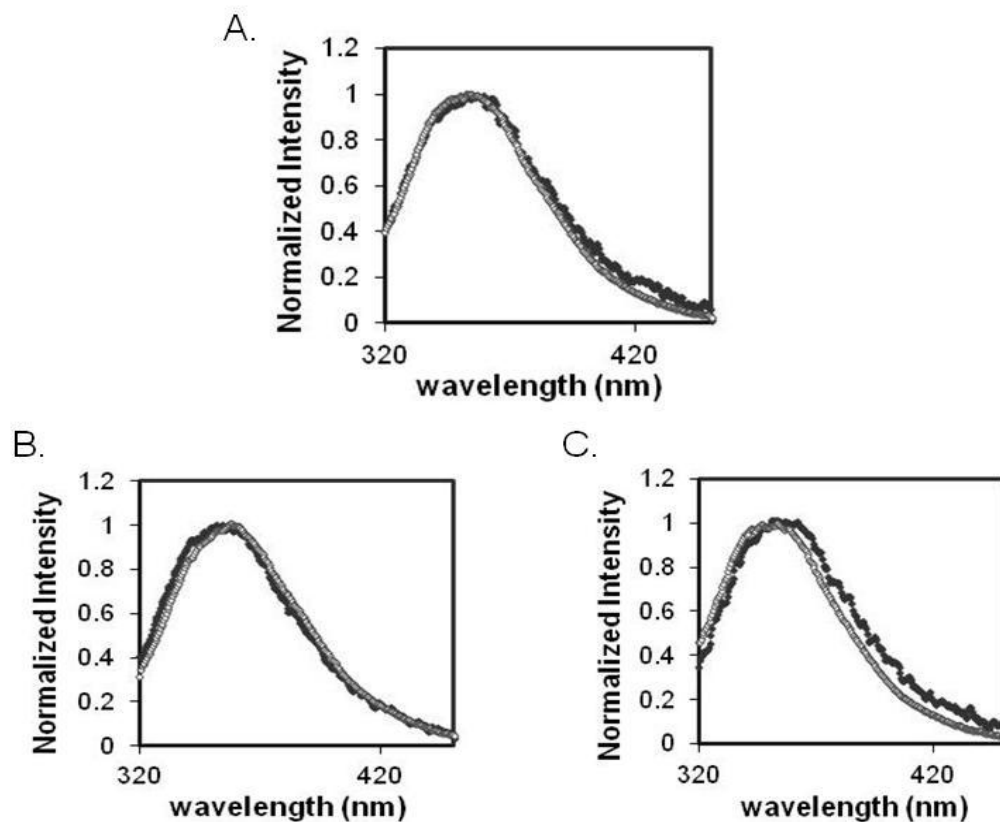


Figure 2.7 Fluorescence emission spectra of BSA (A), unfolded OmpA (B) and OmpT (C) in the absence (open) and the presence (filled) of Ficoll 70.

*2.3.5 Unfolded OmpA assumed a more compact structure under the crowded condition as revealed by limited protease digestion experiment*

Limited protease digestion is another technique that has been used to investigate protein structures, especially in the unfolded state. Trypsin and chymotrypsin recognize specific sequences. When such recognition sites are exposed at the surface of a protein or in a flexible region of the protein, they are more accessible to digestion. Therefore, by monitoring the rate and efficiency of digestion, we can obtain information about protein structure and structural changes.

We chose two proteases, trypsin and chymotrypsin, in this experiment. Trypsin recognizes lysine and arginine, while chymotrypsin digests peptide bonds after aromatic and large aliphatic amino acids. Before we could use these enzymes to characterize the structures of OMPs, we first needed to determine if the activities of the enzymes themselves were affected by the presence of Ficoll 70. To determine the intrinsic activity of the enzymes in the presence and absence of the crowding agent, we used small synthetic substrates as described in the Materials and Methods section. Experimental data was fitted using Michaelis-Menton kinetics equation:

$$v = \frac{V_{\max} \cdot [s]}{K_m + [s]}$$

where  $v$  represents the reaction rate at a certain concentration of the substrate  $[s]$ .  $V_{\max}$  represents the maximum rate achieved by the system when saturated with substrate. The Michaelis constant,  $K_m$ , is the substrate concentration at which the reaction rate is half of the maximum rate.

The reaction rates for each protease for its specific small substrate were recorded at different substrate concentration and fitted using the Michaelis-Menton equation (Figure 2.8). The fitting results (Table 2.3) showed that the presence of 20% Ficoll 70 had a very small effect on the  $K_m$  and  $V_{\max}$  of the proteases, when we considered the large errors. We found that the enzymatic activities of both proteases toward small substrates were not significantly influenced by the crowding condition, which is consistent with an earlier study that reported that the activity of trypsin was not affected by the presence of the crowding condition <sup>101</sup>.

Table 2.3 Parameters of trypsin and chymotrypsin activities measured with small substrates in the absence and presence of 20% Ficoll 70.

	Trypsin		Chymotrypsin	
	$V_{\max}$ (AU/mg)	$K_m$ (mM)	$V_{\max}$ (AU/mg)	$K_m$ (mM)
No Ficoll 70	87.7±10.9	0.02±0.004	1.5±0.03	0.5±0.15
20% Ficoll 70	104.8±7.9	0.03±0.008	2.1±0.12	0.4±0.07

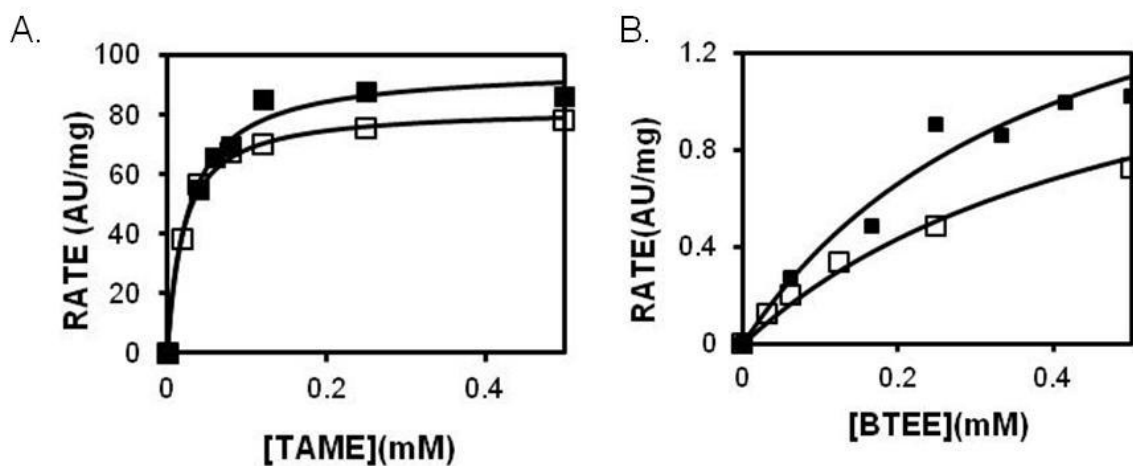


Figure 2.8. Plots of trypsin (A) and chymotrypsin (B) digestion rate in the absence (open) and the presence (filled) of 20% Ficoll 70 versus the concentration of small molecule substrates fitted by Michaelis-Menton equation.

Next, we used BSA as a control for Ficoll 70 effect on the activity of the protease when the substrate is a large globular protein (Figure 2.9A). We found that digestion reaction of trypsin and chymotrypsin was faster in 20% Ficoll solution than in the absence of Ficoll. The increased reaction activity could be a result of the increased binding strength between the protease and BSA, due to the exclusive volume effect during crowding. The presence of 20% Ficoll had a similar effect on the trypsin digestion of OMPs as with BSA (Figure 2.9 left). However, when chymotrypsin was used in the digestion, OmpA was more resistant to digestion, while OmpT was similar to BSA (Figure 2.9 right). The different results between the trypsin and chymotrypsin digestion could be explained by the difference in digestion specificity of the two enzymes. Chymotrypsin preferentially cleaves amide bonds on the carboxyl side, which is an aromatic and large aliphatic residual. Therefore, OmpA underwent a structural change under the crowding condition, in which hydrophobic residues formed a more compact and well protected core. On the other hand, trypsin digests the amide bond after Lys and Arg, which are likely located at solvent exposed surfaces, even in a well-folded protein. Thus, although Ficoll 70 induced OmpA to fold into more a compact structure, the Lys and Arg were still exposed.

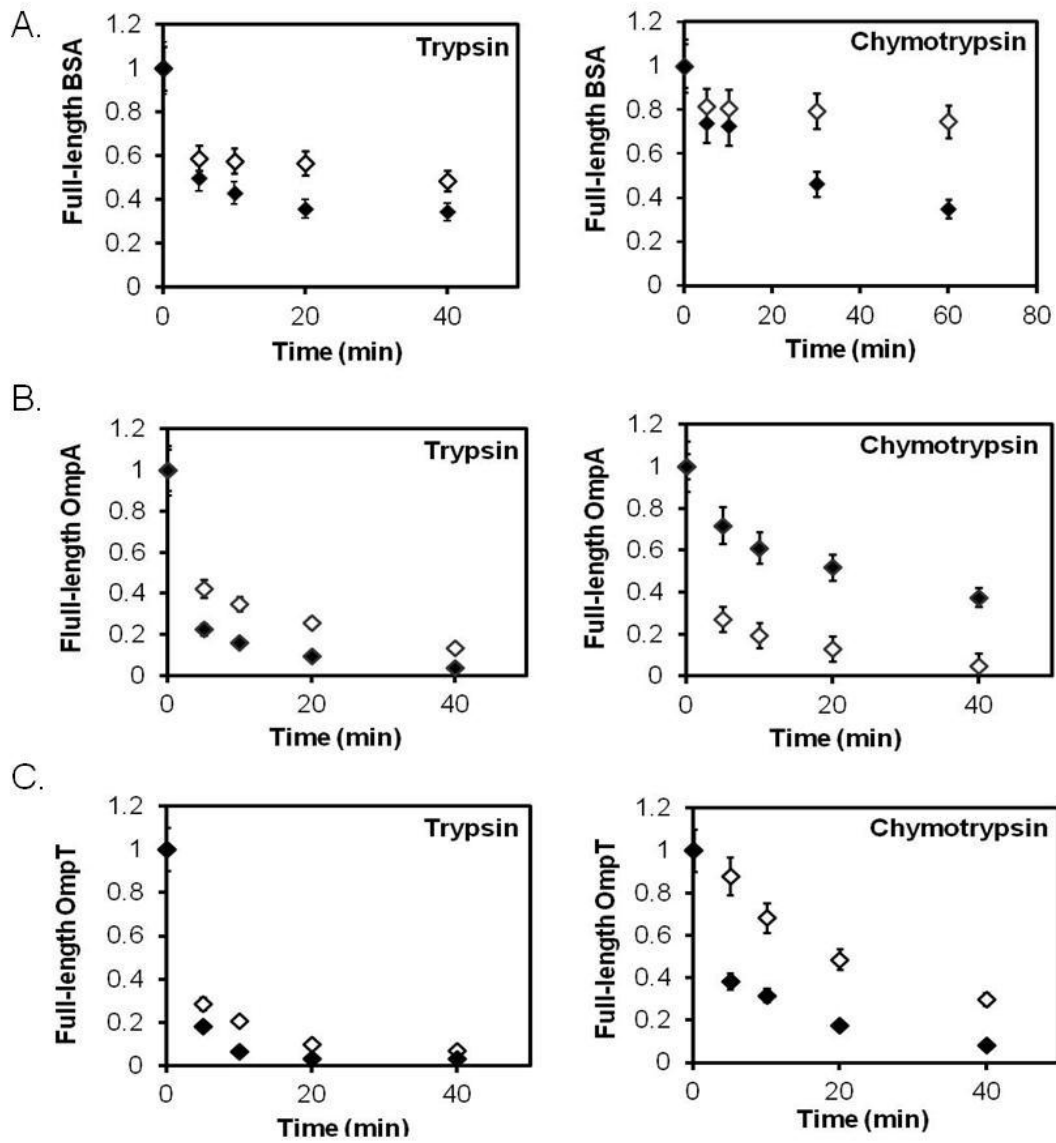


Figure 2.9 Trypsin and chymotrypsin digestion pattern of BSA (A), OmpA (B) and OmpT (C) in pure buffer solution (open) and in 20% Ficoll 70 (filled).

### 2.3.6 Effect of the crowding condition on the rate of membrane insertion of the transmembrane domain of OmpA

Comparing the crystal structures of the two proteins, we noticed that OmpA contains a large C-terminal periplasmic domain, while OmpT has a single transmembrane domain.<sup>88, 89</sup> To investigate if the different behaviors of the two proteins in the presence of Ficoll 70 were due to the periplasmic domain, we constructed a plasmid encoding the sequence of the transmembrane domain of native OmpA (OmpA171). The transmembrane domain of OmpA folds into an eight-stranded  $\beta$ -barrel, and its structure has been determined by both X-ray crystallography and NMR.<sup>102-104</sup> If it is reconstituted into proteoliposomes, the transmembrane fragment of OmpA forms ion conducting channels.<sup>100</sup> We purified the unfolded OmpA171 and conducted a refolding experiment under the similar condition to the full length OmpA. The folded and unfolded OmpA171 were separated on the SDS polyacrylamide gel, in which the unfolded species moved faster than the folded one (Figure 2.10A and 2.10B).<sup>105</sup> In the absence of Ficoll 70, the folding and membrane insertion rate of OmpA171 was  $0.014 \pm 0.002 \text{ min}^{-1}$  and the rate increased approximately twice upon the addition of 20% Ficoll 70 ( $0.028 \pm 0.002 \text{ min}^{-1}$ ), indicating that the addition of Ficoll 70 accelerated the folding and insertion process of OmpA171 (Table 2.2). We also observed that OmpA171 tended to aggregate. High molecular weight bands corresponding to different aggregation states emerged during extended incubation (Figure 2.10D). The presence of Ficoll 70 slightly increased the efficiency of the OmpA171 refolding (Figure 2.10C).



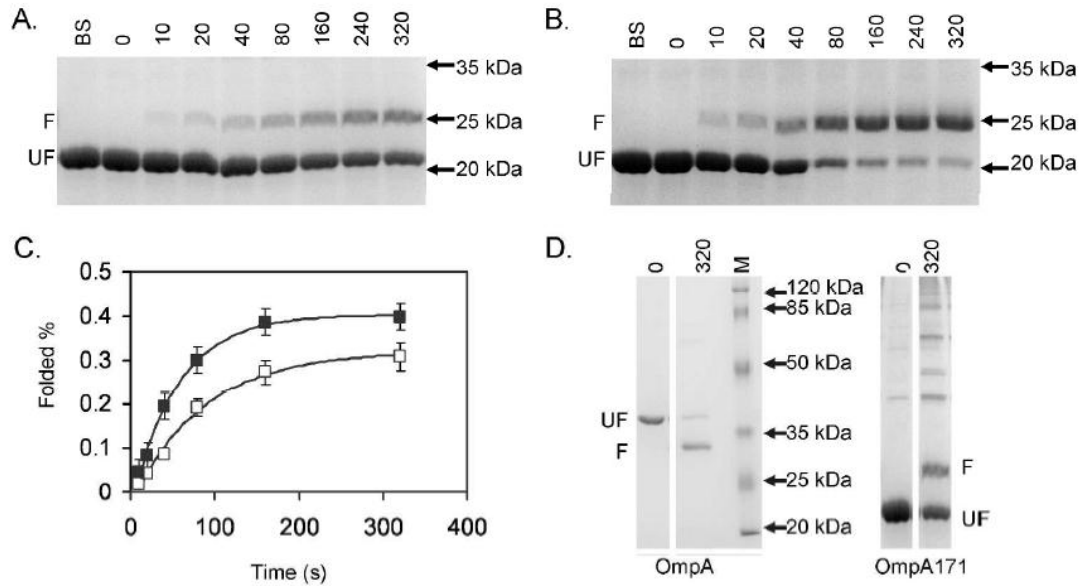


Figure 2.10 OmpA171 refolding and membrane insertion. A. In the absence of Ficoll 70. B. In the presence of 20% Ficoll 70. BS, boiled sample. M, protein molecular weight marker. Numbers represent different incubation time in min. C. Kinetics of OmpA171 refolding in the absence (open) or presence (filled) of 20% Ficoll 70. Data were averages of three independent experiments and fitted to a single exponential equation. D. OmpA171 aggregated over time during the refolding process. Higher molecular weight bands are clearly visible in the refolded OmpA171 sample, but not in the refolded OmpA sample. Positions of folded and unfolded proteins are marked.

## 2.4 Discussion

We used Ficoll 70 as a model crowding agent and studied the crowding effect on the folding and membrane insertion of OmpA and OmpT. First, we found that the folding and membrane insertion rate of OmpA decreased by eight-fold in the presence of 20% Ficoll 70, while the rate of OmpT folding was barely affected. In addition, we noticed

that OmpT folded significantly faster than OmpA under the current experimental condition (Table 2.2). To investigate the mechanism underlying the difference, we examined the structures of the water-soluble intermediates of both proteins. The results indicated that OmpA possessed a more compact structure under crowded condition, while the residual structure of OmpT was barely affected. Finally, we examined whether the presence of the periplasmic domain slowed the membrane insertion of OmpA, we created a truncated OmpA construct containing only the transmembrane domain and investigated its rate of folding and the corresponding effect of crowding. Interestingly, while OmpA171 and full length OmpA had similar folding rates in the dilute buffer solution, the full length OmpA refolded much slower than OmpA171 in the presence of 20% Ficoll 70. The periplasmic domain in the full length OmpA slowed down its folding and membrane insertion under the crowding condition. In addition, we found that the unfolded OmpA171 was less stable than full length OmpA during the refolding. It aggregated and formed oligomeric species of high molecular weight over time. The periplasmic domain of OmpA apparently played a role in stabilizing the structure of OmpA in the unfolded state, prior to its folding and insertion into the OM. Our results are consistent with the conclusion of an earlier study, in which Fleming and coworkers suggested that the periplasmic domain of OmpA serves as a “chaperone” during its folding to keep the protein stable and soluble in the periplasm.<sup>106</sup>

## **2.5 Conclusions**

OMPs play important roles in controlling the membrane permeability for nutrients and toxins. Most studies on the folding mechanism of OMPs were conducted in a dilute

buffer solution. However, the actual folding environment for OMPs is the periplasm, which is a molecularly crowded condition. In this study, we used Ficoll 70 as a model crowding agent and studied the crowding effect on the folding and membrane insertion of OmpA and OmpT. We found that under the crowding condition, refolding and insertion of the transmembrane domain of OmpA was slowed down by the presence of its periplasmic domain in exchange for an improved folding efficiency. This function of the periplasmic domain of OmpA is hardly noticeable in the dilute buffer solution. Macromolecular crowding has long been known to significantly affect the protein folding process. Studying protein folding under the crowding condition will add new our understanding of the protein folding in the living cell.

## CHAPTER III. UNFOLDING STUDY OF A TRIMERIC MEMBRANE

### PROTEIN ACRB

Part of this chapter are taken from “Unfolding study of a trimeric membrane protein AcrB”, 2014, *Protein Sci.* DOI: 10.1002/pro.2471

#### 3.1 Introduction

After their translation, proteins need to fold into and maintain a three-dimensional structure to function. The folding process and thermodynamic stability of proteins have been actively pursued areas of study due to their importance in virtually all life processes. The thermodynamic stability measurement of the integral membrane protein remains to be a challenging task and study on the mechanism of their folding is scant.<sup>74, 107-109</sup> To quantitatively determine the thermodynamic stability of a protein, its reversible unfolding and refolding has to be achieved.<sup>74, 110, 111</sup> The first  $\alpha$ -helical membrane protein that has been successfully refolded from an SDS denatured state is bacteriorhodopsin.<sup>112, 113</sup> Since then, refolding of a few additional  $\alpha$ -helical membrane proteins has been reported, including diacylglycerol kinase<sup>114</sup>, a potassium channel KcsA<sup>115</sup>, and the lactose permease LacY<sup>116</sup>.

Refolding is challenging for helical membrane proteins. The approach taken to unfold a protein is crucial for its refolding efficiency. Methods suitable for soluble proteins such as thermal and acid/base denaturation usually lead to irreversible precipitation or aggregation of  $\alpha$ -helical membrane proteins due to their large hydrophobic core.<sup>74, 117</sup> So far, chemical unfolding using urea, SDS and less commonly trifluoroethanol (TFE)

are the only viable approaches demonstrated to enable successful refolding of  $\alpha$ -helical membrane proteins.<sup>118-120</sup> Urea exerts its effect directly, by binding to the protein, or indirectly, by altering the solvent environment, both resulting in the solvation of the hydrophobic core of the protein,<sup>121</sup> while the mechanism of denaturation by SDS remains a topic of debate.<sup>111, 122, 123</sup> The far UV CD analysis suggests that membrane proteins denatured by SDS tend to maintain a high level of helical structure.<sup>124, 125</sup> This state is arguably a better representative of the unfolded state of helical membrane proteins.<sup>110, 126</sup> An experimental readout that is sensitive to the conformational change of protein during unfolding is another critical factor of the stability measurement. Methods that are extensively used include the far UV CD spectrum which is sensitive to the secondary structure, and the intrinsic fluorescence spectrum that reveals the overall conformational change of a protein.<sup>124, 125, 127</sup>

In this study, we investigated the unfolding and potential of refolding of an *E. coli* IM protein AcrB. Although many attempts have been made to study the folding of  $\alpha$ -helical membrane proteins, these folding studies focus on membrane proteins with relatively simple structures, such as the small multidrug resistance transporter EmrE<sup>128</sup>, the human peripheral myelin protein 22<sup>129</sup>, the ATP-binding cassette transporter BtuCD<sup>130</sup> and the sugar transport protein GalP<sup>131</sup> and LacY<sup>116, 132</sup>, are all helix bundles composed of a small handful of transmembrane helices. Reports on folding of multimeric and multidomain helical membrane proteins are lacking. *E. coli* AcrB is an IM trimeric transporter, in which each monomer contains both a transmembrane domain and a large periplasmic domain formed by two long loops between

transmembrane helices 1 and 2, and helices 7 and 8.<sup>32, 55</sup> The structure of trimeric AcrB is shown in Figure 3.1.<sup>51</sup> Thermal unfolding monitored by CD spectroscopy at 222 nm was measured in a previous study.<sup>133</sup> The protein retained a high helical content even when the temperature was increased to 98 °C. In addition, a clear transition point was lacking. In this study, we examined AcrB unfolding induced by two chemical denaturants, urea and SDS. Intrinsic fluorescence emission and CD signals of the protein were monitored to follow the unfolding and refolding processes. While AcrB failed to refold reversibly under the experimental conditions tested in this study, its monomeric mutant, AcrB $_{\Delta\text{loop}}$ , could be refolded. In addition, the unfolding curve could be fitted by a two-state unfolding model, indicating a lack of folding intermediate states.

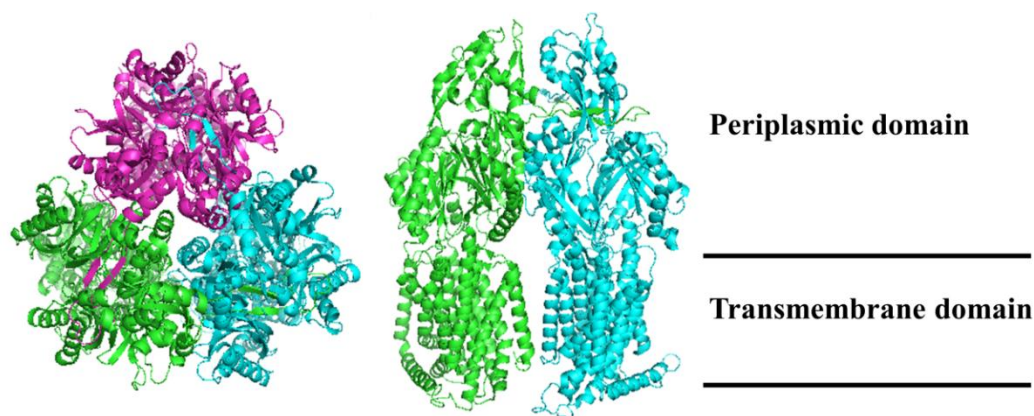


Figure 3.1 Structure of AcrB (created from 2GIF.pdb<sup>51</sup> using Pymol<sup>18</sup>). Top view (left) and side view (right, with the subunit at the back removed for clarity) of an AcrB trimer. Positions of domains as discussed in the text are labeled in the side view. The two lines indicate the position of the cell membrane.

## 3.2 Materials and Methods

### 3.2.1 Plasmid construction, protein expression and purification

Plasmid pQE70-AcrB, pQE70-AcrB $\Delta$ loop and pQE70-AcrB<sub>V225C/A777C</sub> were constructed for an earlier study.<sup>133, 134</sup> Plasmid encoding the triple mutant AcrB<sub>W13F/W515F/W895F</sub> was constructed using the QuikChange Site Directed Mutagenesis Kit (Agilent Technologies) with pQE70-AcrB as the template. Protein was expressed and purified following a published protocol with slight modifications.<sup>135</sup> Cells were cultured at 37 °C in Lysogeny Broth media containing 100 µg mL<sup>-1</sup> ampicillin overnight. The protein expression was conducted under basal condition without induction. Cell was collected by centrifugation at 7,000 g for 15 min at 4 °C and used immediately for purification.

The cell pellets were suspended in a lysis buffer (0.5 mM PMSF, 20 mM Na-phosphate, 0.3 M NaCl, pH 7.9) and sonicated for 25 min in water/ice bath with 5 s on/off intervals. The cell lysate was centrifuged at 15,317×g and 4 °C for 20 min. The pellet was then resuspended in a buffer containing 0.5% (w/v) Triton X-100, 20 mM Na-phosphate, 0.3 M NaCl, pH 7.9. The mixture was then incubated at 4 °C with rotating for 2 hours, followed by centrifugation at 15,317×g and 4 °C for 20 min. The supernatant, containing the AcrB dissolved in detergent, was collected and mixed with Ni-NTA Sepharose resin (Qiagen Inc., Valencia, CA) after the addition of imidazole to a final concentration of 10 mM to reduce non-specific binding to the resin during purification. The binding was allowed to proceed by rotating at 4 °C for 40 min. The suspension was packed into an empty 5 mL column and washed with a wash buffer (50 mM

imidazole, 0.03% n-Dodecyl  $\beta$ -D-maltoside (DDM), 20 mM Na-phosphate, 0.3 M NaCl, pH 7.9). The target protein was eluted using a buffer contained 0.5 M imidazole, 0.03% DDM, 20 mM Na-phosphate, 0.3 M NaCl, pH 7.9. Protein samples were dialyzed overnight in the same buffer in the absence of imidazole at 4 °C overnight. The same buffer was used throughout this study unless otherwise noted. The protein concentration was determined using Pierce BCA Protein Assay Kit (Thermal Scientific, TX).

Protein activity was evaluated by measuring the minimum inhibitory concentration (MIC) of BW25113 $\Delta$ *acrB* containing plasmid encoding this protein as described.<sup>136</sup> BW25113 $\Delta$ *acrB* containing plasmid pQE70-AcrB and the empty vector pQE70 were used as positive and negative controls, respectively.

### 3.2.2 *Unfolding of trimeric AcrB*

Protein unfolding was initiated by titrating concentrated urea (8.0 M) or SDS (0.2% or 2%, w/v) into freshly purified AcrB in the dialysis buffer. A fluorescence emission spectrum between 300 to 400 nm was recorded at each titration point with a LS-55 fluorescence spectrometer (PerkinElmer, Inc., Waltham, MA) with excitation wavelength of 280 nm. The maximum fluorescence intensity of each spectrum was converted into fraction of protein folded using Equation 3.1 and plotted as a function of urea molar concentration or SDS/DDM molar ratio. A titration plot of L-tryptophan with SDS solution as a control was determined similarly.



$$y = \frac{Y - Y_{min}}{Y_{max} - Y_{min}} \quad \text{Eq. 3.1}$$

in which,  $Y$  denotes the fluorescence intensity, and  $Y_{max}$  and  $Y_{min}$  are the maximum and minimum values, respectively.

To reduce the disulfide bonds in AcrB<sub>V225C/A777C</sub>, purified protein was divided into two aliquots: one incubated in solution buffer containing 0.5 mM dithiothreitol (DTT) at 25 °C for 2 hours to reduce disulfide bonds, the other incubated in the absence of DTT under the same conditions. Wild type AcrB was treated similarly and used as the control. Plots of fraction of folded protein versus SDS/DDM molar ratio were obtained as described above.

### 3.2.3 BN- PAGE analysis and far UV CD spectroscopy

Purified AcrB<sub>WT</sub> and AcrB<sub>Dloop</sub> were incubated in a buffer solution in the absence or presence of SDS at a mole ratio of 2.4 at 25 °C for 20 min and then Blue Native polyacrylamide gel electrophoresis (BN-PAGE) was performed as described in a published protocol.<sup>137, 138</sup> Briefly, blue native loading buffer was added into protein sample to give a final concentrations of 0.1 M 6-aminoocaproic acid, 1% Coomassie Brilliant Blue G-250, 1% glycerol. Protein samples were loaded on to a 4-20% gradient polyacrylamide gel (Bio-Rad, Hercules, CA). Electrophoresis was performed using a cathode running buffer containing 50 mM Tricine, 7.5 mM imidazole 0.02% Coomassie Brilliant Blue G-250, pH 7.0 and a anode running buffer (25 mM imidazole, pH adjusted with HCl to 7.0) at 4 °C, at 15 mA for 2 h. The protein bands were visualized with Coomassie blue stain.

Purified AcrB after dialyzed overnight as described above was titrated with 0.2% (w/v) SDS solution at 25 °C. CD spectra in the range of 190 nm and 250 nm were collected with a JASCO J-810 spectrometer. The ratio of the mean residue ellipticities at 222 nm and 208 nm was converted into fraction of folded protein using Equation 3.1 and plotted as a function of DDM/SDS molar ratio.

#### *3.2.4 Refolding of AcrB*

To refold protein denatured by urea, purified AcrB was first incubated in the dialysis buffer containing 4 M urea at 25 °C for 20 min to fully unfold the protein, followed by titration with the urea-free buffer. To refold SDS denatured protein, the buffer solution containing 10% DDM was titrated into the unfolded protein sample containing SDS at the SDS/DDM molar ratio of 11.8. Fluorescence emission spectra and CD spectra were recorded and analyzed to obtain the refolding curve as described above.

### **3.3 Results**

#### *3.3.1 Chemical denaturation of trimeric AcrB monitored by intrinsic fluorescence*

A reversible unfolding/refolding process is a prerequisite for obtaining thermodynamic parameters of protein stability.<sup>74</sup> Urea and SDS have been used successfully in the refolding of membrane proteins.<sup>109, 110</sup> To study the stability of AcrB, we examined its unfolding in these two denaturants and monitored the decrease of intrinsic fluorescence intensity during unfolding. Protein unfolding usually leads to the transition of fluorescent residues to shift from the protected hydrophobic core to a solvent exposed

hydrophilic environment, resulting in a decrease of fluorescence signal and sometimes a red shift of the emission peak.

When AcrB unfolded in urea, a dramatic decrease of tryptophan fluorescence intensity was observed (Figure 3.2A). Therefore, we chose to monitor the decrease of the maximum fluorescence emission as an indicator of protein unfolding. The titration curve with urea (Figure 3.2B) displayed a sigmoid profile with a transition point at around 3.0 M. The unfolding of protein with urea reached the end point when urea concentration was 5.0 M.

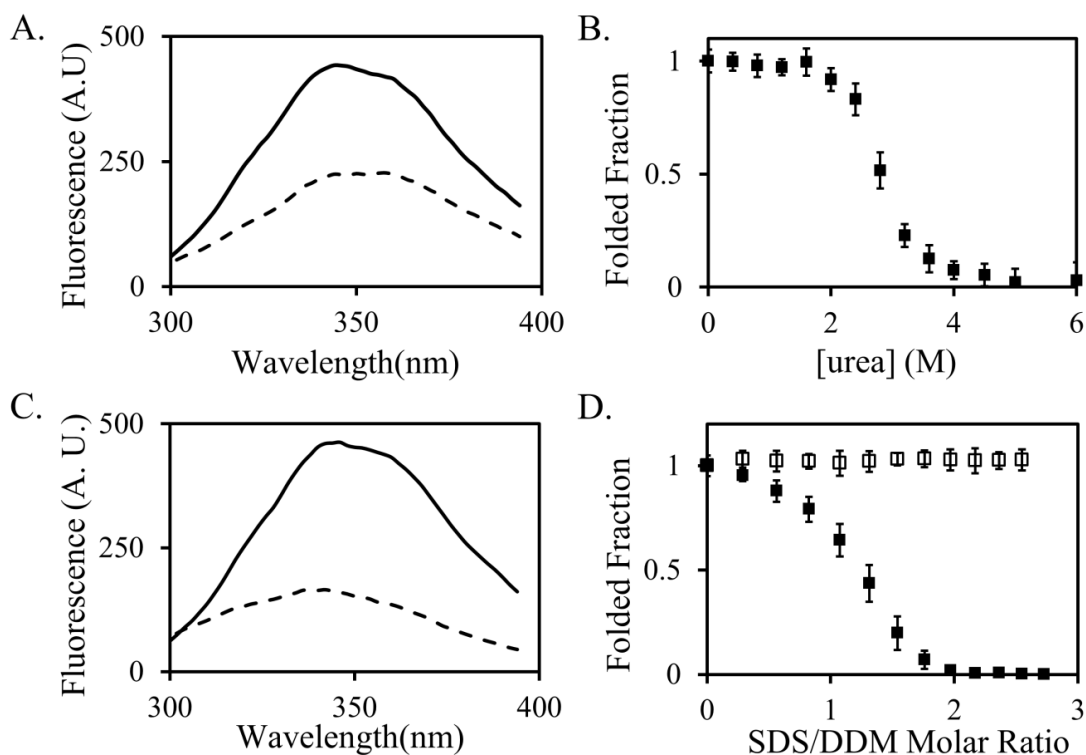


Figure 3.2 Chemical denaturation of AcrB monitored using the intrinsic fluorescence. A. Spectra of AcrB in the absence (solid line) and the presence of (dashed line) of 6 M urea. B. Unfolding of AcrB induced by urea titration. C. Spectra of AcrB in the absence (solid line) and the presence of SDS (dashed line, SDS/DDM molar ratio 2.4). D. Unfolding of AcrB induced by the titration of SDS (black squares). L-tryptophan (open squares) was used as a control to confirm the lack of non-specific effect of SDS on fluorescence emission. Each experiment was repeated at least three times, and the average values and standard deviations are shown.

A significant decrease of the fluorescence signal was also observed when we performed a similar titration using SDS (Figure 3.2C). The transition point occurred at a SDS/DDM molar ratio of around 1.0 (Figure 3.2D). A small fluorescent amino acid L-

tryptophan was titrated similarly with SDS to serve as a control of potential non-specific fluorescence change. As revealed in Figure 3.2D, the presence of SDS had little effect on the fluorescence of L-tryptophan, indicating that the change of buffer condition upon the addition of SDS did not have a non-specific effect on the fluorescence emission. Therefore, the decrease in AcrB fluorescence emission during the titration process was caused by protein structure change. Titration results revealed that the protein reached the unfolding end point in SDS when SDS/DDM molar ratio reached 2.4.

### *3.3.2 Contribution of signal change from trimer dissociation*

Dissociation of AcrB trimer in the presence of SDS was confirmed using BN-PAGE. Only one trimer band was observed when a fresh AcrB sample was analyzed using BN-PAGE (Figure 3.3, lane 1). In the presence of SDS at a molar ratio of 2.4, the trimer band was completely converted into a monomer band, indicating that all AcrB trimers dissociated into monomers (Figure 3.3, lane 2). To confirm that the observed change of migration was not due to the nonspecific association of SDS, we conducted a control experiment using a monomeric AcrB mutant created in a previous study, AcrB $_{\Delta\text{loop}}$ .<sup>134</sup> In AcrB $_{\Delta\text{loop}}$ , the long loop that is critical for the AcrB trimerization is truncated, which leads to the trimer dissociation. However, the overall secondary and tertiary structures of the mutant were comparable to that of the wild type AcrB.<sup>134</sup> As shown in Figure 3.3, lanes 3 and 4, the addition of SDS did not shift the migration of AcrB $_{\Delta\text{loop}}$  in the gel, indicating the observed change in lane 2 was due to trimer dissociation.

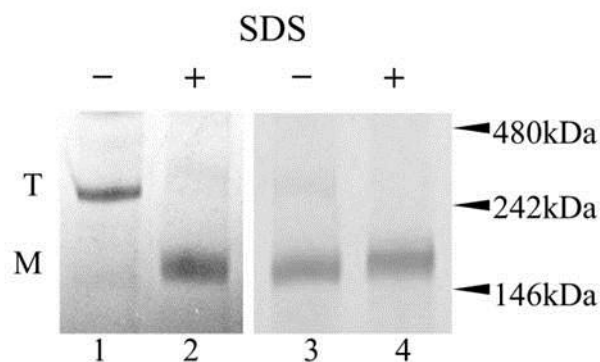


Figure 3.3 AcrB trimer dissociation observed in BN-PAGE gel. A. Representative BN-PAGE gel image of wild type AcrB samples without (lane 1) or with (lane 2) incubation with SDS (SDS/DDM molar ratio 2.4). AcrB $_{\Delta\text{loop}}$  samples were treated similarly and used as controls (lane 3 and 4). Positions of monomer (M) and trimer (T) for both gel as well as molecular weight markers were labeled.

To examine the relative contributions of trimer dissociation and monomer unfolding to the observed change of fluorescence, we monitored the unfolding of a mutant, AcrB $_{\text{V225C/A777C}}$ . AcrB $_{\text{V225C/A777C}}$  contains inter-subunit disulfide bonds between neighboring subunits, and exists as a covalently linked trimer.<sup>139</sup> Formation of the disulfide bond between V225C and A777C of adjacent monomers was complete as revealed by the lack of monomer band when the protein was analyzed on non-reducing SDS-PAGE gel.<sup>138</sup> These inter-molecular disulfide bonds have no effect on AcrB activity, indicating little negative impact on protein structure.<sup>139</sup> We compared the SDS titration curves of AcrB $_{\text{V225C/A777C}}$  with wild type AcrB (Figure 3.4B), and their titration curves under a reducing condition with a non-reducing condition (Figure 3.4C and 3.4D). Incubation in the presence of 0.5 mM of DTT at room temperature for two hours completely reduced disulfide bonds in AcrB $_{\text{V225C/A777C}}$  trimer (Figure 3.4A). The trimer

band was completely converted into a monomer band. Wild type AcrB does not contain any intrinsic disulfide bonds. According to Figure 3.4C, the overlapped titration curves of wild type AcrB in the absence and the presence of DTT confirmed that DTT had little influence on protein structure except for reducing disulfide bonds. The loss of disulfide bonds in AcrB<sub>V225C/A777C</sub> trimer had little effect on protein stability (Figure 3.4D). Therefore AcrB monomer unfolding was the primary cause of the observed sharp decrease in the intrinsic fluorescence intensity.

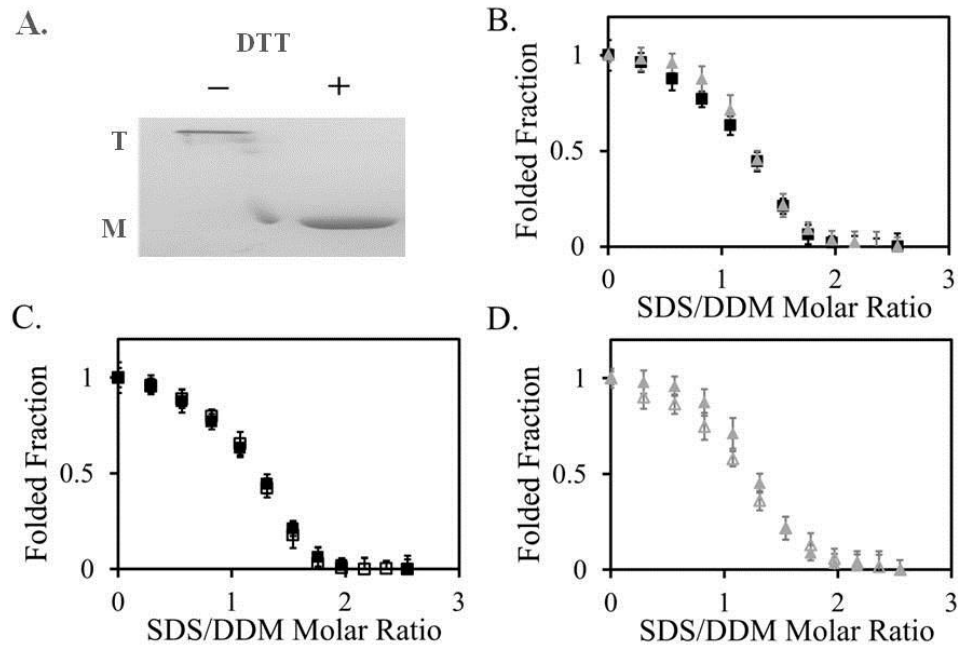


Figure 3.4 SDS-induced unfolding of wild type AcrB and AcrB $\Delta$ loop. A. Representative SDS-PAGE gel image of AcrB<sub>V225C-A777C</sub> before (-) or after (+) the reduction of DTT (0.5 mM). Positions of monomer (M) and trimer (T) are labeled. B. SDS titration of wild type AcrB (black squares) and AcrB<sub>V225C/A777C</sub> (grey triangles). C. SDS titration of wild type AcrB before (black squares) or after (open squares) reduction with DTT. D. SDS titration of AcrB<sub>V225C/A777C</sub> before (grey triangles) or after (open triangles) reduction with DTT. Each experiment was repeated at least three times and the average values and standard deviations are shown.

### 3.3.3 Unfolding of a triple AcrB mutant

As discussed above, the intrinsic fluorescence of a protein can reflect its conformational state. Trp residues are the major contributor to protein intrinsic fluorescence. There are nine Trp residues in the sequence of AcrB, three in the transmembrane domain (W13, W515, and W895) and six in the periplasmic domain (W187, W634, W754,



W789, W809, and W859). We chose to mutate all three Trp in the transmembrane domain to Phe to investigate the effect on the observed unfolding profile. To confirm that the mutations did not drastically alter AcrB structure, we determined the transport activity of the mutant by measuring the MIC of an AcrB knockout strain *BW25113ΔacrB* harboring a plasmid encoding AcrB<sub>W13F/W515F/W895F</sub> (pQE70-AcrB<sub>W13F/W515F/W895F</sub>). The same strain harboring the empty vector (pQE70) or plasmid encoded wild type AcrB (pQE70-AcrB) was used as the negative and positive control, respectively. Two well-established AcrB substrates were tested, erythromycin and novobiocin. For erythromycin, the MIC of the strains containing wild type, mutant, or no AcrB was 160 µg/mL, 160 µg/mL, and 5 µg/mL, respectively. For novobiocin, the MIC of the three strains was 80 µg/mL, 40 µg/mL, and 10 µg/mL, respectively. For the two substrates tested, the mutant retained complete or partial activity, indicating that the overall structure of the protein was largely intact. The replacement of three Trp with Phe residues led to a decrease of the fluorescence intensity by approximately 30%, and the peak of the emission spectrum shifted to a slightly longer wavelength (Figure 3.5A). Next, SDS induced unfolding was measured (Figure 3.5B). The unfolding profile of the triple mutant was very similar to the profile of wild type AcrB. Removal of three Trp from the transmembrane domain did not lead to an observable shift of the unfolding profile, indicating that the observed signal change was actually largely contributed by Trp residues from the periplasmic domain.

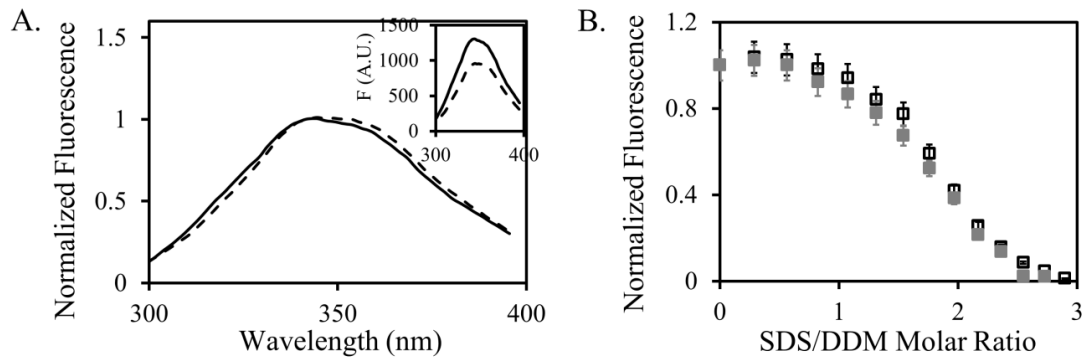


Figure 3.5 SDS-induced AcrB<sub>W13F/W515F/W895F</sub> unfolding. A. A comparison of fluorescence spectra of wild type AcrB (solid line) and mutant AcrB<sub>W13F/W515F/W895F</sub> (dashed line). The spectra were normalized to observe the peak shift. Original concentration adjusted spectra were shown as an inset. B. Unfolding of AcrB<sub>W13F/W515F/W895F</sub> induced by the titration of SDS (open squares). Unfolding of wild type AcrB was also shown as a control (grey squares). Each experiment was repeated at least three times, and the average values and standard deviations were shown.

### 3.3.4 Chemical denaturation of trimeric AcrB monitored by CD spectroscopy

To further examine the structural change of AcrB in the presence of SDS, far UV CD spectra were collected for an AcrB sample in the absence and presence of SDS at a SDS/DDM molar ratio of 2.4. Changes in both intensity and wavelength of the spectrum peak were observed in the CD spectra, revealing an alteration of the secondary structure composition and arrangement (Figure 3.6A). Effort to deconvolute the CD spectra into individual secondary components using online software provided by the DICHROWEB<sup>140</sup> server was not successful, likely due to the lack of an appropriate reference set for membrane proteins. A SDS titration monitored by CD was performed to examine the disruption of secondary structure components during

protein unfolding. The ratio of mean residue ellipticity at 222 nm and 208 nm was used to reflect the secondary structure change (Figure 3.6B). Similar to the results with intrinsic fluorescence, structural change was complete at a SDS/DDM molar ratio of 2.4.

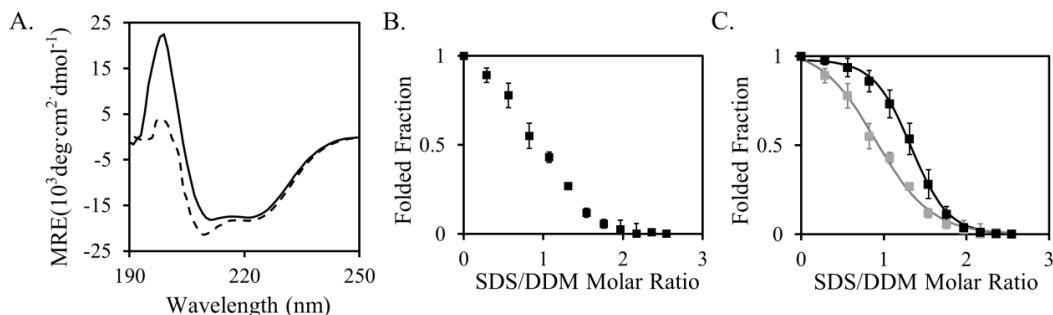


Figure 3.6 SDS-induced denaturation of AcrB monitored by CD. A. Spectra of purified AcrB in the absence (solid line) and the presence (dashed line, SDS/DDM molar ratio 2.4) of SDS. B. AcrB titration with SDS monitored by the ratio of ellipticities at 208 nm and 222 nm. C. Comparison of unfolding profiles. Comparison of the process of unfolding monitored by CD (grey squares) and fluorescence intensity (black square). The curves showed the fitting of the CD and fluorescence intensity data using a simple two-states unfolding model. Each experiment was repeated at least three times and the average value and standard deviation were shown.

### 3.3.5 Comparison of AcrB unfolding plots monitored using fluorescence and CD spectroscopy

While both unfolding plots revealed that the structure change (unfolding) was complete at a SDS/DDM molar ratio of 2.4, the transition points were significantly different (Figure 3.6C). Furthermore, both plots could be fitted with a sigmoidal curve

describing a simple two-state unfolding model from a folded state directly to an unfolded state (Figure 3.6C). The transition point of wild type AcrB unfolding was calculated to be  $0.94 \pm 0.03$  and  $1.32 \pm 0.09$  SDS/DDM molar ratio for CD and fluorescence emission, respectively. Comparison between the plots suggested that the rearrangement of protein secondary structure occurred prior to the global unfolding of the tertiary structure.

### *3.3.6 Refolding of chemically denatured AcrB*

To quantitatively determine the thermodynamic parameters of AcrB, reversible refolding needs to be achieved. We first unfolded AcrB in the presence of 4 M urea, and then diluted the sample to reduce the concentration of urea. As shown in Figure 3.7A and 3.7B, the fluorescence intensity began to increase when the concentration of urea was reduced to below 2 M, and 57% of the fluorescence was recovered when the urea concentration was reduced to 1 M. The presence of two separated unfolding and refolding curves and the low recovery of spectral parameters indicated that AcrB did not refold reversibly from the urea-denatured state under our experimental conditions. We also collected the CD spectra of AcrB unfolded in urea (dotted line), and then after dialyzed overnight (grey line) (Figure 3.7C). The secondary structure of the protein was not regained.

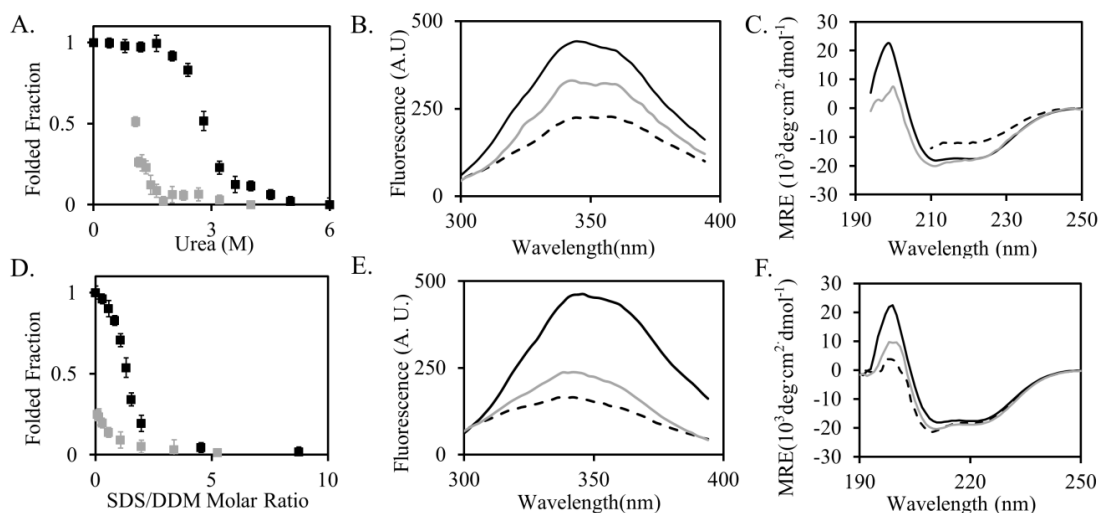


Figure 3.7 Refolding of AcrB. A. Unfolding (black) and refolding (grey) profiles of AcrB in urea. B. Fluorescence emission spectra of AcrB in the native state (black line), unfolded (dashed line, in 6.0 M urea), and after refolding (gray line). C. CD spectra of AcrB in the native state (black line), unfolded state (dashed line, in 6.0 M urea), and after refolding (gray line) in urea. D. Unfolding (black) and refolding (grey) profiles of AcrB in SDS. E. Fluorescence emission spectra of AcrB in the native state (black line), unfolded (dashed line, SDS/DDM molar ratio 2.4), and after refolding (gray line). F. CD spectra of AcrB in the native state (black line), unfolded state (dashed line, SDS/DDM molar ratio 2.4), and after refolding (gray line) in SDS.

To refold the SDS-denatured AcrB, we reduced the molar ratio of SDS in SDS/DDM mixed micelles by adding aliquots of concentrated DDM solution. As shown in Figure 3.7D and 3.7E, the refolding curve did not overlap with the unfolding curve, with around 25% fluorescence recovery at the lowest SDS/DDM molar ratio tested (0.07). The CD spectrum of refolded sample was collected and compared with the spectra of native and unfolded AcrB samples (Figure 3.7F). Again, the secondary structure of the

protein was not fully recovered in the refolding sample. It was clear that the structure of the protein was different from the native-like conformation. We have attempted to refold the protein under a variety of different conditions, including varying the pH, lipid vesicle concentration, and detergent concentration. None of these conditions led to the successful refolding of the protein to the original conformation (data not shown).

Next, we experimented with the refolding of an AcrB mutant, AcrB $\Delta$ loop. As mentioned earlier, AcrB $\Delta$ loop exists as a monomer, but has similar secondary and tertiary structure as a monomeric subunit in a wild type trimer.<sup>134</sup> Since the complete refolding of wild type AcrB involves trimer association, we speculate that the refolding of a monomeric AcrB mutant might be easier to achieve. Unlike the SDS induced unfolding of the wild type protein, the unfolding of AcrB $\Delta$ loop was not as cooperative (Figure 3.8A). However, the unfolding was partially reversible when the SDS/DDM molar ratio was reduced upon the addition of DDM. The CD spectrum of the refolded sample superimposed well with that of the original folded protein, however the fluorescence spectrum was not fully restored (Figure 3.8B and 3.8C).

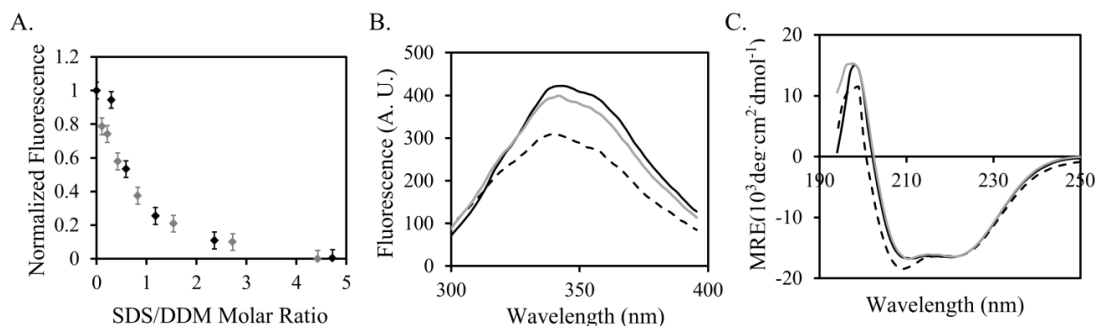


Figure 3.8 Refolding of AcrB $_{\Delta\text{loop}}$ . A. SDS induced unfolding (black diamonds) and refolding (grey diamond) profiles of AcrB $_{\Delta\text{loop}}$ . B. Fluorescence emission spectra of AcrB $_{\Delta\text{loop}}$  in the native state (black line), unfolded (dashed line), and after refolding (grey line). C. CD spectra of AcrB $_{\Delta\text{loop}}$  in the native state (black line), unfolded state (dashed line), and after refolding (grey line).

### 3.4 Discussion

In this study, we monitored the chemical denaturation of trimeric AcrB in the presence of urea and SDS. Both trimer dissociation and monomer unfolding could potentially lead to a change in the intrinsic fluorescence emission. However, we found that the presence of inter-subunit disulfide bonds, which strengthened AcrB trimer stability by covalently linking the three subunits, had little effect on the transition point of AcrB unfolding monitored using fluorescence intensity. There are two potential reasons that may lead to this observation. First, trimer dissociation could be spectroscopically silent. Second, trimer dissociation could have occurred together with the global unfolding of individual subunits. To further investigate the unfolding process, we monitored the folding process using CD. The unfolding profiles monitored using CD was different from that monitored using fluorescent intensity. Even though SDS cannot effectively

unfold  $\alpha$ -helices in the transmembrane domain, it causes a peak shift of the CD spectrum and has been used as a probe of secondary structure change during  $\alpha$ -helical membrane protein unfolding.<sup>118, 119, 127</sup> It is notable in our results that the initiation and transition points of unfolding monitored using CD occurred at a significantly lower SDS concentration than that monitored using fluorescence emission spectroscopy. Therefore, the unfolding of AcrB trimer appeared to start with the structural rearrangement of monomers, and possibly the concurrent dissociation of trimers. The fluorescent intensity change indicates the disruption of the hydrophobic core and exposure of aromatic residues. Based on our result, the change of fluorescence signal was largely contributed by the unfolding of the soluble domain, which could be fitted nicely with a two-state model. The unfolding of the transmembrane domain may not generate a detectable fluorescence signal change, since the change of microenvironment for Trp residues in the transmembrane domain upon unfolding is not likely as dramatic as Trp residues in the soluble domain.

We also attempted to refold the chemically denatured AcrB to quantitatively determine the thermodynamic stability of folding for trimeric AcrB. However, under our experimental conditions, neither urea nor SDS denatured AcrB can be reversibly refolded. Interestingly, an AcrB monomeric mutant, AcrB $\Delta$ loop, could regain its secondary structure composition after SDS induced unfolding. The mutant was not fully refolded into the native conformation as judged by the fluorescence spectrum. The fine-tuning of the tertiary structure during AcrB *in vitro* refolding might require trimerization. We speculate that trimerization, which is the last hurdle for the wild type



AcrB to refold into a native-like structure, might be difficult to achieve in an artificial refolding condition. The complete refolding of AcrB might require a condition more closely mimicking the native cell membrane, in which multiple subunits are accessible to each other and the transmembrane domain is stabilized in a lipid bilayer.

The unfolding process of AcrB trimer was clearly different from the observation of unfolding of the tetrameric GlpF, which occurs via a stable dimeric intermediate state.<sup>141</sup> A larger oligomeric membrane protein, the heterotetrameric BtuCD has been refolded in detergent micelles.<sup>130</sup> The protein complex consists of two trans-membrane protein subunits, BtuC, and two cytoplasmically located nucleotide-binding protein subunits, BtuD. Results from the refolding study support the idea of cooperative folding and assembly of the constituent protein subunits of the BtuCD transporter. This is also consistent with the observed correlation between subunit unfolding and dissociation during the unfolding of an AcrB trimer. Different from AcrB, the structural organization in BtuCD is modular. Therefore, there is a certain degree of flexibility to allow independent folding of BtuC in detergent micelles and BtuD in aqueous solution. In contrast, the sequence segments that fold into the transmembrane domain and segments that fold into the periplasmic domain in AcrB are interdigitated. Folding of these two domains is likely more tightly correlated and reliant on each other. It has been widely accepted that the unfolded state of a transmembrane helix bundle remains to be highly helical. In the case of AcrB, we speculate that the unfolded state of the protein is consisted of a loosely packed transmembrane helix bundle tied to the more disordered periplasmic loops. The anchoring effect of the transmembrane

component could actually be a facilitating factor during the refolding of the periplasmic domain, which subsequently brings the transmembrane helices back to their native-like positions.

### **3.5 Conclusion**

Stability is an important parameter that is essential for investigations on protein structures and functions, including crystallography, protein design and engineering, folding and misfolding, and mechanism of disease-related mutations and aggregation. Thermodynamic stability measurements of  $\alpha$ -helical membrane proteins are rare and are not frequently reported due to the difficulty in achieving reversible unfolding/refolding. So far, quantitative stability measurement has only been achieved for a handful of  $\alpha$ -helical membrane proteins, most of which have simple structures consisting of a transmembrane helix bundle. In this work, we investigated the unfolding and conditions of refolding of a multi-domain trimeric  $\alpha$ -helical membrane protein, *E. coli* inner membrane protein AcrB. Our results suggested that the unfolding of AcrB started with a local structural rearrangement, probably coincidentally with a dissociation of the trimer, and were followed by the collapse of hydrophobic cores in the solvent exposed periplasmic domain. Refolding of trimeric AcrB was not successful, while the refolding of secondary structure in individual monomers could be achieved, suggesting that the re-association of the trimer might be the limiting factor to obtain folded wild type AcrB *in vitro*. Investigation of refolding in a more native-like lipid bilayer is required for more complete refolding and thus more insight in the refolding.

## CHAPTER IV. THE CORRELATION BETWEEN ACRB TRIMER ASSOCIATION AFFINITY AND EFFLUX PUMP ACTIVITY

### 4.1 Introduction

The stabilities of water soluble proteins and protein oligomers are tuned to match their biological functions, the physiological environment, and the regulatory mechanisms.<sup>142-147</sup> Usually a protein is only marginally stable. This modest stability is thought to be critical for protein function, which usually requires a certain degree of structural flexibility involving conformational changes for function. Studies on the stability-activity relationship lag behind in the area of membrane protein research. Such studies have recently become possible due to the advances of techniques and accumulation of knowledge of membrane protein structure and functions. In the past two decades much insight has been obtained on energetics of membrane protein oligomerization in detergent micelles and phospholipid bilayer.<sup>148</sup> Yet, a systematic study investigating the correlation between oligomer stability and *in vivo* activity of a multi-span and multi-domain helical membrane protein is still missing. Here, we used *E. coli* AcrB as a model protein to investigate the relationship between its trimer stability and drug efflux activity.

AcrB is an obligate trimer that exists and functions exclusively in a trimeric form (Figure 4.1A).<sup>149</sup> AcrB conducts the inward flow of protons across the IM to drive conformational changes that facilitate substrate efflux. The structure of AcrB was first solved by x-ray crystallography in the asymmetric trimer form in 2006, which supports a conformational cycling model for drug transport.<sup>51, 55</sup> Up to date, more than thirty

structures of AcrB have been deposited into the Protein Data Bank. However, crystal structures cannot provide insight into how its trimer affinity affects the drug efflux activity.

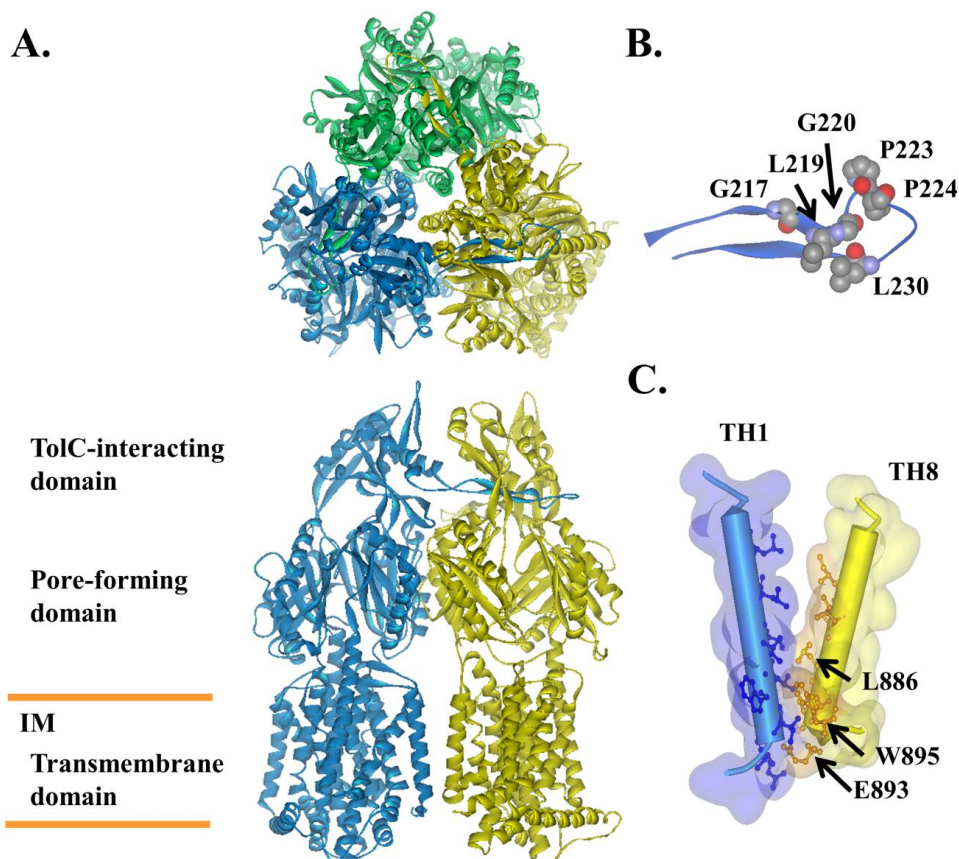


Figure 4.1 Structure of AcrB. A. Top view and side view (with the subunit at the back removed for clarity) of an AcrB trimer. Domains as discussed in the text are labeled for the side view. B. Zoom in view of the protruding loop that is critical for the inter-subunit interaction. Residues discussed in the text are highlighted using space-filled models and labeled. C. Residues lining the interface between TH1 and TH8 are highlighted by ball-and-stick models. L886, E893, and W895 are labeled.

We previously created several AcrB mutants with modifications on the periplasmic inter-subunit interface that displayed different levels of drug efflux activity.<sup>133, 150</sup> These sites of mutation are located on a protruding loop critical of each subunit for trimerization (Figure 4.1B). A single amino acid substitution was shown to almost completely dissociate the trimer structure (AcrB<sub>P223G</sub>). In this work, we introduced additional mutations at three sites on the transmembrane inter-subunit interface, including single, double, and triple replacements (Figure 4.1C), aiming at disrupting trimer association without affecting the overall structure of individual monomers. Structural characterization and stability measurement indicated that the mutations in the protruding loop decreased the stability of individual monomers,<sup>151</sup> while the effect of the mutations in the transmembrane helix was minimal. Therefore, we used the latter to determine their relative trimer affinities and biologically relevant transport activities. When the efflux activity of the AcrB variants were plotted against their relative trimer stabilities, a requirement of a threshold stability was observed.

## **4.2 Materials and Methods**

### *4.2.1 Protein cloning, expression and purification*

Plasmid pQE70-AcrB was created in a previous study by routine molecular cloning methods.<sup>135</sup> Mutations were introduced into the *acrB* gene in plasmid pQE70-AcrB using the QuikChange Site-Directed Mutagenesis Kit according to the manufacturer's instructions (Agilent Technologies) and confirmed through DNA sequencing. Plasmid containing *acrB* gene or its mutations was then transformed into *E. coli* BW25113  $\Delta$ *acrB* strain for protein expression. Expression level of each protein was determined

using Western blot as described.<sup>152</sup> Plasmids used in this study were constructed by Dr. Wei Lu and Dr. Linliang Yu.

#### *4.2.2 Structural characterization using CD and fluorescence spectroscopy*

CD spectra and SDS induced unfolding monitored by fluorescence spectroscopy of purified wild type AcrB and its mutants were collected as described in Materials and Methods section of Chapter III.<sup>136</sup> Titration data was fitted with a single exponential equation to calculate the transition point of unfolding as described.<sup>118</sup>

#### *4.2.3 Measurement of drug susceptibility, ethidium bromide accumulation and nile red efflux*

Drug susceptibility of each AcrB construct was determined by measuring the MIC of BW25113 $\Delta$ *acrB* containing plasmid encoding each protein as described.<sup>136</sup> Ethidium bromide (EtBr) accumulation and nile red efflux were performed following published protocols.<sup>153, 154</sup> The slope of a plot of fluorescence intensity versus time in second was obtained as the accumulation or efflux rate in s<sup>-1</sup>. In all assays, BW25113 $\Delta$ *acrB* containing plasmid pQE70-AcrB or the empty vector pQE70 were used as positive and negative controls, respectively. MIC measurements of all AcrB mutants were performed by Dr. Wei Lu and Dr. Linliang Yu.

To compare data from different measurements, MIC values for the four substrates and EtBr accumulation rates were normalized against the positive control and converted into the residual percent activities. For example, the MIC of erythromycin (Ery)

obtained for the strain containing wild type AcrB (positive control) was 32-fold of the MIC obtained for the strain without AcrB (negative control). If a mutant (for example, AcrB<sub>L886G/E893G/W895G</sub>) has a MIC of 20 µg/ml, which is 8-fold of the MIC of the negative control, we would convert it into 25% residual activity. EtBr accumulation rate was normalized similarly. For instance, the EtBr accumulation rate of BW25113Δ*acrB* was reduced by 15.7-fold of that of wild type AcrB. If the accumulation rate of BW25113Δ*acrB* was reduced by 1.6-fold after the expression of an AcrB mutant (AcrB<sub>L886G/E893G/W895G</sub>, for instance), then the residual activity would be calculated by dividing 1.6 by 15.7 to get 10.7%.

#### *4.2.4 Method to calculate apparent trimer affinity of AcrB in detergent micelles*

To determine the relative stability of AcrB mutants, protein was expressed and purified as described in Materials and Methods section of Chapter III.<sup>133, 135, 136</sup> Freshly purified samples were analyzed using BN-PAGE as described.<sup>136</sup> Software ImageJ was used to quantify the trimer and monomer bands, which were used to calculate the percentages of monomer and trimer in the sample.<sup>155</sup> Concentration of AcrB was determined using Pierce BCA Protein Assay Kit (Thermal Scientific INC., TX).

### **4.3 Results**

#### *4.3.1 AcrB variants with mutations at the inter-subunit interface*

Since the goal of this study is to investigate how a change of trimer affinity would affect AcrB efflux activity, we introduced mutations to disrupt protein-protein interactions. To identify sites for mutation, we analyzed the inter-subunit interface

using the online server ProtorP<sup>156</sup> and the AcrB crystal structure 2DHH<sup>55</sup>. When two AcrB subunits associate, ~12% of the overall decrease in accessible surface area (ASA) is contributed by interactions between transmembrane helices (TH) (Figure 4.1C), and the rest from the periplasmic domain, including a loop-and-tunnel contacting site (Figure 4.1B). The interaction between TH1 (blue) from one subunit and TH8 (yellow) of the neighboring subunit is highlighted in Figure 4.1C, with residues lining the inter-subunit interface shown as ball-and-stick models.

The interaction between the protruding loop from one subunit and multiple residues that form a tunnel around the loop from the other subunit is the major contributor to the binding interface in AcrB, contributing ~47% of the overall decrease of ASA. Among amino acids in the loop sequence, three residues are Ala, Ala215, Ala216, and Ala232 (Figure 4.2A). In a previous study, we conducted an Ala scanning experiment, mutated each non-Ala residue in the loop into Ala, and measured their drug efflux activity.<sup>157</sup> We identified five residues in the loop that when replaced with Ala, the mutant displayed decreased substrate efflux activity. These residues are Gly217, Leu219, Gly220, Pro223, and Leu230 (Figure 4.1B). None of other residues in the loop was sensitive to Ala mutation. Therefore, mutants containing Ala at these five positions were chosen for this study. In addition, we have also included AcrB<sub>P224G</sub>. P224 immediately follows the invariable residue P223. While the activity of AcrB<sub>P223G</sub> was close to that of the negative control, the activity of AcrB<sub>P224G</sub> was comparable to that of the wild type AcrB.<sup>158</sup> AcrB<sub>P224G</sub> was used as an example of a drastic change of amino acid not leading to an observable change of activity.



To increase the pool of AcrB variants with decreased trimer affinity, we also created several additional AcrB variants with mutations at the inter-subunit interface in the transmembrane domain. Although each AcrB subunit contains 12 THs, only a few residues from TH1 and TH8 which are close to the cytoplasmic side of the membrane are involved in inter-subunit interaction (Figure 4.1C). Based on the analysis of the crystal structure as well as sequence alignment result, we chose to mutate three invariant residues, Leu886, Glu893, and Trp895, in TH8 into Gly (Figure 4.2B). No mutational study was conducted in TH1 due to concerns that mutations in TH1 might interfere with membrane insertion. To create partially active mutant with defect in TH1-TH8 packing, we trimmed down the size of the side chains of these three residues by replacing them with Gly. We constructed single as well as double and triple mutants involving these residues.

```

A. EC 213QVAAGQLGGTTPPVKGQ-QLNASIIAQTR239 B. 871NQAPSLYAISLIVVFLCLAALYESWSI897
PA QISSGQLGGLPAVKGQ-QLNATIIIGKTR SQAPALYALSILVVFLCLAALYESWSI
NM QISAGSIGSLPAVRGQ-TVTATVTAQGQ SQTLLIYGLAVAAVFLVLAALYESWSI
HC QFAAGFFGQEPVRKDL-DFTYTVTTQGR GTGVIAFIFGLVFLILAAQYERWLM
SE QVAAGQLGGTTPPVKGQ-QLNASIIAQTR NQAPALYAISLIVVFLCLAALYESWSI
LL EISSGQIGAPPSAGTP-AYQFTVNVPGQ NLSYYIFMLSLLVYLILAGQYENWVA
SM QVAIGQLGGAPSVKGGQ-QLNATINAQSR SQTPLLYTLSLIVVFLCLAALYESWSV
MC QVSAGQLGTLPTNTDRVVINATISVQSY GQAPILYALSILVVFLCLAALYESWSV
: . : * : * * * * * * * * * * * * * * * * * * * * * * * * * * * *

```

Figure 4.2 Sequence alignment of residues in the loop (A) and TH8 (B), residues at the interface are shown as white fonts in black box). Numbers indicate the position of the starting and ending residues in the sequence of *E. coli* AcrB. Asterisks, colons and periods indicate identical, conserved and semi-conserved residues, respectively. The sequences are: EC, AcrB from *E. coli*; PA, MexB from *Pseudomonas aeruginosa*; NM, MtrD from *Neisseria meningitidis*; HC, HcanM9\_00968 from *Helicobacter canadensis*; SE, acridine efflux pump from *Salmonella enterica*; LL, AcrB from *Legionella longbeachae*; SM, HAE1 from *Tenotrophomonas maltophilia*; MC, AcrB from *Moraxella catarrhalis RH4*.

#### 4.3.2 AcrB variants displayed partial or full activities

To determine the effect of mutations on protein activity, we measured activities of AcrB constructs using both drug susceptibility and ethidium bromide (EtBr) accumulation. Drug susceptibility was performed as described.<sup>133</sup> Briefly, *E. coli* strain BW25113 $\Delta$ *acrB* was transformed with plasmids encoding the indicated AcrB constructs. The same bacterial strain containing plasmid encoding wild type AcrB or the empty cloning vector pQE70 was used as positive and negative controls, respectively. MIC was measured under the basal expression conditions. Four well established AcrB substrates, erythromycin (Ery), novobiocin (Nov), rhodamine-6-G

(R6G), and tetraphenylphosphonium (TPP) were chosen to represent the diversity of AcrB substrates of different polarity, structure, and charges. In addition, the presence or absence of AcrB causes a large MIC change for these drugs (ranging from 32-to 128-fold), which provides a wide dynamic range to reveal differences between the residual levels of activities of different mutants (Table 4.1). As shown in Table 4.1, AcrB tolerated mutations at the TM interface much better than mutations in the loop. In several cases a single mutation in the loop had a more dramatic effect on the activity of AcrB than the simultaneous mutation of three invariable residues in TH8.

Table 4.1 MIC and EtBr accumulation rate of BW25113 $\Delta$ *acrB* containing plasmid encoding the corresponding protein, and monomer stability of AcrB constructs.

Protein	MIC ( $\mu$ g/ml)				EtBr accumulation rate ( $s^{-1}$ )	Transition point ( $X_{SDS}$ )
	Ery	Nov	R6G	TPP		
No AcrB*	2.5	5	5	5	$1.4 \times 10^{-1}$	/
AcrB	80	160	320	640	$8.9 \times 10^{-3}$	$1.6 \pm 0.1$
AcrB <sub>G217A</sub>	10	40	80	80	/	/
AcrB <sub>L219A</sub>	5	20	20	10	/	/
AcrB <sub>G220A</sub>	5	40	80	20	/	/
AcrB <sub>P223G</sub>	5	10	20	20	/	/
AcrB <sub>P223A</sub>	10	40	40	40	/	/
AcrB <sub>P224G</sub>	80	160	320	640	/	/
AcrB <sub>L230A</sub>	5	20	20	10	/	/
AcrB <sub>L886G</sub>	80	160	320	640	$1.1 \times 10^{-2}$	$1.5 \pm 0.1$
AcrB <sub>E893G</sub>	80	160	320	640	$7.6 \times 10^{-3}$	$1.5 \pm 0.1$
AcrB <sub>W895G</sub>	80	160	320	640	$1.0 \times 10^{-2}$	$1.5 \pm 0.1$
AcrB <sub>L886G/E893G</sub>	40	40	320	40	$4.9 \times 10^{-2}$	$1.4 \pm 0.1$
AcrB <sub>E893G/W895G</sub>	40	40	320	40	$2.3 \times 10^{-2}$	$1.5 \pm 0.1$
AcrB <sub>L886G/E893G/W895G</sub>	20	10	160	20	$8.3 \times 10^{-2}$	$1.5 \pm 0.1$

\*: BW25113 $\Delta$ *acrB* transformed with the empty vector pQE70 was used as the negative control for activity.

To confirm that the increased drug susceptibility was due to a slower active efflux, we examined the substrate efflux rate of AcrB constructs using EtBr accumulation. Accumulation of EtBr by live *E. coli* cells was monitored by following the increase of fluorescence of EtBr.<sup>153</sup> Accumulation rate was inversely correlated with the capacity of efflux pumps transporting EtBr out of bacterial cells. EtBr is a substrate of AcrB and the EtBr accumulation has been used in several studies to reveal the activity of AcrB.<sup>153, 159, 160</sup> We measured the accumulation rate of BW25113 $\Delta$ *acrB* containing plasmid encoding AcrB with mutations in the transmembrane interface. The strains containing plasmids encoding AcrB with mutations in the loop were not included in

this measurement, since we observed changes in the stabilities of individual monomers due to those mutations (the result was published recently).<sup>151</sup> The same strain containing plasmid encoding wild type AcrB or the empty cloning vector pQE70 were used as positive and negative controls, respectively. As shown in Table 4.1, removal of AcrB led to approximately 16-fold increase in the accumulation rate. In the triple mutant, the accumulation rate was approximately 10-fold that of cells containing wild type AcrB. The increase of accumulation was consistent with the observed decrease of MIC in strains expressing AcrB mutants.

Neither MIC nor EtBr accumulation directly measures the drug efflux rate. They reflect the combined effects of the drug entering the cell, mainly via diffusion, and exiting via active efflux and passive diffusion. We have also attempted to measure AcrB activity directly using the recently developed Nile Red efflux assay.<sup>154</sup> We found that the difference between the positive ( $0.03 \pm 0.01 \text{ s}^{-1}$ ) and the negative controls ( $0.02 \pm 0.01 \text{ s}^{-1}$ ), *BW25113ΔacrB* containing wild type AcrB or no AcrB, was not large enough and the resolution was not high enough to resolve the differences in efflux activities among different mutants.

#### *4.3.3 Most AcrB variants used in this study have similar expression levels*

We measured the relative expression levels of all mutants used in this study. Plasmids encoding different AcrB constructs were transformed into *BW25113ΔacrB* for protein expression under the basal condition. Detergent-dissolved cell membrane samples obtained from freshly prepared log phase cells were analyzed using SDS-PAGE and

Western Blot analysis (Figure 4.3). The expression levels of all mutants were similar to the expression level of wild type AcrB except for AcrB<sub>E893G</sub>, which appeared to have a significantly higher expression level. Although it was not clear why the expression level of AcrB<sub>E893G</sub> was higher, these results indicated that the increased drug sensitivities and EtBr accumulation rates of *E. coli* strains that expressed AcrB mutants was not a result of reduced AcrB expression.

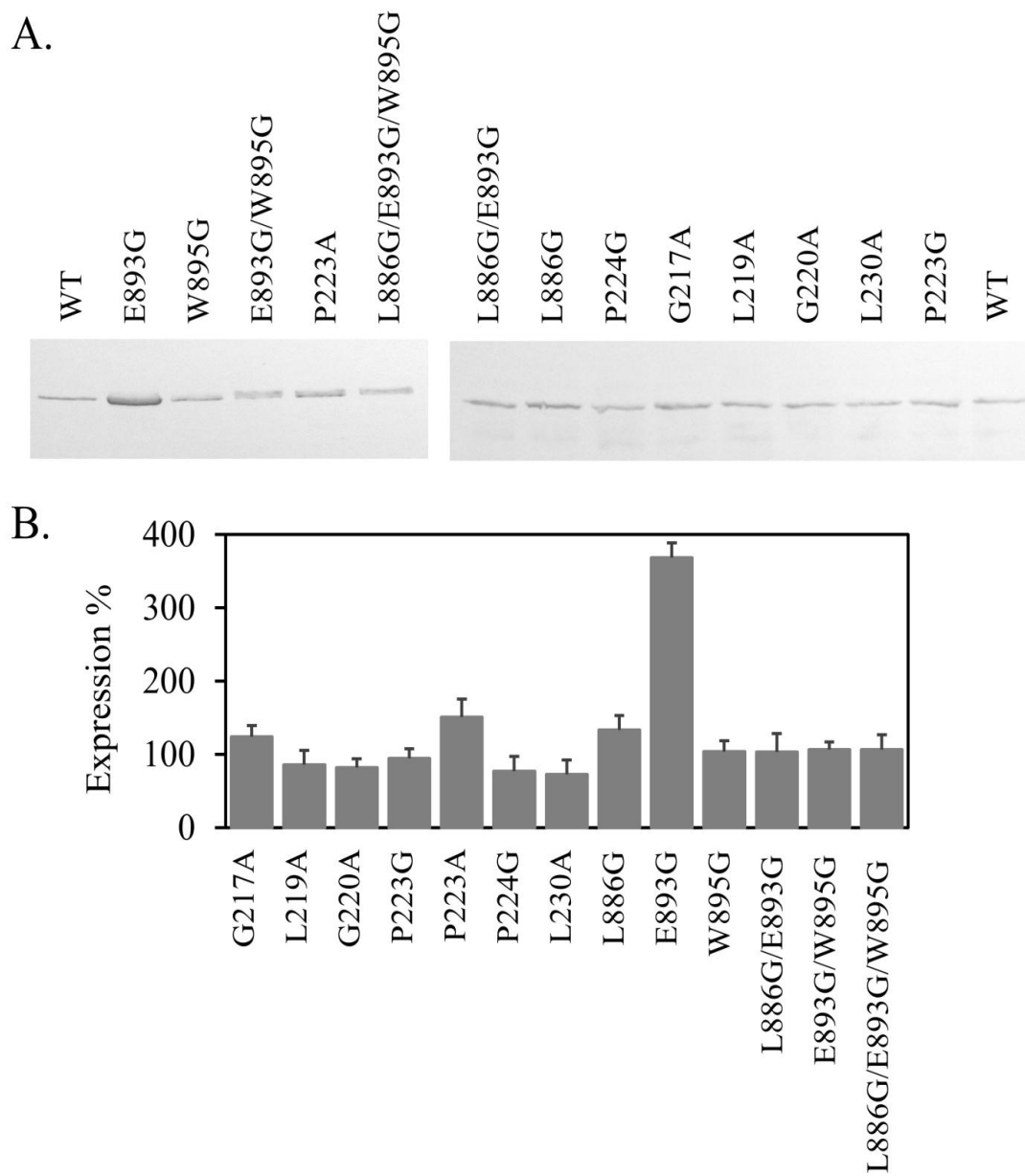


Figure 4.3 Western blot analysis of expression levels of all AcrB constructs. A. Image of representative blots. B. Expression of AcrB mutants normalized to the expression level of the wild type AcrB. Experiments were performed three times. The average value and standard deviation are shown.

#### *4.3.4 Mutations introduced in TH8 had little influence on the structure of monomers.*

The interaction between the protruding loop from one subunit and residues that collectively form a tunnel around the loop from the other subunit is the major contributor to the binding interface in AcrB. However, mutations in the loop or the tunnel that lead to changes of efflux activity have been shown to affect the stability of individual monomers.<sup>151</sup> To confirm whether mutations in the transmembrane domain would alter individual monomers, AcrB mutants were purified and examined using CD spectroscopy and fluorescence emission spectroscopy. As shown in Figure 4.4, all mutants had similar CD spectra as that of the wild type AcrB, suggesting that mutations in the transmembrane interface had little influence on the overall protein structure.



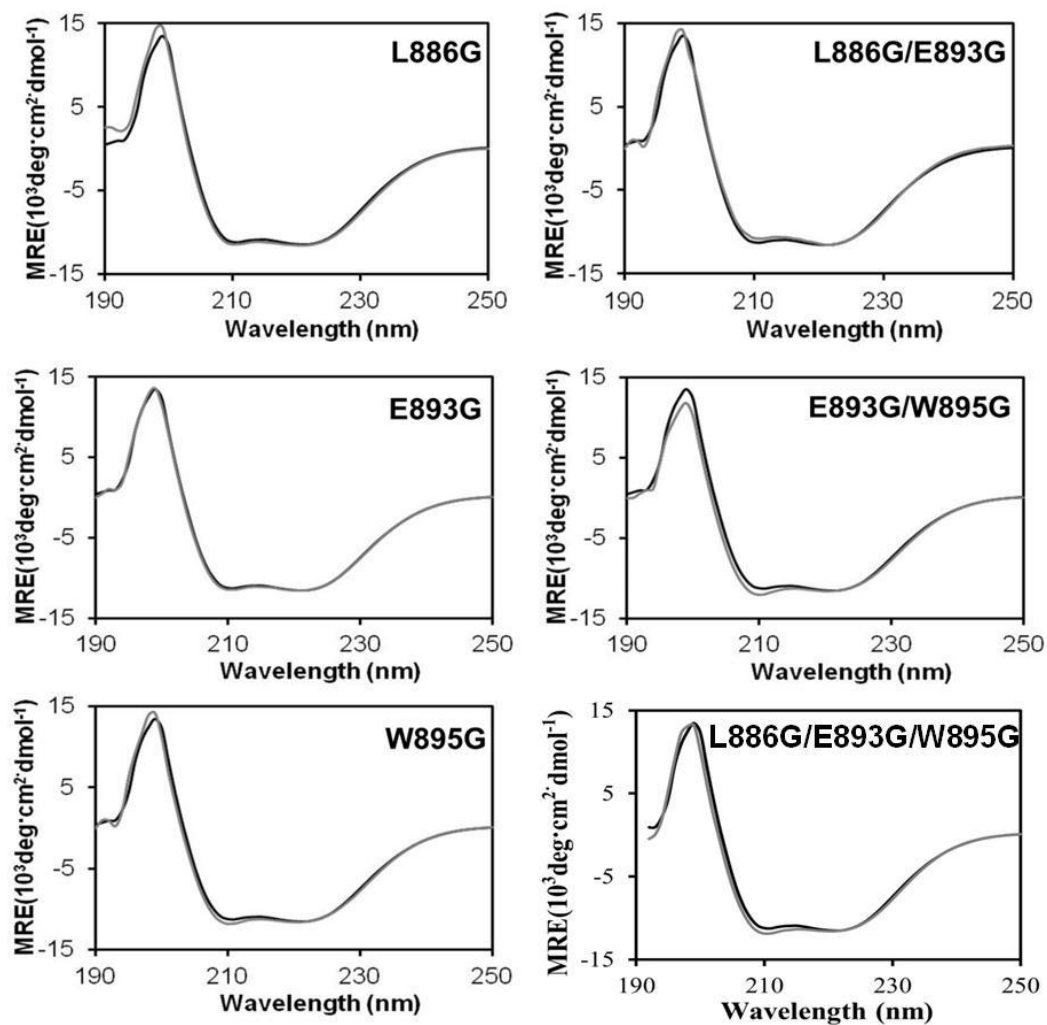


Figure 4.4 CD spectrum of each AcrB construct (grey) superimposed onto the spectrum of wild type AcrB (black). All mutants had similar overall structure as that of the wild type AcrB.

Furthermore, we performed SDS-induced denaturation monitored by intrinsic fluorescence. We previously showed that the sharp decrease of fluorescence observed was most likely due to the unfolding of monomers,<sup>151</sup> which was further confirmed by the observation that the unfolding profile and the molar ratio of SDS ( $X_{\text{SDS}}$ ) at the

transition point  $T_m$  was not affected by the introduction of an inter-subunit disulfide bond (C225-C777), which strengthened trimer association via a covalent bond (Figure 3.3 in Chapter III). Here we used this method to study the monomer stability in each AcrB construct. The denaturation profiles of all mutants tested were very similar to the profile of the wide type AcrB. Figure 4.5A shows the unfolding profiles of AcrB<sub>WT</sub> and the mutants. The transition point was calculated for comparison by fitting the curve with a single exponential equation as described in Materials and Methods section (Table 4.1). There was no drastic change in transition point in all mutants, suggesting that the mutations we introduced did not significantly disrupt the stabilities of AcrB monomers.

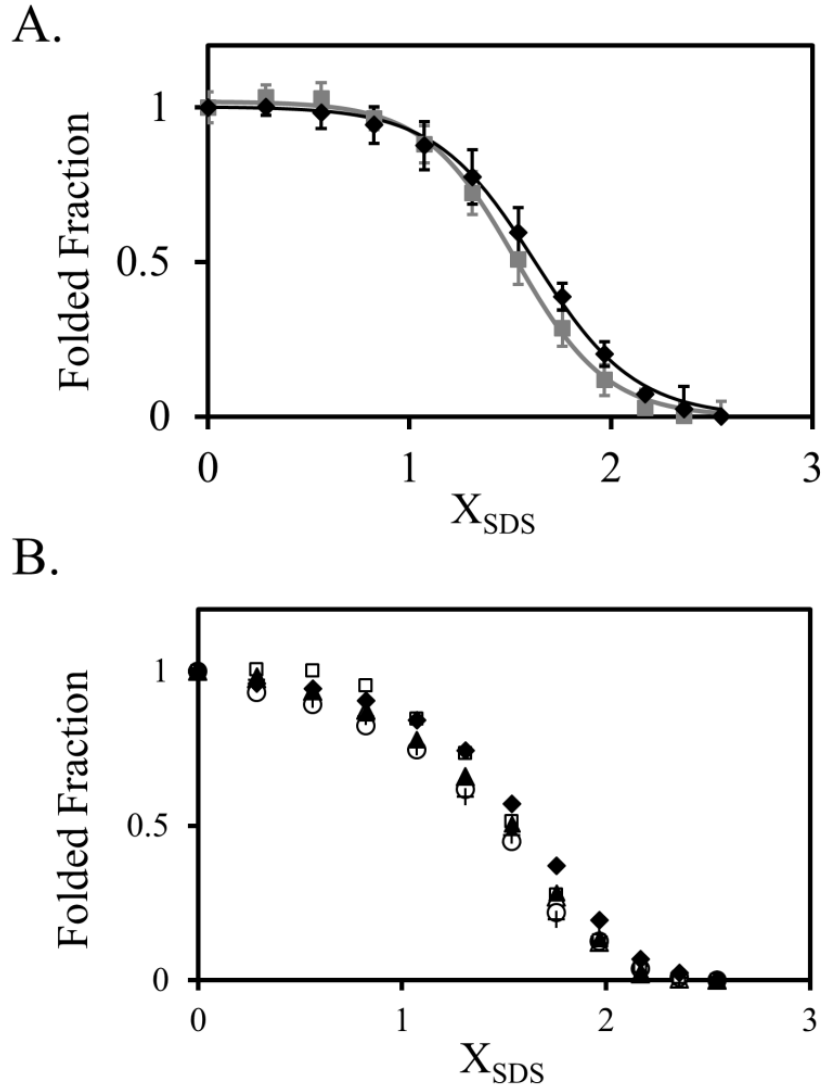
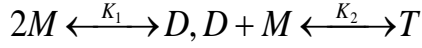


Figure 4.5 Stability characterizations. **A.** SDS induced unfolding profile of wild type AcrB (black diamonds) and AcrB<sub>L886G/E893G/W895G</sub> (grey squares) monitored by fluorescence emission. The curves showed the fitting using a single exponential equation. **B.** SDS induced unfolding profile of wild type AcrB (black diamonds) and AcrB<sub>L886G</sub> (black triangles), AcrB<sub>E893G</sub> (open triangles), AcrB<sub>W895G</sub> (open circles), AcrB<sub>L886G/E893G</sub> (black crosses), and AcrB<sub>E893G/W895G</sub> (open squares). Curves of fitting were omitted for visual clarity.

#### 4.3.5 Determination of the trimer association constant of purified AcrB variants

In the equilibration between AcrB monomer (M), dimer (D), and trimer (T):



The apparent trimer association constant  $K_{app}$  is:

$$K_{app} = K_1 K_2 = \frac{M_D}{M_M^2} \times \frac{M_T}{M_D M_M} = \frac{M_T}{M_M^3} \quad (\text{Eq. 4.1})$$

in which  $M_T$ ,  $M_D$ , and  $M_M$  are the molar concentrations of trimer, dimer, and monomer, respectively. For detergent solubilized membrane proteins, the actual volume that a protein can occupy is limited by the volume defined by detergent micelles.<sup>161, 162</sup>

Therefore, a mole fraction concentration of protein versus detergent is a more proper expression of the association constant of AcrB trimer in detergent micelles:

$$K_X = \frac{n_T / n_{Det}}{(n_M / n_{Det})^3} \quad (\text{Eq. 4.2})$$

in which  $n_T$ ,  $n_M$  and  $n_{Det}$  are moles of trimer, monomer, and detergent, respectively.<sup>161</sup>

The relationship between  $K_X$  and  $K_{app}$  is:

$$K_X = \frac{n_T / n_{Det}}{(n_M / n_{Det})^3} = \frac{n_T}{n_M^3} \times n_{Det}^2 = \left[ \frac{n_T / V}{(n_M / V)^3} \times \frac{V}{V^3} \right] \times \left[ \frac{n_{Det}^2}{V^2} \times V^2 \right] = \frac{M_T}{M_M^3} \times M_{Det}^2 = K_{app} \times M_{Det}^2 \quad (\text{Eq. 4.3})$$

in which  $V$  is the total volume, and  $M_{Det}$  is the molar concentration of detergent. Using this equation, we estimated and compared relative trimer stability of AcrB mutants.

BN-PAGE was used to estimate the trimer to monomer ratio, and thus their concentrations in the sample. BN-PAGE is a well-established method that has been

used broadly in the characterization of membrane protein oligomers.<sup>137, 163</sup> All AcrB constructs migrated as a mixture of trimer and monomer. The positions of AcrB monomer and trimer in BN-PAGE have been previously established.<sup>133, 136</sup> No dimer band was observed in any AcrB construct, indicating that the portion of dimer was negligible and therefore neglected during calculation. The concentrations of AcrB monomer and trimer were obtained by multiplying the total AcrB concentration in the sample by the percent of AcrB existed as monomer or trimer, respectively. A trimer association constant  $K_X$  was calculated using Equations 4.2 and 4.3 from the concentrations of detergent, and AcrB monomer and trimer (Table 4.2). The relative affinity,  $K_r$ , is the ratio between the  $K_X$  of each mutant and the  $K_X$  of the wild type AcrB. The free energy of trimer association of the wild type AcrB was calculated from  $K_X$  using the equation  $\Delta G_X = -RT \ln(K_X)$ , which was  $-11.9 \pm 0.8$  kcal/mol. The free energy difference of trimer association,  $\Delta \Delta G_X$ , was calculated from  $K_r$ . Representative BN-PAGE gel images were shown in Figure 4.6.

Table 4.2 Trimer stabilities of AcrB constructs.

Protein	$K_X$	$K_r$	$\Delta\Delta G_X$ (kcal/mol)
AcrB	$(6.6 \pm 3.2) \times 10^8$	1	/
AcrB <sub>L886G</sub>	$(3.8 \pm 2.1) \times 10^6$	$5.8 \times 10^{-3}$	3.1
AcrB <sub>E893G</sub>	$(3.0 \pm 0.8) \times 10^7$	$4.5 \times 10^{-3}$	1.8
AcrB <sub>W895G</sub>	$(3.0 \pm 0.9) \times 10^5$	$4.6 \times 10^{-4}$	4.6
AcrB <sub>L886G/E893G</sub>	$(1.8 \pm 0.6) \times 10^5$	$2.8 \times 10^{-4}$	4.8
AcrB <sub>E893G/W895G</sub>	$(1.7 \pm 0.9) \times 10^5$	$2.6 \times 10^{-4}$	4.9
AcrB <sub>L886G/E893G/W895G</sub>	$(1.9 \pm 1.0) \times 10^5$	$2.8 \times 10^{-4}$	4.8

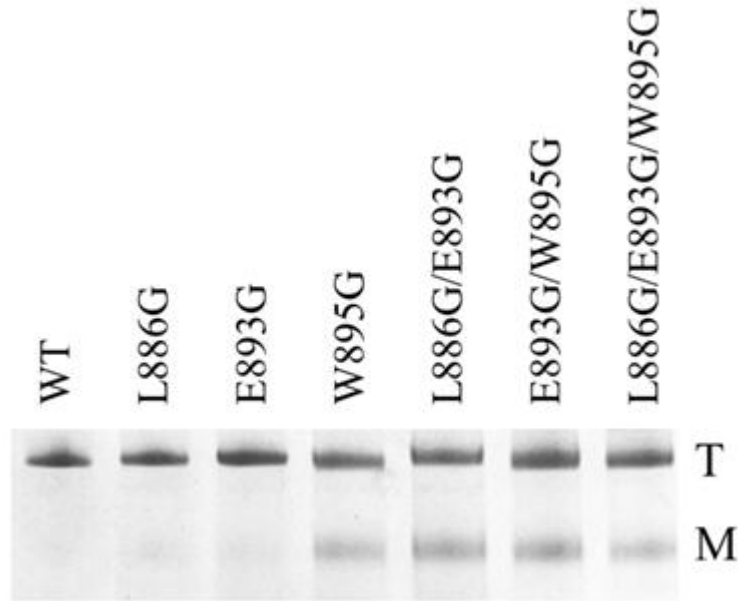


Figure 4.6 BN-PAGE gel of purified AcrB constructs. Positions of monomer and trimer bands are marked by M and T, respectively.

#### *4.3.6 Correlation between AcrB trimer stability and transport activity.*

To quantitatively review the relation between the relative trimer stability of a mutant and its biological activity, we plotted the relative trimer affinity ( $K_r$ ) of each mutant in detergent micelles versus the MIC (Figure 4.7A) and EtBr accumulation rate (Figure 4.7B) of wild type AcrB and its variants (only the AcrB constructs with mutations in the transmembrane interface). Relative trimer affinity  $K_r$  was obtained by designating the affinity of wild type AcrB as 1 (Table 4.2). Data for all substrates showed the same trend. The correlation between the trimer stability and drug efflux activity was clearly not linear.

To compare efflux activity measured using MIC and EtBr accumulation, we normalized MIC values for four substrates and EtBr accumulation rates to obtain the residual percent activity. Various substrates are intrinsically different in their binding affinities and interactions with AcrB. Therefore it was not surprising that the fold change on MIC and accumulation rate caused by the same mutation were not always the same. However, an overall trend could be observed, in which a mutant with lower activity transported all substrates with lower efficiency (Table 4.1). These residual activities were plotted against the relative trimer stability for seven AcrB constructs examined in this study (Figure 4.7C). The switch from no function to full function occurred in a very narrow stability range. The threshold trimer stability was required for efflux activity. This threshold value in terms of relative affinity is approximately 0.001, or three orders of magnitude lower than the affinity of the wild type trimer.

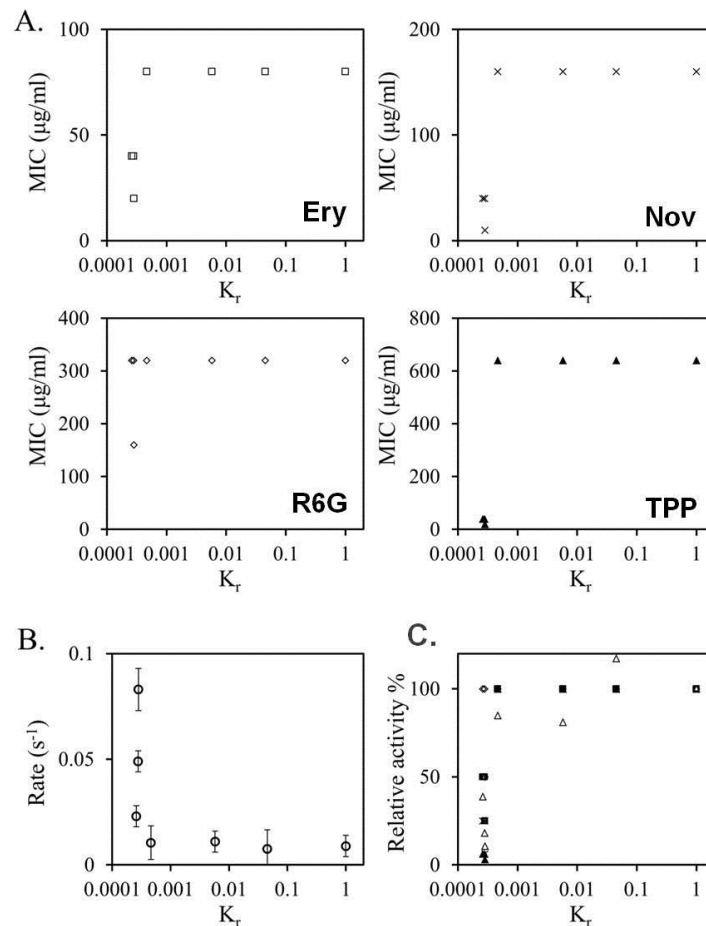


Figure 4.7 Correlation between AcrB trimer affinity and substrate efflux activity. A. MIC of four different AcrB substrates determined for BW25113 $\Delta$ acrB containing plasmid-encoded wild type AcrB or AcrB mutants plotted against their relative affinity. Substrate for each plot is indicated. B. EtBr accumulation rate of BW25113 $\Delta$ acrB containing plasmid-encoded wild type AcrB or AcrB mutants plotted against their relative affinity. C. Normalized MIC values and EtBr accumulation rate (diamonds) plotted against the relative trimer affinity. Substrates tested were Ery (open squares), TPP (black triangles), R6G (open diamonds), and Nov (black crosses). EtBr accumulation data are shown as open triangles.



#### 4.4 Discussion

Accurate determination of the oligomer's association constant of proteins in the cell membrane remains very challenging. Here we examined the correlation between the relative oligomer association affinity of purified AcrB mutants in detergent micelles and their biological activity. We have to acknowledge the limitations of the method used in this study. During the purification process, membrane protein was transferred from a native biological bilayer membrane environment to a less favorable detergent micelle environment. The transfer might cause a certain degree of reduction in trimer amount. The association constant that we obtained using purified AcrB in DDM detergent micelles might also be very different from the actual association constant in cell membrane. It is generally believed that the oligomer affinities of membrane proteins are much higher in phospholipid bilayers than in detergent micelles. For example, in two studies the association constants of model transmembrane helices are found 100-fold stronger in lipid bilayers than in detergent micelles.<sup>164, 165</sup> In addition, the relative trimer and monomer content in each mutant was estimated using BN-PAGE. BN-PAGE is a non-equilibrium method. During electrophoresis, the trimeric species and monomeric species are physically separated, which may cause more trimers to dissociate during the process and lead to a negative bias in the measured association constants. However, we speculate that a similar trend as we observed here likely exist between the trimer stability of AcrB in the actually cell membrane and its substrate efflux activity.

The first important observation of this study is that the stability-activity correlation was not linear. The trimer stability of an AcrB mutant needed to reach a threshold value for the protein to display activity. A drastic increase of activity occurred within a narrow range of trimer stability. To discuss the affinity in the thermodynamic energy terms, we calculated the free energy difference of trimer association ( $\Delta\Delta G_X$ ) from the relative association constant  $K_r$  (Table 4.2). When measured in the current system in detergent-dissolved state, this threshold value was approximately 5 kcal/mol. In other words, the association energy of the wild type trimer was 5 kcal/mol higher than the threshold value. We also calculated the free energy of trimer association of the wild type AcrB, which was approximately 12 kcal/mol. The value is in good agreement with membrane protein oligomerization energetics reported in the literature. Association energies have been determined for a few model membrane proteins and peptides in detergent micelles and phospholipids (Table 4.3). Glycophorin A transmembrane fragment (GpATM) was used as the model protein in three such studies, while fibroblast growth factor receptor 3 (FGFR3) and the transmembrane fragment of the M2 protein from influenza A virus were used in the other two studies. All model proteins form single transmembrane helices. Both GpATM and FGFR3 dimerize, while the M2 protein fragment forms a tetramer. The dimerization energy of GpATM in detergent micelles is 7 kcal/mol. The association constant for the tetrameric M2 protein fragment is determined to be  $2 \times 10^6$  in detergent micelles, corresponding to an association free energy of 8.6 kcal/mol. The larger association energy of the wild type AcrB trimer (approximately 12 kcal/mol) could arise from the larger intersubunit interface in AcrB as it is a much larger protein than the models. For both soluble and

membrane proteins, the oligomerization free energy per subunit are quite modest, that might be necessary to maintain flexibility of protein structure and association/dissociation state to suit functional requests. Changes in the quaternary state often affect a protein's biological function or activity, therefore stability of protein-protein interactions in such complexes is an important regulator for biological functions.<sup>135, 142, 143, 166-169</sup>

On a final note, substrate efflux facilitated by AcrB was measured as readout of AcrB activity. While we cannot completely rule out the possibility that the mutations studied affected substrate efflux via additional mechanisms such as substrate binding, proton relay, or interaction with AcrA/TolC, such possibilities are not very likely since the residues mutated were distant from these sites.

Table 4.3 Oligomer association constant and energy reported in literature.

System	Method	$K_x$	$\Delta G_x$
Glycophorin A transmembrane fragment (GpATM) in detergent micelles <sup>125, 161</sup>	Analytical ultracentrifugation	/	-7 kcal/mol
Transmembrane fragment of the M2 protein from influenza A virus in detergent micelles and phospholipid bilayer <sup>164</sup>	Thiol-disulfide equilibrium	$2 \times 10^6$ in detergent micelles $2 \times 10^8$ in lipid bilayer	/
Fibroblast growth factor receptor 3 (FGFR3) in phospholipid bilayer <sup>170</sup>	FRET	/	-3 kcal/mol
GpATM in vesicles derived from mammalian cell membranes <sup>171</sup>	Quantitative Imaging FRET	/	$-3.9 \pm 0.2^*$ kcal/mol
GpATM in detergent micelles and phospholipid bilayer <sup>165</sup>	Steric trap	/	-7 kcal/mol in detergent micelles -12 kcal/mol in bilayer

\*Standard state was defined as  $K_D=1$  per  $\text{nm}^2$ .

## 4.5 Conclusion

The majority of membrane proteins function as oligomers. However, it is not yet clear how the oligomer stabilities of these complexes correlate with their function. Understanding of the relationship between oligomer stability and activity is essential to protein research, and to virtually each and every cellular process that depends on the function of protein complexes. In this study, we obtained one of the first set of data

describing a direct correlation between the oligomer association constant and activity of a multiple spanning helical membrane protein. A non-linear correlation between AcrB trimer affinity and transport activity was observed, in which a threshold trimer stability was required to maintain efflux activity. Once the threshold was met, further increase of stability in the range observed had no observable effect on protein activity.

## CHAPTER V. MOLECULAR ENGINEERING OF AQUAPORIN Z

### 5.1 Introduction

Over 30% of the world's population lives in countries facing water shortage. This figure is predicted to double in 2025.<sup>172-174</sup> The overall fresh water storage on our planet is a largely fixed number. The only methods that can increase the usable fresh water supply beyond what is available from the water cycle are desalination of sea water, purification of ground water, and recycling of waste water. All these methods depend on the availability of efficient techniques to separate water from solutes and insoluble substances co-existing with water. The traditional process for desalting is distillation (i.e., the boiling of water), such as multi-effect distillation (MED) and multistage flash (MSF).<sup>175-178</sup> The membrane based desalting techniques, principally the reverse osmosis technology, are currently most applied method to separate water from salts with a lower energy cost than thermal distillations.<sup>179</sup> In the reverse osmosis desalting system, an applied pressure is used to overcome the osmotic pressure to drive water molecules through a semipermeable membrane and thus separate them from other chemical species. However, the low water permeability of the synthetic membrane currently used in the reverse osmosis diminishes their performance.<sup>178</sup> Therefore, the development of a synthetic membrane with a high water permeability becomes a hot topic in this area.

Biological membranes have an efficient water transportation system that allows water molecules to rapidly cross the hydrophobic membrane bilayer. The movement of the water molecules is facilitated by specific water channels (also called aquaporins)

embedded in the cell membrane, as discovered by Peter Agre in 1992.<sup>180</sup> Aquaporins are found in almost all organisms and are especially rich in the organisms with a strong ability to regulate the permeability.<sup>181-183</sup> Aquaporins give high water permeability and selectivity to biological membranes. Aquaporin Z (AqpZ) is an integral membrane protein discovered a decade ago as an effective water channel in *E. coli*.<sup>184</sup> Studies showed that the expression of AqpZ cRNA yielded *Xenopus* oocytes with a 15-fold increase in the osmotic water permeability, but failed to transport nonionic solutes such as urea and glycerol.<sup>184</sup> Due to its superb specificity and high permeability, AqpZ has been incorporated into artificial membranes used for water filtration and desalination.<sup>185-187</sup> In this study, we attempt to develop molecular engineering strategies to improve the stability of AqpZ, so that it can work under the high pressure and high salinity when used in water purification.

AqpZ forms a symmetric tetramer in the cell membrane, with each monomer acting as an independent water channel (Figure 5.1). Each AqpZ monomer is made up of six transmembrane  $\alpha$ -helices forming a right handed bundle.<sup>188</sup> The high-resolution crystal structure of AqpZ suggested that the channel is long (approximately 28 Å in length) and narrow (less than 4Å in diameter). AqpZ acts as a two-stage filter. The first stage with two highly conserved NPA (Asn-Pro-Ala) motifs forms a very narrow pathway (the narrowest point with a diameter of approximately 2 Å), and excludes most of the solutes due to the steric hindrance. The second stage (aromatic/arginine region) is proposed to repel positive charged ions (such as protons, hydronium) by arginine.<sup>189</sup> Native AqpZ tetramer is a highly stable complex and can maintain its oligomeric state

even in 1% SDS at neutral pH. In this work, we tested several molecular engineering approaches to stabilize the AqpZ structure and estimated the stability of the mutants by CD spectroscopy. Our results indicated that the structure of AqpZ is intrinsically stable and none of the mutation tested in this work has significantly improved its thermal stability. Additional investigation of the factors stabilizing AqpZ may reveal the molecular interactions critical for the AqpZ stability, which may be applicable to stabilize other membrane proteins.

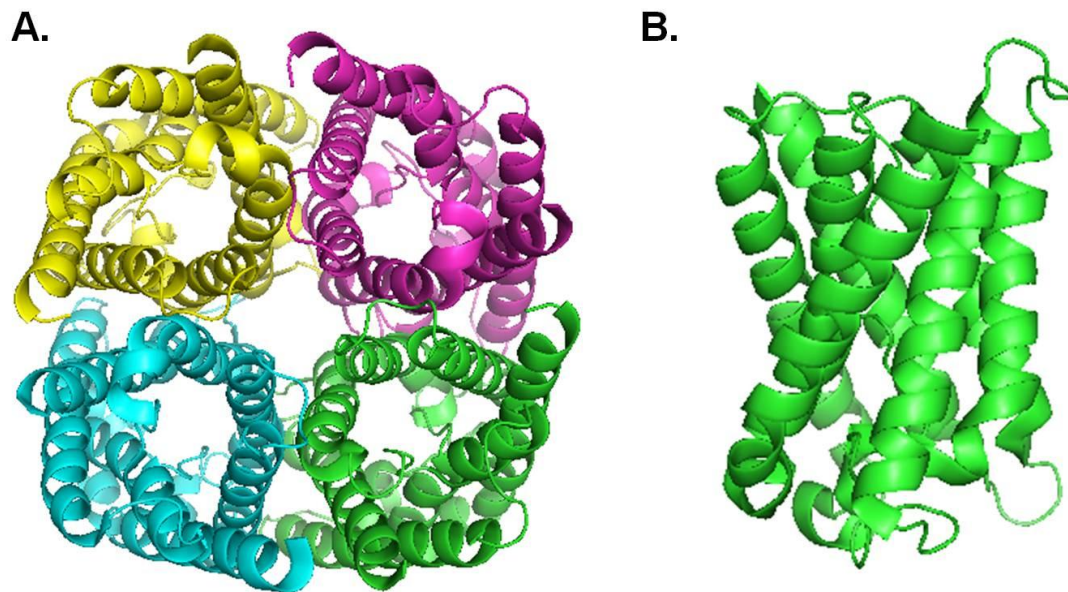


Figure 5.1 Structure of AqpZ (created from 2ABM.pdb<sup>19</sup> using Pymol<sup>18</sup>). A. Top view of AqpZ tetramer. Each subunit has a water conducting channel in the center of the helix bundle. B. Side view of one AqpZ subunit.



## 5.2 Materials and Methods

### 5.2.1 Plasmid construction, protein expression and purification

Genes encoding AqpZ was amplified from the genomic DNA of *E. coli* K-12 and inserted into plasmid pET28a between two restriction enzymatic sites (NdeI and XhoI). A six-histidine tag was introduced at the N terminal of protein for the convenience of the protein purification. Complementary primers used in the construction of expression plasmids were as follows: 5'-CATATGTTCAGAAAATTAGCAGCTGA-ATGTTTTGG and 5'-CTCGAGTTAATCACGCTTTTCCAGCAGGGTC with restriction enzymatic sites underlined. Mutations were introduced into the *aqpZ* gene in plasmid pET28a-AqpZ using the QuikChange Site-Directed Mutagenesis Kit following the manufacturer's instructions (Agilent Technologies) and confirmed through DNA sequencing. Plasmid containing *aqpZ* gene or its mutations was then transformed into *E. coli* strain C43 for protein expression.

Cells were cultured at 37 °C in Lysogeny Broth media containing 50 µg mL<sup>-1</sup> kanamycin to an OD<sub>600nm</sub> of approximately 0.6. Protein expression was induced by the addition of IPTG to a final concentration of 1 mM. After three hours at 37 °C, cells were harvested by centrifugation at 7,000 g for 10 min at 4 °C. Cell pellets were stored at -20 °C before purification. AqpZ was purified following the published protocol for AcrB with minor modifications.<sup>135</sup> In the elution step, the elution buffer contained 0.25 M imidazole, 0.03% DDM, 20 mM Na-phosphate, 0.3 M NaCl, pH 7.9. Protein samples were dialyzed overnight against the same buffer without imidazole at 4 °C. The same buffer was used throughout this study unless otherwise noted.

Purified protein was analyzed by SDS-PAGE and visualized after the gels were stained using Coomassie Blue. Protein concentration was determined using Pierce BCA Protein Assay Kit (Thermal Scientific INC., TX).

### *5.2.2 Quantification of the disulfide bonds formed in AqpZ<sub>G91C</sub>*

The efficiency of disulfide bond formation in AqpZ<sub>G91C</sub> was evaluated following a published protocol with minor modifications.<sup>135</sup> The entire process consists of three steps: the blockage of the free cysteines, the reduction of the disulfide bonds, and fluorescent labeling. Briefly, the purified protein was treated with iodoacetamide (IAM) and SDS at the final concentrations of 10 mM and 4% (w/v), respectively, for 30 min at 37 °C. IAM blocks the free Cys residues, but has no effect on the disulfide bonds. After the blockage, DTT was added to the mixture to a final concentration of 50 mM to break the disulfide bonds into free thiols. After 1 h incubation at 37 °C, protein was precipitated using 15% trichloroacetic acid (TCA). After centrifugation, the precipitate was washed with cold acetone and then resolubilized in a buffer solution containing 4% SDS and 50 mM Tris (pH 8.0). The precipitation and washing steps removed DTT from the protein sample. The freshly generated thiol groups were immediately labeled using 5mM 5-maleimido-fluorescein (F-MAL). The labeling reaction was incubated at room temperature for 15 min before it was stopped by the addition of 50 mM of DTT. The protein sample was subjected to SDS-PAGE. After the remaining free fluorescence dye migrated out of the gel, the gel was removed and the fluorescence image was taken under the UV light. The same gel was then stained using Coomassie

blue stain and the image of the gel was taken again under normal white light. Positive and negative controls were performed without the absence of the blockage or the reduction step. Gel images were analyzed using software ImageJ to obtain the percentage of the disulfide bonds.<sup>93</sup> Assuming that all Cys have the same labeling efficiency, fraction of Cys involved in the formation of the disulfide bonds was calculated using following equation:

$$F = \frac{F_s}{F_p \times \frac{2}{3}}$$

where  $F$  is the fraction of Cys that formed disulfide bonds;  $F_s$  and  $F_p$  are the fluorescence intensities of the sample and positive control, respectively.  $\frac{2}{3}$  indicates that two out of three Cys in AqpZ<sub>G91C</sub> could potentially form a disulfide bond.

### *5.2.2 Protein thermal denaturation monitored using CD spectroscopy and fluorescence spectroscopy*

CD spectra and thermal denaturation experiments were conducted on a JASCO J-810 spectrometer following a published protocol.<sup>136</sup> Purified wild type AqpZ was first treated with different concentrations of urea (0, 4 M, 6 M, and 8 M). After incubation at 4 °C for 30 min, ellipticity at 222 nm of protein sample was measured as temperature was increased from 40 °C to 100 °C with a temperature interval of 1 °C/min. Spectral scans were collected at 40 °C and 100 °C in the wavelength range between 210 to 250 nm. The CD signals below 210 nm could not be obtained due to the presence of urea.

Thermal denaturation of the purified AqpZ was monitored by intrinsic tryptophan fluorescence by a LS-55 fluorescence spectrometer (PerkinElmer, Inc., Waltham, MA). The decrease of the intensity of fluorescence emission was recorded at the excitation wavelength of 280 nm as the temperature increased from 20 °C to 80 °C.

## 5.3 Results and Discussion

### 5.3.1 A rational design of positions to be mutated

We used two methods to improve the intrinsic stability of AqpZ: one was the introduction of proline into  $\beta$ -turns, and the other was the introduction of a disulfide bond into AqpZ monomer by site directed mutagenesis. Pro is commonly found in  $\beta$ -turns, due to its rigid backbone structure.<sup>190, 191</sup> An increase of conformational entropy is one of the major forces driving protein unfolding. To stabilize their structure, proteins prefer a residue with a rigid side chain (such as Pro) to one with a flexible side chain in their  $\beta$ -turn structure to minimize the entropy gain of the unfolding. The majority of naturally occurring membrane proteins do not have their stability highly optimized. This is likely due to a certain degree of the flexibility required for conformational change. One of our approaches to improve the stability of AqpZ was to replace flexible amino acid residues with a more rigid Pro residue. Several studies have shown that the introduction of Pro into  $\beta$ -turns is an effective way to stabilize the protein tertiary structure, especially if Pro is introduced at the secondary site ( $i + 1$ ) in a  $\beta$ -turn (Figure 5.2A).<sup>192-195</sup> AqpZ contains eight  $\beta$ -turns (Figure 5.3). Three of the eight  $\beta$ -turns contain Pro at the  $i+1$  position (turns number 1, 5, and 8). We replaced the  $i+1$  residues in two (T107 and A27) out of other five  $\beta$ -turns with Pro to examine

whether the method would improve the stability of AqpZ. Since the residue is not conserved, we speculated that such mutations would not affect the structure and function of AqpZ.

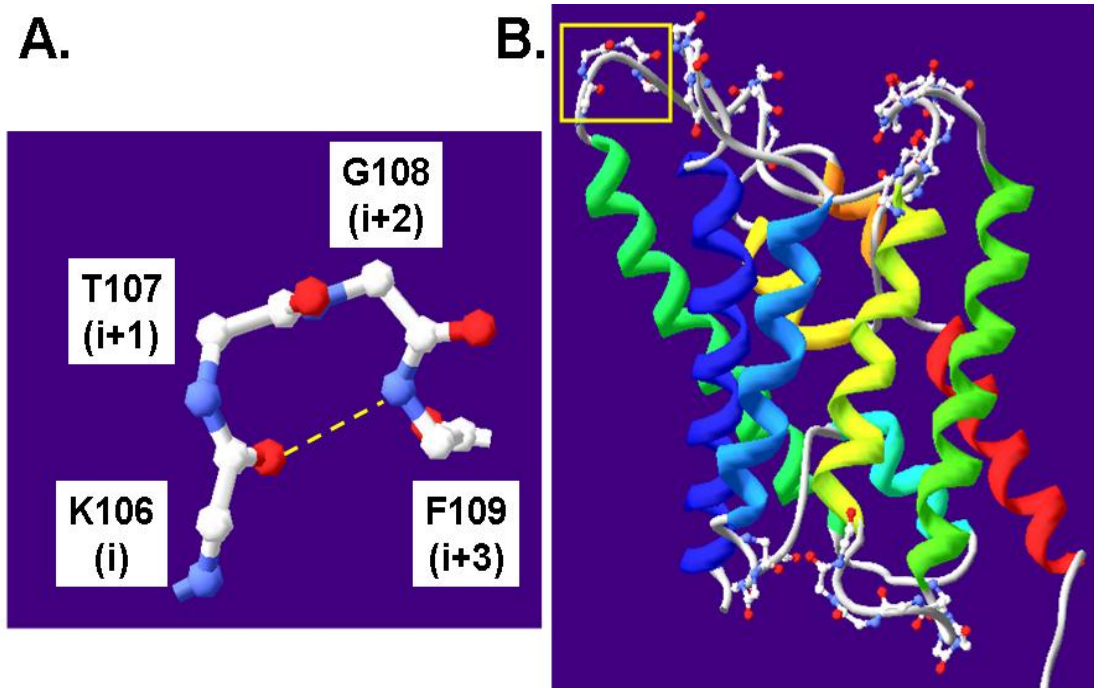


Figure 5.2  $\beta$ -Turns and their presence in AqpZ structure. A. The backbone trace of a representative  $\beta$ -turn from AqpZ (residues K106 to F109). The carbonyl of residue  $i$  forms a hydrogen bond with the amine of  $i+3$ . B. The ribbon diagram of an AqpZ monomer (1RC2.pdb<sup>188</sup>). Backbone trace is shown for stretches that form  $\beta$ -turns, with the  $\beta$ -turn formed by K106 to F109 as shown in A.

```

                                     1-----1-----11
AqpZ M-----FRKLAACEFGTFWLVFVGCGSAVLAAGF-----P-----ELGIGFAGVALAFGLTVLTMFAFV
Aqp0 MWE---LRSASFWRICAEEFFASLFYVFFGLGASLRW---AP-----GPLHVLQVALAFGLALATLVQAV
Aqp1 MAS--EFKKLFWRAVVAEFLATTLFVFIISIGSALGF-KYPVGNQ-----TAVQDNVKVSLAFGLSIATLAQSV
AqpM MVS-----LTKRCIAEFIGTFILVFFGAGSAATLMIASGGTSPNPFNIGIGLLGGLGDWVAIGLAFGFAIAASIYAL
GlpF MSQT-----STLKGQCIAEFLGTGLLIFVGVGVAAL-KVAG-----ASFGQWEISVIWGLGVAMAIYLT
*          * * . . : . * .          : . : . :
                                     2222          3333          44445
AqpZ GHISGGHFNPAVTIGLWAGGRFPAKEVVGIVIAQVVGIVAAALLYLIAS-----GKTGFDAASGFASNGYGEHS
Aqp0 GHISGAHVNPVTF AFLVGSQMSLLRAICYMVAQLLGAVAGA AVLYSVTP-----PAVR-----G-----NLALNT
Aqp1 GHISGAHLNPAVTLGLLLSCQISIFRALMYIIAQCVGAIVATAILSGITS-----SLTG-----N-----SLGRND
AqpM GNISGCHINPAVTIGLWSVKKFPGREVVPYIIAQLLGAAGFSFIFLQCAGIG-----AATV-----G-----GLGATA
GlpF AGVSGAHLNPAVTIALWLFACFDKRVIPFIVSQVAGAFCAAALVYGLYYNLFFDFEQTHHIVRGSVESVDLA--GTFSY
. : * * * . * * * : * . . : : * * . . : . .
                                     -555          66-66777-7          8888
AqpZ -PGGYMSLSALVVELVLSAGFLLVIHGAT-DK-FAPAG-FAPIAIGLALTLIHLISIPVTNTSVNPARSTAVAFQG--GW
Aqp0 LHPGVSVGQATIVEIFLTLQFVLCIFATYDERRNRLG-SVALAVGFSLTLGHLFGMYITGAGMNPARSFAPAILTR--NF
Aqp1 LADGVNSGQGLGIEIIGTLQVLVLCVLTATDERRRDLGG-SAPLAIGLSVALGHLLAIDYTGCGINPARSFGSAVITH--NF
AqpM PFPGISYQAMLAEVVGTFLMITMGI AVDE-RAPKG-FAGIIIGLTVAGIITTLGNISGSSLNPARTFGPYLNDM--IF
GlpF PNPHINFVQAFVAVEMVITAILMGLILALTDGNGVPRGPLAPLLIGLLIAVIGASMGPLTGFMNPARDFGPKVFAWLAW
. . . * . : : : . . * : : * : : . . : * * * * . : : :

```

Figure 5.3 Sequence alignment of AqpZ with its homologues with known structures. Asterisks, colons and periods indicate identical, conserved and semi-conserved residues, respectively. Positions of  $\beta$ -turns in the structure of AqpZ are highlighted by the numbers on top of the AqpZ sequence. Of the 8  $\beta$ -turns in AqpZ, three intrinsically contain Pro at the  $i+1$  position (turns number 1, 5, and 8). The corresponding structure files in the protein data bank for the proteins used in the alignment are: 1R2C.pdb for AqpZ,<sup>188</sup> 1YMG.pdb for Aqp0,<sup>196</sup> 1FQY.pdb for Aqp1,<sup>197</sup> 2F2B.pdb for AqpM,<sup>198</sup> and 1FX8.pdb for GlpF.<sup>199</sup>

The introduction of disulfide bonds is another simple and effective strategy that could be used to improve the protein tertiary stability by creating new linkages between neighboring helices. There are two intrinsic Cys in the sequence of AqpZ, C9 and C20 (Figure 5.4A), both existing as free sulfhydryl groups. While the side chain of C20 points to the water transduction channel, the side chain of C9 is exposed to the lipid bilayer. We took advantage of C9, which is within the disulfide bond distance to two

residues from neighboring helices, A87 and G91 (Figure 5.4B). We replaced A87 or G91 with Cys and expected that the introduced disulfide bond would enhance the interaction between the neighboring helices. In addition, since the function of AqpZ does not involve a large-scale conformational change, we expect the introduction of a disulfide bond at a location distant from the water conducting channel should have a minimum impact on activity.

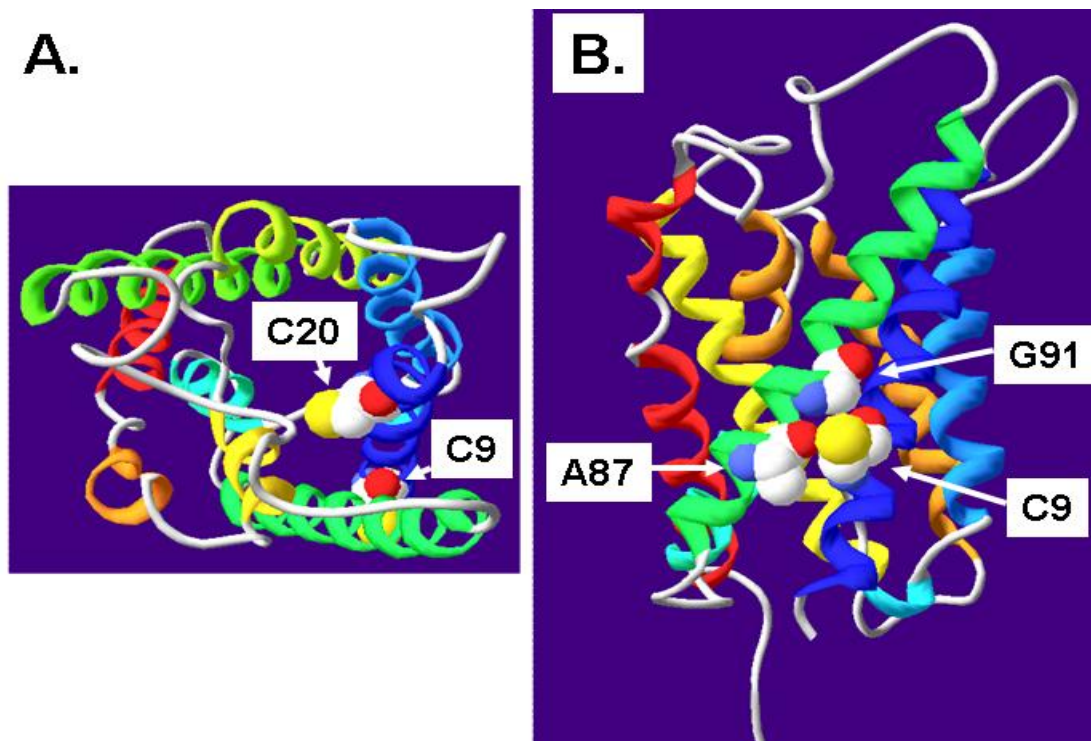


Figure 5.4. Ribbon diagram of AqpZ monomer structure (1RC2.pdb<sup>188</sup>). A. Top view of the structure with positions of the two intrinsic Cys highlighted using space filled model. B. Side view of the structure with positions of C9 and two residues close to C9 in space, A87 and G91.

### 5.3.2 None of mutations increased the thermal stability of AqpZ

To assess the effect of mutations on the stability of AqpZ, we conducted temperature-induced denaturation monitored by far UV CD spectroscopy. As described in previous chapters, CD is one of most general and basic tools to study protein unfolding, in which a melting temperature ( $T_m$ ) could be determined as a measurement of the thermal stability of a protein. For  $\alpha$ -helical proteins, an increase of temperature disrupts structures of the protein, resulting in a drop of CD signal at two characteristic negative peaks (208 nm and 222 nm) (Figure 5.5A). Protein unfolding thus could be observed by following the decrease of CD signal at 222 nm. The denaturation profile of wild type AqpZ (Figure 5.5B) was obtained. A high  $T_m$  (approximately 94 °C) suggested the high thermal stability of AqpZ.

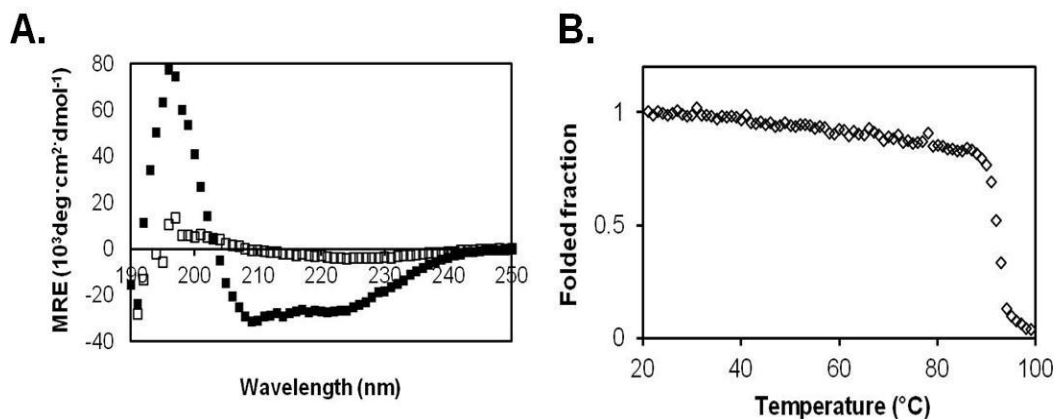


Figure 5.5 Thermal denaturation of AqpZ monitored using far UV CD spectroscopy. A. CD spectra of AqpZ at 20 °C (filled) and 100 °C (open). B. Temperature induced unfolding profile of AqpZ followed by fixing the wavelength to 222 nm.



We repeated the denaturation experiment in the presence of urea, a widely used protein denaturant. CD signals below 210 nm could not be observed because of a very strong absorption of urea at and below this wavelength.<sup>200</sup> The presence of urea up to 8 M barely affected the secondary structure of AqpZ (Figure 5.6A), but significantly reduced its thermal stability (Figure 5.6B).  $T_m$  of wild type AqpZ decreased by approximately 10 °C and 20 °C in the presence of 6 M and 8 M urea, respectively. On the other hand, the presence of 4 M urea had little effect on the melting temperature.

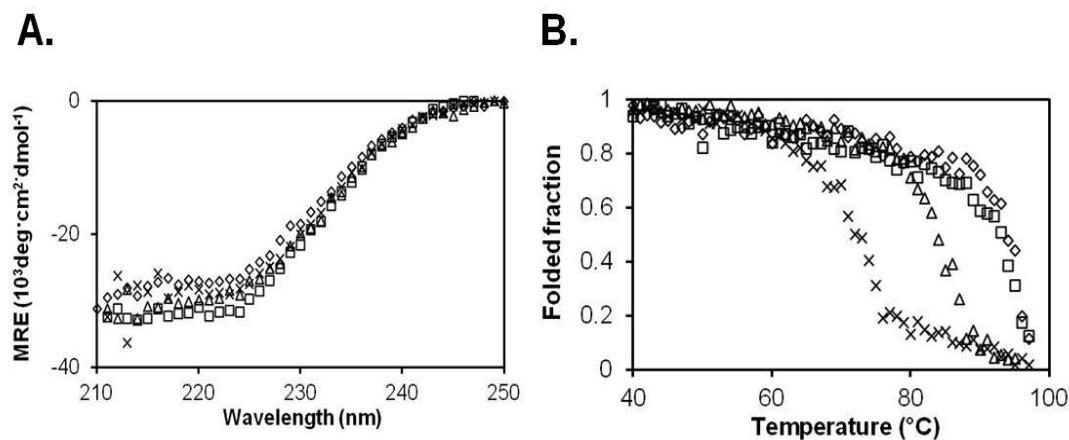


Figure 5.6 Effect of urea on secondary structure and melting point of AqpZ. A. CD spectra of AqpZ in the absence (diamonds) and presence of urea at 20 °C. B. Thermal denaturation of AqpZ followed by fixing the wavelength to 222 nm. Urea concentrations tested are 4 M (squares), 6 M (triangles), and 8 M (crosses).

CD spectra and temperature scans of all AqpZ mutations were performed in the presence of 6 M urea. A higher concentration of urea than 6 M significantly increased the spectral noise. The CD spectra of all AqpZ mutants, except A27P, overlapped with that of the wild type protein, suggesting that mutations did not alter the overall protein

structure (Figure 5.7A). The loss of the AqpZ<sub>A27P</sub> secondary structure in the presence of urea indicated a less stable structure caused by the introduction of the Pro residue. The temperature-induced unfolding curves of all other AqpZ mutants were obtained and compared with the wild type protein (Figure 5.7B). The  $T_m$  of the protein was not enhanced by the introduction of the designed mutations.

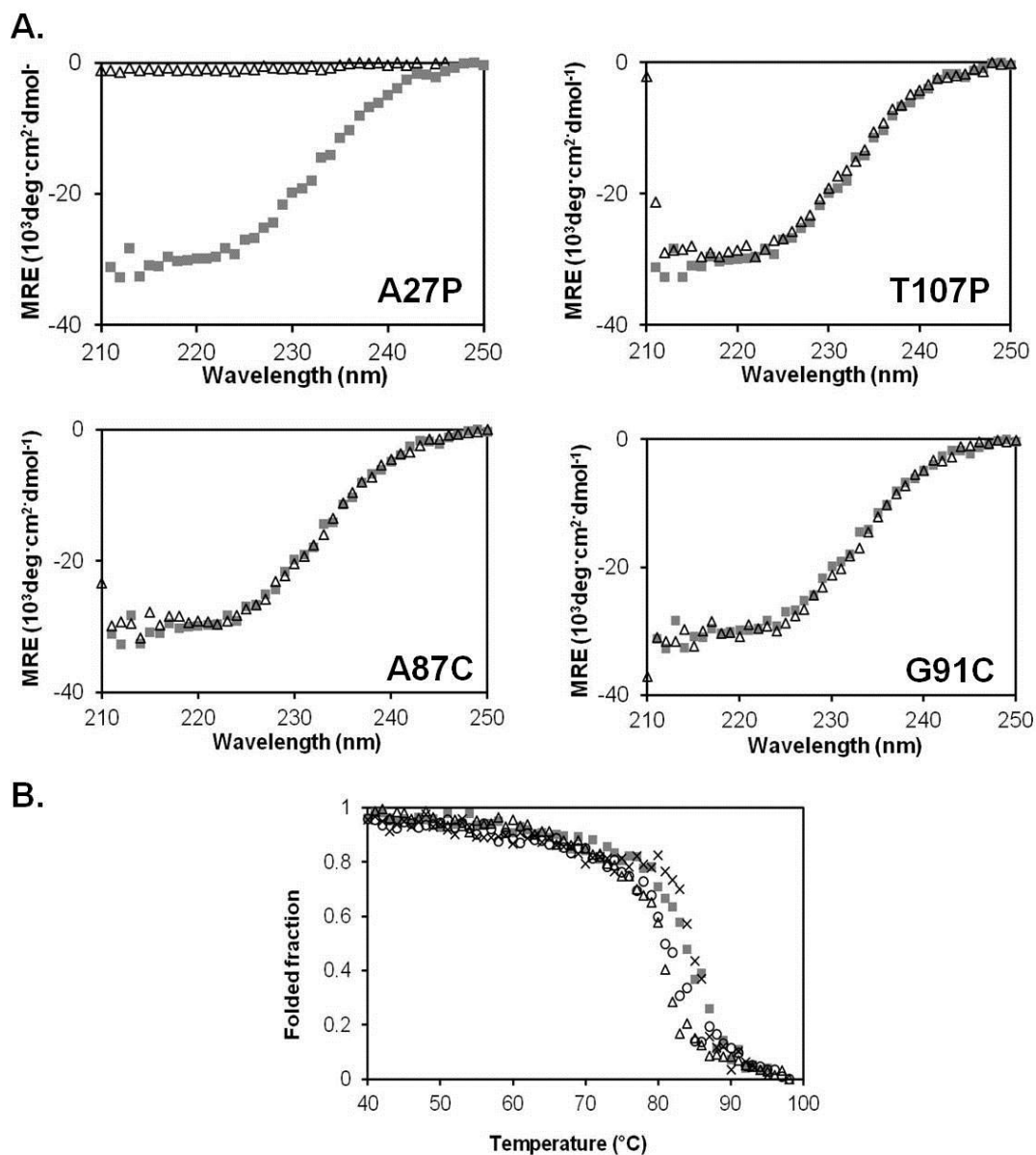


Figure 5.7 Thermal stabilities of AqpZ and its mutants measured by CD spectroscopy.

A. CD spectra of AqpZ (grey squares) and its mutants (triangles) at 20 °C. Mutations are indicated in graphs. B. Unfolding profiles of AqpZ (grey squares) and its mutants (AqpZ<sub>T107P</sub>, circles; AqpZ<sub>A87C</sub>, triangles; AqpZ<sub>G91C</sub>, crosses).

### 5.3.3 Disulfide bond formations in AqpZ<sub>G91C</sub>

To confirm that the introduced Cys actually formed a disulfide bond with Cys9, we monitored the formation of the disulfide AqpZ<sub>G91C</sub>.<sup>135</sup> According to the method, cys involved in the formation of the disulfide bond could be labeled by F-MAL (Figure 5.8B/D, lane 2). Therefore, the presence or absence of the disulfide bond could be observed by examining the fluorescence labeling. The positive control was the same protein with all cys labeled by F-MAL (Figure 5.8A/D, lane 1). The negative control was included to confirm the lack of non-specific labeling to non-Cys sites (Figure 5.8C/D, lane 3). Approximately 50% of C9 and C91 formed a disulfide bond. However, the introduction of a disulfide bond did not improve the stability of the protein tertiary structure.

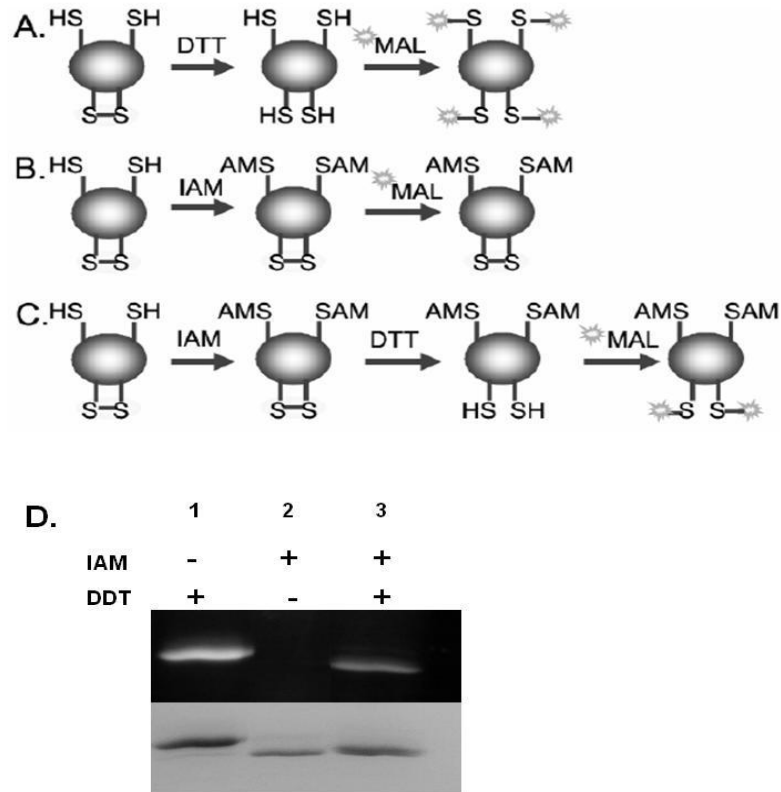


Figure 5.8 Disulfide bond formation in AqpZ<sub>G91C</sub>. A. Positive control. Purified protein was incubated with DTT, followed by labeling using F-MAL. All Cys residues in the protein could be labeled. B. Negative control. Purified protein was treated by IAM before F-MAL labeling. None of the Cys could be labeled. C. Experimental group. Purified protein was first treated by IAM, reduced using DTT, and then labeled using F-MAL. Original free Cys could not be labeled, while Cys protected by a disulfide bond during the IAM treatment could be labeled after DTT reduction. D. Purified AqpZ<sub>G91C</sub> was divided into three aliquots, and then treated according to the procedure described in A (lane 1), B (lane 2), and C (lane 3), respectively. Purified AqpZ<sub>G91C</sub> contains one free Cys and one disulfide bond. Protein bands analyzed using SDS-PAGE was photographed under UV light (top) and then visualized by Coomassie blue stain under white light (bottom).

## 5.4 Prospectus

Our results indicated that the thermal stability of AqpZ has been highly optimized. This is not common for membrane proteins. It was shown by Bowie and co-workers that the frequency of stability-enhancing mutations is remarkably high for membrane proteins.<sup>118, 201-203</sup> Roughly 10% of random mutants were found to improve the stability of a membrane protein, indicating the prevalence of the membrane proteins with moderate stability. Investigation of the mechanism behind the remarkable stability of AqpZ is a future direction of this project. Knowledge about the stabilizing factors could be used in rational design efforts to stabilize the membrane proteins used in the structural determination and therapeutic application. Searching for a method to quantitatively assess the overall stability of AqpZ will be a second subproject. In this study, the protein stability is primarily assessed through measuring the melting temperature using CD spectroscopy, which reveals the stability of the protein secondary structure. A more comprehensive evaluation on the entire structure of the protein is desirable for better understanding its stabilizing factors.

To investigate stabilization factors of AqpZ, the first task is to figure out the reasons for the membrane proteins instability. One of the reasons is considered to be related to protein dynamics.<sup>204</sup> The operation of many membrane proteins relies on conformational changes. An increase in the stability may lead to a decrease of the structural flexibility and a lower activity. Secondly, the stability of the membrane proteins is usually measured in detergent micelles, not in the natural cell membrane. It is possible that they have already achieved a degree of stability in the cell membrane

that is sufficient for cell viability.<sup>203, 205</sup> As discussed in Introduction, the selectivity of AqpZ relies on the size exclusion and electrostatic repulsion in the central pores of monomers. The transportation of water molecules mediated by AqpZ is driven by the osmotic pressure generated between the cytoplasm and the environment, suggesting that AqpZ does not undergo a conformational change to perform its function. This feature might be one of the prerequisites for proteins with a highly optimized stability. However, other known aquaporins fold into similar structures and have similar transport characteristics, but with much lower stabilities. For example, spinach aquaporin SoPIP2;1 could only maintain its tetrameric state in a mild detergent like DDM,<sup>206</sup> whereas AqpZ tolerances harsh detergent like SDS up to 1% at neutral pH.<sup>207</sup> AqpZ is very hydrophobic and its tetramer appears to be tightly packed.<sup>207</sup> Trypsin failed to cleave at any of amino acids in AqpZ when the protein was reconstituted into proteoliposomes. Therefore, studies on factors stabilizing AqpZ could start with an investigation of the interface between AqpZ monomers. The interface between the monomers in several aquaporins could be calculated and compared using the online server ProtorP.<sup>156</sup> Mutagenesis studies could be performed subsequently to determine the critical residues and interactions in the subunit association. The tetramer stability of AqpZ could be determined using both SDS-PAGE and fluorescence polarization spectroscopy as described in Section 3.3.4.

Another technical difficulty encountered in this study is the lack of a proper method to monitor the unfolding of the AqpZ tertiary structure. Fluorescence spectroscopy has been extensively used to evaluate the stability of protein tertiary structure.<sup>114, 208, 209</sup>

Thermal unfolding of AqpZ monitored using intrinsic fluorescence emission was attempted. However, an obvious transition was missing in the unfolding profile (Figure 5.9). A recently reported dye-based fluorescence assay is a potential method to assess the stability of the tertiary structure of AqpZ.<sup>210</sup> This assay is based on the fact that the dye *N*-[4-(7-diethylamino-4-methyl-3-coumarinyl) phenyl]-maleimide (CPM) becomes fluorescent after reacting with a free sulfhydryl group. Cys residues are frequently at helix-helix interaction site in the transmembrane segment of the membrane proteins, which makes them ideal sensors for the overall integrity of the helical membrane protein structure. Those Cys residues protected by the neighboring helices in the native protein were gradually exposed to the CPM dye as the protein structure collapses with an increase of temperature or concentration of a denaturant, resulting in a surge of fluorescence signal. AqpZ unfolding could potentially be monitored using this CPM based method.

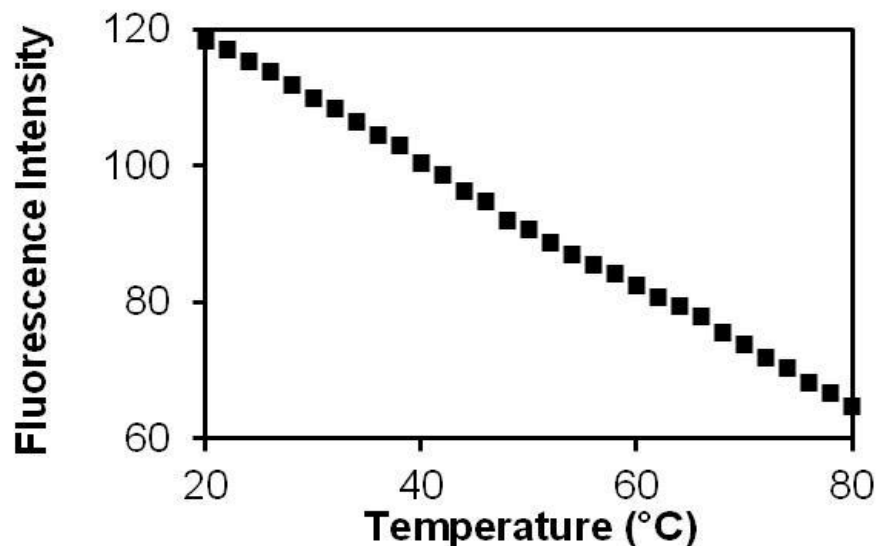


Figure 5.9 Thermal unfolding of AqpZ monitored using intrinsic fluorescence.

Copyright © Cui Ye 2014



## REFERENCES

1. Aronson, S. M. (1997) The naming of antibiotics, *Med. Health R I.* 80, 180.
2. Calderon, C. B., and Sabundayo, B. P. (2007) Antimicrobial classifications: drugs for bugs, in Schwalbe R, Steele-Moore L, Goodwin AC. Antimicrobial Susceptibility Testing Protocols. CRC Press.
3. von Nussbaum, F., Brands, M., Hinzen, B., Weigand, S., and Habich, D. (2006) Antibacterial natural products in medicinal chemistry--exodus or revival? *Angew. Chem. Int. Ed. Engl.* 45, 5072-5129.
4. Butler, M. S. (2004) The role of natural product chemistry in drug discovery, *J. of Nat. Prod.* 67, 2141-2153.
5. Pommier, Y., Leo, E., Zhang, H. L., and Marchand, C. (2010) DNA Topoisomerases and Their Poisoning by Anticancer and Antibacterial Drugs, *Chem. Biol.* 17, 421-433.
6. Tenson, T., Lovmar, M., and Ehrenberg, M. (2003) The mechanism of action of macrolides, lincosamides and streptogramin B reveals the nascent peptide exit path in the ribosome, *J. Mol. Biol.* 330, 1005-1014.
7. Fisher, J. F., Meroueh, S. O., and Mobashery, S. (2005) Bacterial resistance to beta-lactam antibiotics: compelling opportunism, compelling opportunity, *Chem. Rev.* 105, 395-424.
8. Axelsen, P. H. (2008) A chaotic pore model of polypeptide antibiotic action, *Biophys. J.* 94, 1549-1550.
9. Calvori, C., Frontali, L., Leoni, L., and Tecce, G. (1965) Effect of rifamycin on protein synthesis, *Nature* 207, 417-418.

10. Team, E. E. (2013) CDC publishes report on antibiotic resistance threats in the United States for the first time, *Eurosurveillance* 18, 28-28.
11. Smolinski M. S., Hamburg M. A., Lederberg J. (2003) Microbial Threats to Health: Emergence, Detection, and Response. National Academy of Sciences; Washington DC
12. Dever, L. A., and Dermody, T. S. (1991) Mechanisms of Bacterial-Resistance to Antibiotics, *Arch. Intern. Med.* 151, 886-895.
13. Levy, S. B. (1998) The challenge of antibiotic resistance, *Sci. Am.* 278, 46-53.
14. McManus, M. C. (1997) Mechanisms of bacterial resistance to antimicrobial agents, *Am. J. Health Syst. Pharm.* 54, 1420-1433.
15. Austrian, R. (1960) The Gram Stain and the Etiology of Lobar Pneumonia, an Historical Note, *Bacteriol. Rev.* 24, 261-265.
16. Vollmer, W., Blanot, D., and de Pedro, M. A. (2008) Peptidoglycan structure and architecture, *FEMS Microbiol. Rev.* 32, 149-167.
17. Vaara, M. (1993) Antibiotic-Supersusceptible Mutants of Escherichia-Coli and Salmonella-Typhimurium, *Antimicrob. Agents Chemother.* 37, 2255-2260.
18. Schrodinger, L. (2010) The PyMOL Molecular Graphics System, Version 1.3r1.
19. Jiang, J. S., Daniels, B. V., and Fu, D. (2006) Crystal structure of AqpZ tetramer reveals two distinct Arg-189 conformations associated with water permeation through the narrowest constriction of the water-conducting channel, *J. Biol. Chem.* 281, 454-460.

20. Vandeputte-Rutten, L., Kramer, R. A., Kroon, J., Dekker, N., Egmond, M. R., and Gros, P. (2001) Crystal structure of the outer membrane protease OmpT from *Escherichia coli* suggests a novel catalytic site, *EMBO J.* 20, 5033-5039.
21. Delcour, A. H. (2009) Outer membrane permeability and antibiotic resistance, *Biochim. Biophys. Acta* 1794, 808-816.
22. Vaara, M. (1992) Agents that increase the permeability of the outer membrane, *Microbiol. Rev.* 56, 395-411.
23. Vaara, M., Vaara, T., and Sarvas, M. (1979) Decreased binding of polymyxin by polymyxin-resistant mutants of *Salmonella-typhimurium*, *J. Bacteriol.* 139, 664-667.
24. Vaara, M., Vaara, T., Jensen, M., Helander, I., Nurminen, M., Rietschel, E. T., and Makela, P. H. (1981) Characterization of the lipopolysaccharide from the polymyxin-resistant pmrA mutants of *Salmonella-typhimurium*, *FEBS Lett.* 129, 145-149.
25. Nikaido, H. (1989) Outer membrane barrier as a mechanism of antimicrobial resistance, *Antimicrob. Agents Chemother* 33, 1831-1836.
26. Higgins, C. F. (2007) Multiple molecular mechanisms for multidrug resistance transporters, *Nature* 446, 749-757.
27. Piddock, L. J. V. (2006) Clinically relevant chromosomally encoded multidrug resistance efflux pumps in bacteria, *Clin. Microbiol. Rev.* 19, 382-402.
28. Nikaido, H. (1996) Multidrug efflux pumps of gram-negative bacteria, *J. Bacteriol.* 178, 5853-5859.

29. Saier, M. H., Jr., Tam, R., Reizer, A., and Reizer, J. (1994) Two novel families of bacterial membrane proteins concerned with nodulation, cell division and transport, *Mol. Microbiol.* *11*, 841-847.
30. Dinh, T., Paulsen, I. T., and Saier, M. H. (1994) A family of extracytoplasmic proteins that allow transport of large molecules across the outer membranes of gram-negative bacteria, *J. Bacteriol.* *176*, 3825-3831.
31. Sulavik, M. C., Houseweart, C., Cramer, C., Jiwani, N., Murgolo, N., Greene, J., DiDomenico, B., Shaw, K. J., Miller, G. H., Hare, R., and Shimer, G. (2001) Antibiotic susceptibility profiles of *Escherichia coli* strains lacking multidrug efflux pump genes, *Antimicrob. Agents Chemother.* *45*, 1126-1136.
32. Murakami, S., Nakashima, R., Yamashita, E., and Yamaguchi, A. (2002) Crystal structure of bacterial multidrug efflux transporter AcrB, *Nature* *419*, 587-593.
33. Long, F., Su, C. C., Zimmermann, M. T., Boyken, S. E., Rajashankar, K. R., Jernigan, R. L., and Yu, E. W. (2010) Crystal structures of the CusA efflux pump suggest methionine-mediated metal transport, *Nature* *467*, 484-488.
34. Sennhauser, G., Bukowska, M. A., Briand, C., and Grutter, M. G. (2009) Crystal Structure of the Multidrug Exporter MexB from *Pseudomonas aeruginosa*, *J. Mol. Biol.* *389*, 134-145.
35. Pak, J. E., Ekende, E. N., Kifle, E. G., O'Connell, J. D., De Angelis, F., Tessema, M. B., Derfoufi, K. M., Robles-Colmenares, Y., Robbins, R. A., Goormaghtigh, E., Vandebussche, G., and Stroud, R. M. (2013) Structures of intermediate

- transport states of ZneA, a Zn(II)/proton antiporter, *Pro. Natl. Acad. Sci. U. S. A.* *110*, 18484-18489.
36. Paulsen, I. T., Brown, M. H., and Skurray, R. A. (1996) Proton-dependent multidrug efflux systems, *Microbiol. Rev.* *60*, 575-608.
  37. Paulsen, I. T., Skurray, R. A., Tam, R., Saier, M. H., Jr., Turner, R. J., Weiner, J. H., Goldberg, E. B., and Grinius, L. L. (1996) The SMR family: a novel family of multidrug efflux proteins involved with the efflux of lipophilic drugs, *Mol. microbiol.* *19*, 1167-1175.
  38. Lewis, K. (1994) Multidrug resistance pumps in bacteria: variations on a theme, *Trends Biochem. Sci.* *19*, 119-123.
  39. Li, X. Z., Ma, D., Livermore, D. M., and Nikaido, H. (1994) Role of efflux pump(s) in intrinsic resistance of *Pseudomonas aeruginosa*: active efflux as a contributing factor to beta-lactam resistance, *Antimicrob. Agents Chemother* *38*, 1742-1752.
  40. Ma, D., Cook, D. N., Alberti, M., Pon, N. G., Nikaido, H., and Hearst, J. E. (1993) Molecular cloning and characterization of *acrA* and *acrE* genes of *Escherichia coli*, *J. Bacteriol.* *175*, 6299-6313.
  41. Li, X. Z., Nikaido, H., and Poole, K. (1995) Role of *mexA-mexB-oprM* in antibiotic efflux in *Pseudomonas aeruginosa*, *Antimicrob. Agents Chemother* *39*, 1948-1953.
  42. Kohler, T., Kok, M., Michea-Hamzhepour, M., Plesiat, P., Gotoh, N., Nishino, T., Curty, L. K., and Pechere, J. C. (1996) Multidrug efflux in intrinsic

- resistance to trimethoprim and sulfamethoxazole in *Pseudomonas aeruginosa*, *Antimicrob. Agents Chemother* 40, 2288-2290.
43. Seeger, M. A., Diederichs, K., Eicher, T., Brandstatter, L., Schiefner, A., Verrey, F., and Pos, K. M. (2008) The AcrB efflux pump: conformational cycling and peristalsis lead to multidrug resistance, *Curr. Drug Targets* 9, 729-749.
  44. Tikhonova, E. B., and Zgurskaya, H. I. (2004) AcrA, AcrB, and TolC of *Escherichia coli* form a stable intermembrane multidrug efflux complex, *J. Biol. Chem.* 279, 32116-32124.
  45. Symmons, M. F., Bokma, E., Koronakis, E., Hughes, C., and Koronakis, V. (2009) The assembled structure of a complete tripartite bacterial multidrug efflux pump, *Proc. Natl. Acad. Sci. U. S. A.* 106, 7173-7178.
  46. Zgurskaya, H. I., and Nikaido, H. (1999) AcrA is a highly asymmetric protein capable of spanning the periplasm, *J. Mol. Biol.* 285, 409-420.
  47. Eswaran, J., Koronakis, E., Higgins, M. K., Hughes, C., and Koronakis, V. (2004) Three's company: component structures bring a closer view of tripartite drug efflux pumps, *Curr. Opin. Struct. Biol.* 14, 741-747.
  48. Koronakis, V., Sharff, A., Koronakis, E., Luisi, B., and Hughes, C. (2000) Crystal structure of the bacterial membrane protein TolC central to multidrug efflux and protein export, *Nature* 405, 914-919.
  49. Kobayashi, N., Nishino, K., and Yamaguchi, A. (2001) Novel macrolide-specific ABC-type efflux transporter in *Escherichia coli*, *J. Bacteriol.* 183, 5639-5644.

50. Higgins, M. K., Eswaran, J., Edwards, P., Schertler, G. F. X., Hughes, C., and Koronakis, V. (2004) Structure of the ligand-blocked periplasmic entrance of the bacterial multidrug efflux protein TolC, *J. Mol. Biol.* 342, 697-702.
51. Seeger, M. A., Schiefner, A., Eicher, T., Verrey, F., Diederichs, K., and Pos, K. M. (2006) Structural asymmetry of AcrB trimer suggests a peristaltic pump mechanism, *Science* 313, 1295-1298.
52. Mikolosko, J., Bobyk, K., Zgurskaya, H. I., and Ghosh, P. (2006) Conformational flexibility in the multidrug efflux system protein AcrA, *Structure* 14, 577-587.
53. Yamaguchi, A., Murakami, S., Nakshima, R., and Yamashita, E. (2003) Crystal structure of bacterial multidrug efflux transporter AcrB, *FASEB J* 17, A1185-A1185.
54. Husain, F., and Nikaido, H. (2010) Substrate path in the AcrB multidrug efflux pump of *Escherichia coli*, *Mol. Microbiol.* 78, 320-330.
55. Murakami, S., Nakashima, R., Yamashita, E., Matsumoto, T., and Yamaguchi, A. (2006) Crystal structures of a multidrug transporter reveal a functionally rotating mechanism, *Nature* 443, 173-179.
56. Eicher, T., Cha, H. J., Seeger, M. A., Brandstatter, L., El-Delik, J., Bohnert, J. A., Kern, W. V., Verrey, F., Grutter, M. G., Diederichs, K., and Pos, K. M. (2012) Transport of drugs by the multidrug transporter AcrB involves an access and a deep binding pocket that are separated by a switch-loop, *Proc. Natl. Acad. Sci. U. S. A.* 109, 5687-5692.

57. Pos, K. M. (2009) Drug transport mechanism of the AcrB efflux pump, *Biochim. Biophys. Acta* 1794, 782-793.
58. Schulz, G. E. (2002) The structure of bacterial outer membrane proteins, *Biochim. Biophys. Acta* 1565, 308-317.
59. Tokuda, H. (2009) Biogenesis of outer membranes in gram-negative bacteria, *Biosci. Biotech. Biochem.* 73, 465-473.
60. Bos, M. P., Robert, V., and Tommassen, J. (2007) Biogenesis of the gram-negative bacterial outer membrane, *Annu. Rev. Microbiol.* 61, 191-214.
61. Ruiz, N., Kahne, D., and Silhavy, T. J. (2006) Advances in understanding bacterial outer-membrane biogenesis, *Nat. Rev. Microbiol.* 4, 57-66.
62. Bernstein, H. D. (2000) The biogenesis and assembly of bacterial membrane proteins, *Curr. Opin. Microbiol.* 3, 203-209.
63. Walther, D. M., Rapaport, D., and Tommassen, J. (2009) Biogenesis of beta-barrel membrane proteins in bacteria and eukaryotes: evolutionary conservation and divergence, *Cell Mol. Life Sci.* 66, 2789-2804.
64. Gold, V. A. M., Duong, F., and Collinson, I. (2007) Structure and function of the bacterial Sec translocon, *Mol. Membr. Biol.* 24, 387-394.
65. Missiakas, D., Betton, J. M., and Raina, S. (1996) New components of protein folding in extracytoplasmic compartments of *Escherichia coli* SurA, FkpA and Skp/OmpH, *Mol. Microbiol.* 21, 871-884.
66. Mogensen, J. E., and Otzen, D. E. (2005) Interactions between folding factors and bacterial outer membrane proteins, *Mol. Microbiol.* 57, 326-346.



67. Sklar, J. G., Wu, T., Kahne, D., and Silhavy, T. J. (2007) Defining the roles of the periplasmic chaperones SurA, Skp, and DegP in *Escherichia coli*, *Genes Dev.* 21, 2473-2484.
68. Ricci, D. P., and Silhavy, T. J. (2012) The Bam machine: A molecular cooper, *Biochim. Biophys. Acta* 1818, 1067-1084.
69. Hagan, C. L., Kim, S., and Kahne, D. (2010) Reconstitution of Outer Membrane Protein Assembly from Purified Components, *Science* 328, 890-892.
70. Tamm, L. K., Arora, A., and Kleinschmidt, J. H. (2001) Structure and assembly of beta-barrel membrane proteins, *J. Biol. Chem.* 276, 32399-32402.
71. Huysmans, G. H. M., Baldwin, S. A., Brockwell, D. J., and Radford, S. E. (2010) The transition state for folding of an outer membrane protein, *Proc. Natl. Acad. Sci. U. S. A.* 107, 4099-4104.
72. Hong, H. D., and Tamm, L. K. (2004) Elastic coupling of integral membrane protein stability to lipid bilayer forces, *Proc. Natl. Acad. Sci. U. S. A.* 101, 4065-4070.
73. Burgess, N. K., Dao, T. P., Stanley, A. M., and Fleming, K. G. (2008) beta-barrel proteins that reside in the *Escherichia coli* outer membrane in vivo demonstrate varied folding behavior in vitro, *J. Biol. Chem.* 283, 26748-26758.
74. Stanley, A. M., and Fleming, K. G. (2008) The process of folding proteins into membranes: Challenges and progress, *Arch. Biochem. Biophys.* 469, 46-66.
75. Hong, H., Szabo, G., and Tamm, L. K. (2006) Electrostatic couplings in OmpA ion-channel gating suggest a mechanism for pore opening, *Nat. Chem. Biol.* 2, 627-635.

76. Hong, H. D., Park, S., Jimenez, R. H. F., Rinehart, D., and Tamm, L. K. (2007) Role of aromatic side chains in the folding and thermodynamic stability of integral membrane proteins, *J. Am. Chem. Soc.* *129*, 8320-8327.
77. Zimmerman, S. B., and Minton, A. P. (1993) Macromolecular Crowding: Biochemical, Biophysical, and Physiological Consequences, *Annu. Rev. Biophys. Biomol. Struct.* *22*, 27-65.
78. Ellis, R. J. (2001) Macromolecular crowding: obvious but underappreciated, *Trends Biochem. Sci.* *26*, 597-604.
79. Hobot, J. A., Carlemalm, E., Villiger, W., and Kellenberger, E. (1984) Periplasmic Gel: new concept resulting from the reinvestigation of bacterial cell envelope ultrastructure by new methods, *J. Bacteriol.* *160*, 143-152.
80. Minton, A. P., and Wilf, J. (1981) Effect of macromolecular crowding upon the structure and function of an enzyme: glyceraldehyde-3-phosphate dehydrogenase, *Biochemistry* *20*, 4821-4826.
81. Minton, A. P. (2006) Macromolecular crowding, *Curr. Biol.* *16*, R269-R271.
82. Dong, H., Qin, S., and Zhou, H. X. (2010) Effects of macromolecular crowding on protein conformational changes, *PLoS Comput. Biol.* *6*, e1000833.
83. McNulty, B. C., Young, G. B., and Pielak, G. J. (2006) Macromolecular crowding in the *Escherichia coli* periplasm maintains  $\alpha$ -synuclein disorder, *J. Mol. Biol.* *355*, 893-897.
84. Wieczorek, G., and Zielonkiewicz, P. (2008) Influence of macromolecular crowding on protein-protein association rates: a Brownian dynamics study, *Biophys. J.* *95*, 5030-5036.

85. Engel, R., Westphal, A. H., Huberts, D. H. E. W., Nabuurs, S. M., Lindhoud, S., Visser, A. J. W. G., and van Mierlo, C. P. M. (2008) Macromolecular crowding compacts unfolded apoflavodoxin and causes severe aggregation of the off-pathway intermediate during apoflavodoxin folding, *J. Biol. Chem.* *283*, 27383-27394.
86. Hong, J., and Gierasch, L. M. (2010) Macromolecular crowding remodels the energy landscape of a protein by favoring a more compact unfolded state, *J. Am. Chem. Soc.* *132*, 10445-10452.
87. Mukherjee, S., Waegelé, M. M., Chowdhury, P., Guo, L., and Gai, F. (2009) Effect of macromolecular crowding on protein folding dynamics at the secondary structure level, *J. Mol. Biol.* *393*, 227-236.
88. Pautsch, A., and Schulz, G. E. (2000) High-resolution structure of the OmpA membrane domain, *J. Mol. Biol.* *298*, 273-282.
89. Vandeputte-Rutten, L., Kramer, R. A., Kroon, J., Dekker, N., Egmond, M. R., and Gros, P. (2001) Crystal structure of the outer membrane protease OmpT from *Escherichia coli* suggests a novel catalytic site, *EMBO J.* *20*, 5033-5039.
90. Zhou, H. X., Rivas, G., and Minton, A. P. (2008) Macromolecular crowding and confinement: biochemical, biophysical, and potential physiological consequences, *Annu. Rev. Biophys.* *37*, 375-397.
91. Dix, J. A., and Verkman, A. S. (2008) Crowding effects on diffusion in solutions and cells, *Annu. Rev. Biophys.* *37*, 247-263.

92. Dauty, E., and Verkman, A. S. (2004) Molecular crowding reduces to a similar extent the diffusion of small solutes and macromolecules: measurement by fluorescence correlation spectroscopy, *J. Mol. Recognit* 17, 441-447.
93. Gassmann, M., Grenacher, B., Rohde, B., and Vogel, J. (2009) Quantifying Western blots: Pitfalls of densitometry, *Electrophoresis* 30, 1845-1855.
94. Hummel, B. C. W. (1959) A modified spectrophotometric determination of chymotrypsin, trypsin, and thrombin, *Can. J. Biochem. Physiol.* 37, 1393-1399.
95. Kleinschmidt, J. H. (2006) Folding kinetics of the outer membrane proteins OmpA and FomA into phospholipid bilayers, *Chem. Phys. Lipids* 141, 30-47.
96. Kleinschmidt, J. H. (2006) Folding kinetics of the outer membrane proteins OmpA and FomA into phospholipid bilayers, *Chem. Phys. Lipids* 141, 30-47.
97. Kleinschmidt, J. H., and Tamm, L. K. (1996) Folding intermediates of a  $\beta$ -barrel membrane protein. Kinetic evidence for a multi-Step membrane insertion mechanism, *Biochemistry* 35, 12993-13000.
98. Rodionova, N. A., Tatulian, S. A., Surrey, T., Jaehnig, F., and Tamm, L. K. (1995) Characterization of two membrane-bound forms of OmpA, *Biochemistry* 34, 1921-1929.
99. Dornmair, K., Kiefer, H., and Jaehnig, F. (1990) Refolding of an integral membrane protein. OmpA of Escherichia coli, *J. Biol. Chem.* 265, 18907-18911.
100. Arora, A., Rinehart, D., Szabo, G., and Tamm, L. K. (2000) Refolded outer membrane protein A of Escherichia coli forms ion channels with two conductance states in planar lipid bilayers, *J. Biol. Chem.* 275, 1594-1600.

101. Asaad, N., and Engberts, J. B. F. N. (2003) Cytosol-Mimetic Chemistry: Kinetics of the Trypsin-Catalyzed Hydrolysis of p-Nitrophenyl Acetate upon Addition of Polyethylene Glycol and N-tert-Butyl Acetoacetamide, *J. Am. Chem. Soc.* *125*, 6874-6875.
102. Pautsch, A., and Schulz, G. E. (2000) High-resolution Structure of the OmpA Membrane Domain, *J. Mol. Biol.* *298*, 273-282.
103. Cierpicki, T., Liang, B., Tamm, L. K., and Bushweller, J. H. (2006) Increasing the accuracy of solution NMR structures of membrane proteins by application of residual dipolar couplings. High-resolution structure of outer membrane protein A, *J. Am. Chem. Soc.* *128*, 6947-6951.
104. Arora, A., Abildgaard, F., Bushweller, J. H., and Tamm, L. K. (2001) Structure of outer membrane protein A transmembrane domain by NMR spectroscopy, *Nat. Struct. Biol.* *8*, 334-338.
105. Verhoeven, G. S., Alexeeva, S., Dogterom, M., and den Blaauwen, T. (2009) Differential bacterial surface display of peptides by the transmembrane domain of OmpA, *PLoS One* *4*, e6739.
106. Danoff, E. J., and Fleming, K. G. (2011) The soluble, periplasmic domain of OmpA folds as an independent unit and displays chaperone activity by reducing the self-association propensity of the unfolded OmpA transmembrane beta-barrel, *Biophys. Chem.* *159*, 194-204.
107. Bowie, J. U. (2005) Solving the membrane protein folding problem, *Nature* *438*, 581-589.

108. Booth, P. J., and Curnow, P. (2006) Membrane proteins shape up: understanding *in vitro* folding, *Curr. Opin. Struct. Biol.* *16*, 480-488.
109. Harris, N. J., and Booth, P. J. (2012) Folding and stability of membrane transport proteins *in vitro*, *Biochim. Biophys. Acta* *1818*, 1055-1066.
110. Hong, H., Joh, N. H., Bowie, J. U., and Tamm, L. K. (2009) Methods for measuring the thermodynamic stability of membrane proteins, *Methods Enzymol.* *455*, 213-236.
111. Renthal, R. (2006) An unfolding story of helical transmembrane proteins, *Biochemistry* *45*, 14559-14566.
112. Huang, K. S., Bayley, H., Liao, M. J., London, E., and Khorana, H. G. (1981) Refolding of an integral membrane protein. Denaturation, renaturation, and reconstitution of intact bacteriorhodopsin and two proteolytic fragments, *J. Biol. Chem.* *256*, 3802-3809.
113. London, E., and Khorana, H. G. (1982) Denaturation and renaturation of bacteriorhodopsin in detergents and lipid-detergent mixtures, *J. Biol. Chem.* *257*, 7003-7011.
114. Nagy, J. K., Lonzer, W. L., and Sanders, C. R. (2001) Kinetic study of folding and misfolding of diacylglycerol kinase in model membranes, *Biochemistry* *40*, 8971-8980.
115. Valiyaveetil, F. I., MacKinnon, R., and Muir, T. W. (2002) Semisynthesis and folding of the potassium channel KcsA, *J. Am. Chem. Soc.* *124*, 9113-9120.

116. Harris, N. J., Findlay, H. E., Simms, J., Liu, X., and Booth, P. J. (2014) Relative domain folding and stability of a membrane transport protein, *J. Mol. Biol.* *426*, 1812-1825.
117. Haltia, T., and Freire, E. (1995) Forces and factors that contribute to the structural stability of membrane proteins, *Biochim. Biophys. Acta* *1228*, 1-27.
118. Lau, F. W., and Bowie, J. U. (1997) A method for assessing the stability of a membrane protein, *Biochemistry* *36*, 5884-5892.
119. Curnow, P., and Booth, P. J. (2007) Combined kinetic and thermodynamic analysis of alpha-helical membrane protein unfolding, *Proc. Natl. Acad. Sci. U. S. A.* *104*, 18970-18975.
120. Valiyaveetil, F. I., Zhou, Y. F., and Mackinnon, R. (2002) Lipids in the structure, folding, and function of the KcsA K<sup>+</sup> channel, *Biochemistry* *41*, 10771-10777.
121. Bennion, B. J., and Daggett, V. (2003) The molecular basis for the chemical denaturation of proteins by urea, *Proc. Natl. Acad. Sci. U. S. A.* *100*, 5142-5147.
122. Sehgal, P., and Otzen, D. E. (2006) Thermodynamics of unfolding of an integral membrane protein in mixed micelles, *Protein Sci.* *15*, 890-899.
123. Mattice, W. L., Riser, J. M., and Clark, D. S. (1976) Conformational properties of the complexes formed by proteins and sodium dodecyl sulfate, *Biochemistry* *15*, 4264-4272.
124. Faham, S., Yang, D., Bare, E., Yohannan, S., Whitelegge, J. P., and Bowie, J. U. (2003) Side-chain contributions to membrane protein structure and stability, *J. Mol. Biol.* *335*, 297-305.

125. Fleming, K. G., Ackerman, A. L., and Engelman, D. M. (1997) The effect of point mutations on the free energy of transmembrane alpha-helix dimerization, *J. Mol. Biol.* 272, 266-275.
126. Popot, J. L., and Engelman, D. M. (1990) Membrane protein folding and oligomerization - the two-stage model, *Biochemistry* 29, 4031-4037.
127. Otzen, D. E. (2003) Folding of DsbB in mixed micelles: A kinetic analysis of the stability of a bacterial membrane protein, *J. Mol. Biol.* 330, 641-649.
128. Miller, D., Charalambous, K., Rotem, D., Schuldiner, S., Curnow, P., and Booth, P. J. (2009) In vitro unfolding and refolding of the small multidrug transporter EmrE, *J. Mol. Biol.* 393, 815-832.
129. Schlebach, J. P., Peng, D., Kroncke, B. M., Mittendorf, K. F., Narayan, M., Carter, B. D., and Sanders, C. R. (2013) Reversible folding of human peripheral myelin protein 22, a tetraspan membrane protein, *Biochemistry* 52, 3229-3241.
130. Di Bartolo, N. D., Hvorup, R. N., Locher, K. P., and Booth, P. J. (2011) In vitro folding and assembly of the *Escherichia coli* ATP-binding cassette transporter, BtuCD, *J. Biol. Chem.* 286, 18807-18815.
131. Findlay, H. E., Rutherford, N. G., Henderson, P. J. F., and Booth, P. J. (2010) Unfolding free energy of a two-domain transmembrane sugar transport protein, *Proc. Natl. Acad. Sci. U. S. A.* 107, 18451-18456.
132. He, M. M., and Kaback, H. R. (1998) In vitro folding of a membrane protein: effect of denaturation and renaturation on substrate binding by the lactose permease of *Escherichia coli*, *Mol. Membr. Biol.* 15, 15-20.



133. Yu, L. L., Lu, W., and Wei, Y. N. (2011) AcrB Trimer Stability and Efflux Activity, Insight from Mutagenesis Studies, *PloS One* 6, e28390.
134. Lu, W., Zhong, M., and Wei, Y. N. (2011) Folding of AcrB Subunit Precedes Trimerization, *J. Mol. Biol.* 411, 264-274.
135. Lu, W., Zhong, M., and Wei, Y. N. (2011) A Reporter Platform for the Monitoring of In Vivo Conformational Changes in AcrB, *Protein Pept. Lett.* 18, 863-871.
136. Lu, W., Zhong, M., and Wei, Y. (2011) Folding of AcrB Subunit Precedes Trimerization, *J. Mol. Biol.* 411, 264-274.
137. Wittig, I., Braun, H. P., and Schagger, H. (2006) Blue native PAGE, *Nat. Protoc.* 1, 418-428.
138. Yu, L., Lu, W., Ye, C., Wang, Z., Zhong, M., Chai, Q., Sheetz, M., and Wei, Y. (2013) Role of a Conserved Residue R780 in Escherichia coli Multidrug Transporter AcrB, *Biochemistry* 52, 6790-6796.
139. Seeger, M. A., von Ballmoos, C., Eicher, T., Brandstatter, L., Verrey, F., Diederichs, K., and Pos, K. M. (2008) Engineered disulfide bonds support the functional rotation mechanism of multidrug efflux pump AcrB, *Nat. Struct. Mol. Biol.* 15, 199-205.
140. Whitmore, L., and Wallace, B. A. (2004) DICHROWEB, an online server for protein secondary structure analyses from circular dichroism spectroscopic data, *Nucleic Acids Res.* 32, W668-W673.

141. Veerappan, A., Cymer, F., Klein, N., and Schneider, D. (2011) The tetrameric alpha-helical membrane protein GlpF unfolds via a dimeric folding intermediate, *Biochemistry* 50, 10223-10230.
142. Miller, S., Lesk, A. M., Janin, J., and Chothia, C. (1987) The accessible surface area and stability of oligomeric proteins, *Nature* 328, 834-836.
143. Blundell, T. L., and Srinivasan, N. (1996) Symmetry, stability, and dynamics of multidomain and multicomponent protein systems, *Proc. Natl. Acad. Sci. U. S. A.* 93, 14243-14248.
144. Shoichet, B. K., Baase, W. A., Kuroki, R., and Matthews, B. W. (1995) A relationship between protein stability and protein function, *Proc. Natl. Acad. Sci. U. S. A.* 92, 452-456.
145. Fersht, A. (1999) *structure and mechanism in protein science*, W. H. Freeman and Company, New York.
146. Bloom, J. D., Labthavikul, S. T., Otey, C. R., and Arnold, F. H. (2006) Protein stability promotes evolvability, *Proc. Natl. Acad. Sci. USA* 103, 5869-5874.
147. Fields, P. A. (2001) Review: Protein function at thermal extremes: balancing stability and flexibility, *Comp. Biochem. Phys. A Mol. Integr. Physiol.* 129, 417-431.
148. Hong, H., Joh, N. H., Bowie, J. U., and Tamm, L. K. (2009) Methods for measuring the thermodynamic stability of membrane proteins, *Method Enzymol.* 455, 213-236.

149. Takatsuka, Y., and Nikaido, H. (2009) Covalently linked trimer of the AcrB Multidrug Efflux Pump Provides Support for the Functional Rotating Mechanism, *J. Bacteriol.* *191*, 1729-1737.
150. Fang, J., Yu, L. L., Wu, M., and Wei, Y. N. (2013) Dissecting the function of a protruding loop in AcrB trimerization, *J. Biomol. Struct. Dyn.* *31*, 385-392.
151. Yu, L., Lu, W., Ye, C., Wang, Z., Zhong, M., Chai, Q., Sheetz, M., and Wei, Y. (2013) Role of a conserved residue R780 in *Escherichia coli* multidrug transporter AcrB, *Biochemistry* *52*, 6790-6796.
152. Lu, W., Chai, Q., Zhong, M., Yu, L. L., Fang, J., Wang, T., Li, H. L., Zhu, H. N., and Wei, Y. N. (2012) Assembling of AcrB trimer in cell membrane, *J. Mol. Biol.* *423*, 123-134.
153. Li, X. Z., Poole, K., and Nikaido, H. (2003) Contributions of MexAB-OprM and an EmrE homolog to intrinsic resistance of *Pseudomonas aeruginosa* to aminoglycosides and dyes, *Antimicrob. Agents Chemother* *47*, 27-33.
154. Bohnert, J. A., Karamian, B., and Nikaido, H. (2010) Optimized Nile red efflux assay of AcrAB-TolC multidrug efflux system shows competition between substrates, *Antimicrob. Agents Chemother* *54*, 3770-3775.
155. Abramoff, M. D., Magelhaes, P. J. & Ram, S. J. (2004) Image processing with ImageJ., *Biophoton. Int.* *11*, 36-42.
156. Reynolds, C., Damerell, D., and Jones, S. (2009) ProtorP: a protein-protein interaction analysis server, *Bioinformatics* *25*, 413-416.
157. Fang, J., Yu, L. L., Wu, M., and Wei, Y. N. (2013) Dissecting the function of a protruding loop in AcrB trimerization, *J. Biomol. Struct. Dyn.* *31*, 385-392.

158. Yu, L. L., Lu, W., and Wei, Y. N. (2011) AcrB Trimer Stability and Efflux Activity, Insight from Mutagenesis Studies, *PLoS ONE*, 6, e28390.
159. Viveiros, M., Martins, A., Paixao, L., Rodrigues, L., Martins, M., Couto, I., Fahrnich, E., Kern, W. V., and Amaral, L. (2008) Demonstration of intrinsic efflux activity of *Escherichia coli* K-12 AG100 by an automated ethidium bromide method, *Int. J. Antimicrob. Agents* 31, 458-462.
160. Paixao, L., Rodrigues, L., Couto, I., Martins, M., Fernandes, P., de Carvalho, C. C., Monteiro, G. A., Sansonetty, F., Amaral, L., and Viveiros, M. (2009) Fluorometric determination of ethidium bromide efflux kinetics in *Escherichia coli*, *J. Biol. Eng.* 3, 18.
161. Fleming, K. G. (2002) Standardizing the free energy change of transmembrane helix-helix interactions, *J. Mol. Biol.* 323, 563-571.
162. Sehgal, P., Mogensen, J. E., and Otzen, D. E. (2005) Using micellar mole fractions to assess membrane protein stability in mixed micelles, *Biochim. Biophys. Acta* 1716, 59-68.
163. Heuberger, E. H. M. L., Veenhoff, L. M., Duurkens, R. H., Friesen, R. H. E., and Poolman, B. (2002) Oligomeric state of membrane transport proteins analyzed with blue native electrophoresis and analytical ultracentrifugation, *J. Mol. Biol.* 317, 591-600.
164. Cristian, L., Lear, J. D., and DeGrado, W. F. (2003) Use of thiol-disulfide equilibria to measure the energetics of assembly of transmembrane helices in phospholipid bilayers, *Proc. Natl. Acad. Sci. USA* 100, 14772-14777.

165. Hong, H., Blois, T. M., Cao, Z., and Bowie, J. U. (2010) Method to measure strong protein-protein interactions in lipid bilayers using a steric trap, *Proc. Natl. Acad. Sci. USA* *107*, 19802-19807.
166. Ali, M. H., and Imperiali, B. (2005) Protein oligomerization: How and why, *Bioorgan Med Chem* *13*, 5013-5020.
167. Goodsell, D. S., and Olson, A. J. (2000) Structural symmetry and protein function, *Annu. Rev. Biophys. Biomol. Struct.* *29*, 105-153.
168. Goodsell, D. S. (1991) Inside a Living Cell, *Trends Biochem. Sci.* *16*, 203-206.
169. Nooren, I. M. A., and Thornton, J. M. (2003) Diversity of protein-protein interactions, *EMBO J.* *22*, 3486-3492.
170. You, M., Li, E., Wimley, W. C., and Hristova, K. (2005) Foerster resonance energy transfer in liposomes: Measurements of transmembrane helix dimerization in the native bilayer environment, *Anal. Biochem.* *340*, 154-164.
171. Chen, L. R., Novicky, L., Merzlyakov, M., Hristov, T., and Hristova, K. (2010) Measuring the energetics of membrane protein dimerization in mammalian membranes, *J. Am. Chem. Soc.* *132*, 3628-3635.
172. Harhay, M. O. (2011) Water stress and water scarcity: a global problem, *Am. J. Public Health* *101*, 1348-1349
173. Falkenmark, M. (2013) Growing water scarcity in agriculture: future challenge to global water security, [\*Philos. Trans. A Math Phys. Eng. Sci.\* \*371\*](#), 20120410.
174. Hoekstra, A. Y., Mekonnen, M. M., Chapagain, A. K., Mathews, R. E., and Richter, B. D. (2012) Global monthly water scarcity: blue water footprints versus blue water availability, *PloS One* *7*, e32688.

175. Shannon, M. A., Bohn, P. W., Elimelech, M., Georgiadis, J. G., Marinas, B. J., and Mayes, A. M. (2008) Science and technology for water purification in the coming decades, *Nature* 452, 301-310.
176. Semiat, R. (2008) Energy issues in desalination processes, *Environ. Sci. Technol.* 42, 8193-8201.
177. Elimelech, M., and Phillip, W. A. (2011) The future of seawater desalination: energy, technology, and the environment, *Science* 333, 712-717.
178. Tang, C. Y. Y., Kwon, Y. N., and Leckie, J. O. (2009) Effect of membrane chemistry and coating layer on physiochemical properties of thin film composite polyamide RO and NF membranes I. FTIR and XPS characterization of polyamide and coating layer chemistry, *Desalination* 242, 149-167.
179. Fritzmann, C., Lowenberg, J., Wintgens, T., and Melin, T. (2007) State-of-the-art of reverse osmosis desalination, *Desalination* 216, 1-76.
180. Agre, P., Preston, G. M., Smith, B. L., Jung, J. S., Raina, S., Moon, C., Guggino, W. B., and Nielsen, S. (1993) Aquaporin CHIP: the archetypal molecular water channel, *Am. J. Physiol.* 265, F463-F476.
181. Knepper, M. A., Wade, J. B., Terris, J., Ecelbarger, C. A., Marples, D., Mandon, B., Chou, C. L., Kishore, B. K., and Nielsen, S. (1996) Renal aquaporins, *Kidney Int.* 49, 1712-1717.
182. Preston, G. M., Carroll, T. P., Guggino, W. B., and Agre, P. (1992) Appearance of water channels in *Xenopus* oocytes expressing red-cell chip28 protein, *Science* 256, 385-387.

183. Nielsen, S., Smith, B. L., Christensen, E. I., and Agre, P. (1993) Distribution of the aquaporin chip in secretory and resorptive epithelia and capillary endothelia, *Proc. Natl. Acad. Sci. U. S. A.* *90*, 7275-7279.
184. Calamita, G., Bishai, W. R., Preston, G. M., Guggino, W. B., and Agre, P. (1995) Molecular cloning and characterization of Aqpz, a water channel from *Escherichia coli*, *J. Biol. Chem.* *270*, 29063-29066.
185. Wang, H. L., Chung, T. S., Tong, Y. W., Jeyaseelan, K., Armugam, A., Chen, Z. C., Hong, M. H., and Meier, W. (2012) Highly permeable and selective pore spanning biomimetic membrane embedded with Aquaporin Z *Small* *8*, 1969.
186. Kumar, M., Grzelakowski, M., Zilles, J., Clark, M., and Meier, W. (2007) Highly permeable polymeric membranes based on the incorporation of the functional water channel protein Aquaporin Z, *Proc. Natl. Acad. Sci. U. S. A.* *104*, 20719-20724.
187. Zhao, Y., Qiu, C. Q., Li, X. S., Vararattanavech, A., Shen, W. M., Torres, J., Helix-Nielsen, C., Wang, R., Hu, X., Fane, A. G., and Tang, C. Y. (2012) Synthesis of robust and high-performance aquaporin-based biomimetic membranes by interfacial polymerization-membrane preparation and RO performance characterization, *J. Membrane Sci.* *423*, 422-428.
188. Savage, D. F., Egea, P. F., Robles-Colmenares, Y., O'Connell, J. D., and Stroud, R. M. (2003) Architecture and selectivity in aquaporins: 2.5 Å X-ray structure of aquaporin Z, *PloS Biol.* *1*, 334-340.

189. de Groot, B. L., and Grubmuller, H. (2001) Water permeation across biological membranes: mechanism and dynamics of aquaporin-1 and GlpF, *Science* 294, 2353-2357.
190. Hutchinson, E. G., and Thornton, J. M. (1994) A revised set of potentials for beta-turn formation in proteins, *Protein Sci.* 3, 2207-2216.
191. Guruprasad, K., and Rajkumar, S. (2000) beta-and gamma-turns in proteins revisited: A new set of amino acid turn-type dependent positional preferences and potentials, *J. Biosci.* 25, 143-156.
192. Trevino, S. R., Schaefer, S., Scholtz, J. M., and Pace, C. N. (2007) Increasing protein conformational stability by optimizing beta-turn sequence, *J. Mol. Biol.* 373, 211-218.
193. Hardy, F., Vriend, G., Veltman, O. R., Vandervinne, B., Venema, G., and Eijsink, V. G. H. (1993) Stabilization of *Bacillus-stearothermophilus* neutral protease by introduction of prolines, *FEBS Lett.* 317, 89-92.
194. Nicholson, H., Tronrud, D. E., Bechtel, W. J., and Matthews, B. W. (1992) Analysis of the effectiveness of proline substitutions and glycine replacements in increasing the stability of phage-T4 lysozyme, *Biopolymers* 32, 1431-1441.
195. Yi, Z. L., Pei, X. Q., and Wu, Z. L. (2011) Introduction of glycine and proline residues onto protein surface increases the thermostability of endoglucanase CelA from *Clostridium thermocellum*, *Bioresour. Technol.* 102, 3636-3638.
196. Harries, W. E., Akhavan, D., Miercke, L. J., Khademi, S., and Stroud, R. M. (2004) The channel architecture of aquaporin 0 at a 2.2 Å resolution, *Proc. Natl. Acad. Sci. U. S. A.* 101, 14045-14050.



197. Murata, K., Mitsuoka, K., Hirai, T., Walz, T., Agre, P., Heymann, J. B., Engel, A., and Fujiyoshi, Y. (2000) Structural determinants of water permeation through aquaporin-1, *Nature* 407, 599-605.
198. Lee, J. K., Kozono, D., Remis, J., Kitagawa, Y., Agre, P., and Stroud, R. M. (2005) Structural basis for conductance by the archaeal aquaporin AqpM at 1.68 Å, *Proc. Natl. Acad. Sci. U. S. A.* 102, 18932-18937.
199. Fu, D., Libson, A., Miercke, L. J., Weitzman, C., Nollert, P., Krucinski, J., and Stroud, R. M. (2000) Structure of a glycerol-conducting channel and the basis for its selectivity, *Science* 290, 481-486.
200. Kelly, S. M., Jess, T. J., and Price, N. C. (2005) How to study proteins by circular dichroism, *Biochim. Biophys. Acta* 1751, 119-139.
201. Kang, H. J., Lee, C., and Drew, D. (2013) Breaking the barriers in membrane protein crystallography, *Int. J. Biochem. Cell Biol.* 45, 636-644.
202. Lau, F. W., Nauli, S., Zhou, Y. F., and Bowie, J. U. (1999) Changing single side-chains can greatly enhance the resistance of a membrane protein to irreversible inactivation, *J. Mol. Biol.* 290, 559-564.
203. Bowie, J. U. (2001) Stabilizing membrane proteins, *Curr. Opin. Struct. Biol.* 11, 397-402.
204. Joseph, D., Petsko, G. A., and Karplus, M. (1990) Anatomy of a conformational change - hinged lid motion of the triosephosphate isomerase loop, *Science* 249, 1425-1428.
205. Bowie, J. U. (1997) Helix packing in membrane proteins, *J. Mol. Biol.* 272, 780-789.

206. Hansen, J. S., Vararattanavech, A., Plasencia, I., Greisen, P. J., Bomholt, J., Torres, J., Emneus, J., and Helix-Nielsen, C. (2011) Interaction between sodium dodecyl sulfate and membrane reconstituted aquaporins: A comparative study of spinach SoPIP2;1 and *E. coli* AqpZ, *Biochim. Biophys. Acta* 1808, 2600-2607.
207. Borgnia, M. J., Kozono, D., Calamita, G., Maloney, P. C., and Agre, P. (1999) Functional reconstitution and characterization of AqpZ, the *E. coli* water channel protein, *J. Mol. Biol.* 291, 1169-1179.
208. Eftink, M. R. (1994) The use of fluorescence methods to monitor unfolding transitions in proteins, *Biophys. J.* 66, 482-501.
209. Barrera, F. N., Renart, M. L., Poveda, J. A., De Kruijff, B., Killian, J. A., and Gonzalez-Ros, J. M. (2008) Protein self-assembly and lipid binding in the folding of the potassium channel KcsA, *Biochemistry* 47, 2123-2133.
210. Alexandrov, A. I., Mileni, M., Chien, E. Y. T., Hanson, M. A., and Stevens, R. C. (2008) Microscale fluorescent thermal stability assay for membrane proteins, *Structure* 16, 351-359.

## VITA

### PERSONAL INFORMATION

- Name Cui Ye
- Place of Birth Jiangxi, China
- Nationality China

### EDUCATION

- B.E. in Bioengineering, 2008  
Nanchang University, Nanchang, Jiangxi, China

### PUBLICATIONS AND SELECTED PRESENTATIONS

- Ye C., Lu W., Zhong M. Chai Q., and Wei Y. (2013) Correlation between AcrB trimer association affinity and efflux activity. (Submitted on Jan. 20, 2014)
- Ye C., Wang Z., Lu W., and Wei Y. (2014) Unfolding study of a trimeric membrane protein AcrB. Protein Sci. DOI: 10.1002/pro.2471
- Ye C., Chai Q., Zhong M., and Wei Y. (2013) Effect of crowding by Ficolls on OmpA and OmpT refolding and membrane insertion. Protein Sci. 22, 239-245
- Yu L., Lu W., Ye C., Wang Z., Zhong M., Chai Q., Sheetz M., and Wei Y. (2013) Role of a conserved residue R780 in Escherichia coli multidrug transporter AcrB. Biochemistry 52, 6790-6796
- Ye C., Wang Z., Lu W., and Wei Y., “Unfolding study of a trimeric membrane protein AcrB.” 99th Kentucky Academic Science meeting, Morehead, KY (Nov. 9, 2013)

- Ye C., Combs T., and Wei Y., “Supporting extended space travel through basic research on membrane proteins.” KY EPSCoR Annual Conference, Louisville, KY (Oct. 17, 2013)
- Ye C., Lu W., Zhong M. Chai Q., and Wei Y., “Correlation between AcrB trimer association affinity and efflux activity.” Frontiers in Structure Biology of Membrane Proteins, Birmingham, AL (Apr. 4, 2013)
- Ye C., Combs T., and Wei Y., “Molecular engineering of Aquaporin.” Kentucky Water Resources Research Institute Annual Symposium, Lexington, KY (Mar. 18, 2013)
- Ye C., Chai Q., Zhong M., and Wei Y., “Effect of Ficolls on OmpA and OmpT Membrane Insertion.” Gibbs Conference on Biological Thermodynamics, Carbondale, IL (Sep. 23, 2012)
- Ye C., Wu M., Chai Q., Zhong M., Wei Y. “Macromolecular Crowding Effect on the Structure of Unfolded Outer Membrane Proteins.” Graduate Course on Neutron Scattering Application in Structural Biology, Oak Ridge National Laboratory, Oak Ridge, TN (May 23, 2011)

#### AWARDS AND HONORS

- First prize graduate research competition award, 99th KAS meeting, Morehead, KY, 2013
- Selected video presentation at KY EPSCoR Annual Conference, Louisville, KY, 2013
- Graduate School Academic Year Fellowship, University of Kentucky, 2011-2012

- Travel award for the Neutrons in Structural Biology workshop, Oak Ridge National Lab, TN, 2011